REGULATION OF INFLUENZA VIRUS RNA SYNTHESIS MACHINERY BY VIRAL AND HOST FACTORS

FANGZHENG WANG

Sir William Dunn School of Pathology

and

Lincoln College

A thesis submitted for the degree of

Doctor of Philosophy

at the University of Oxford, Hilary Term 2024

ABSTRACT

Regulation of influenza virus RNA synthesis machinery by viral and host factors

Fangzheng Wang — Doctor of Philosophy

Lincoln College — Hilary Term, 2024

Influenza A virus transcribes and replicates the viral genome in the context of ribonucleoproteins (RNPs) which are the basic RNA synthesis units of the virus. The function of this viral RNA synthesis machinery is tightly regulated by various viral and host proteins to ensure the optimized virus replication and concomitant evasion or subversion of host immune responses.

ANP32 is recognized as an essential host factor for influenza virus replication due to its role in mediating the formation of influenza viral polymerase asymmetric dimer. In this work, we unravel that ANP32 facilitates recruitment of NP to the nascent RNA products, which is the second function of ANP32 during influenza virus replication, further strengthening the model that FluPol-ANP32 complex represents the replication platform for the influenza virus RNA genome.

Influenza virus nucleoprotein (NP) is the major component of ribonucleoproteins, and it binds to viral RNA and interacts with viral polymerase, underlying its critical role in virus replication. I demonstrate that the C-terminal tail of NP, a region that was previously only characterized by structural analysis, is important for cRNA stabilization and FluPol-NP interactions. Mutation in the C-terminal tail of NP profoundly attenuates the virus, recapitulating the essential role of NP in influenza virus replication. Another important

viral regulator of the viral RNA synthesis machinery is the influenza nuclear export protein (NEP). I establish a split-luciferase assay to measure FluPol-NEP interactions. Based on our resolved structure of FluPol in complex with NEP, we identify critical residues at the interface of the FluPol-NEP complex and link the FluPol-NEP interactions with the regulatory function of NEP.

The interdependent nature of vRNA and cRNA synthesis of influenza virus hinders the understanding of the effect of different factors on each step of virus replication. By combining the RNPs isolation techniques and *in vitro* vRNP reconstitution system, we set up an *in vitro* cRNP reconstitution assay, which allows us to uncouple the vRNA and cRNA synthesis and measure the authentic vRNA synthesis from isolated cRNPs alone.

In summary, the above findings improve our understanding of mechanisms by which ANP32, NP, and NEP regulate influenza virus RNA synthesis. The techniques established in this study also provide powerful tools for future studies on the replication mechanisms of influenza virus.

DECLARATION

I declare that this thesis is entirely my own work and describes my own research, except where stated otherwise by reference or acknowledgment.

ACKNOWLEDGEMENTS

"What's past is prologue."

My DPhil study in the Fodor lab is more like a journey of self-healing. I will be forever grateful for my supervisor Professor Ervin Fodor that he put his trust on a stubborn young man who just barely survived from a hideous farce in academia and had failed the PhD application twice five years ago. After joining his lab, the scientific training that I received from Ervin is remarkable, and most of this work could not have been accomplished without his supervision and guidance. In addition to the elegant science, I also want to appreciate his true kindness, great patience, and wonderful leadership which are valuable traits I have been trying to learn by osmosis in the past four years. Thank you for making doing science a such enjoyable thing!

I would also want to thank my co-supervisor Jonathan Grimes and Haitian Fan for their great insights from structural biology and valuable scientific discussions on my project. Thank you all for leading me into the world of structural virology. I am grateful to Jane Shapes for her timely support and teaching in the lab and George Brownlee for sharing his knowledge and expertise during lab meetings. I also want to appreciate Kuang-yu Chen for her assistance on my experiments and all the ridiculously delicious cakes she has made.

My gratitude also goes to the past and current lab members of the Fodor Lab and the Grimes Lab: Alison Rep, Alaa Baazaoui, Jeremy Keown, Loic Carrique, Jack Whitehead, Ecco Staller, Stephanie Williams for their daily help in the lab. A special thanks goes to Zihan Zhu, my good labmate, friend, and gym partner, who successfully makes exercise become a daily routine for me. I also want to express thanks to all my friends at Dunn School, especially who have spent long nights in the lab together with me. I also appreciate the generous funding from different funding agencies on my studies and projects.

In the end, I want to express my deepest gratitude to my parents who have kindled my initial interest in microbiology. Your unconditional love, encouragement, and support are the reasons that I can freely enjoy the discovery of the unknown.

TABLE OF CONTENTS

ABBREVIATIONS

Units

bp	Base pair
Ci	Curie (1 Ci = 3.7 ×10^{10} becquerels)
Da	Dalton
h	Hour
hpi	Hours post-infection
hpt	Hours post-transfection
g	Standard gravity (9.80665 m/s2)
kDa	KiloDalton
min	Minute
MOI	Multiplicity of infection
nt	Nucleotide
PFU	Plaque-forming unit
RPM	Revolutions per minute
s	Second (s)
U	Enzyme Unit

Other Abbreviations

A	Alanine
ANOVA	Analysis of variance
ANP32A	Acidic nuclear phosphoprotein 32 family member A
ANP32B	Acidic nuclear phosphoprotein 32 family member B
ANP32E	Acidic nuclear phosphoprotein 32 family member E
APS	Ammonium persulfate
ATP	Adenosine triphosphate
cDNA	Complementary DNA
chANP32A	Chicken acidic nuclear phosphoprotein 32 family member A
chANP32B	Chicken acidic nuclear phosphoprotein 32 family member B
CPE	Cytopathogenic effect
CRM1	Chromosomal Maintenance 1
cRNA	Complementary RNA
cRNP	Complementary ribonucleoprotein
CTD	C-terminal domain
D	Aspartic acid
dH2O	Distilled water
DMEM	Dulbecco′s modified Eagle′s medium
DNA	Deoxyribonucleic acid
dNTP	Deoxynucleoside triphosphate
DPBS	Dulbecco's Phosphate-buffered saline
DSMO	Dimethyl sulfoxide
DTT	Dithiothreitol
E	E glutamic acid
ECL	Enhanced chemiluminescence

EDTA	Ethylenediaminetetraacetic acid
EM	Electron microscopy
FCS	Foetal calf serum
FluPol	Influenza A virus RNA polymerase
$FluPol_E$	Encapsidating influenza A virus RNA polymerase
$FluPol_R$	Replicating influenza A virus RNA polymerase
G	Glycine
GST	Glutathione S-transferase
H	Histidine
HA	Haemagglutinin
HCl	Hydrochloric acid
HEPES	4-(2-hydroxyethyl)-1-piperazineethanesulfonic acid
HRP	Horseradish peroxidase
huANP32A	Human acidic nuclear phosphoprotein 32 family member A
huANP32B	Human acidic nuclear phosphoprotein 32 family member B
huANP32E	Human acidic nuclear phosphoprotein 32 family member E
HIV	Human immunodeficiency virus
I	Isoleucine
IPTG	Isopropyl β- d-1-thiogalactopyranoside
IP	Immunoprecipitation
K	Lysine
LB	Lysogeny broth
LCAR	Low-complexity acidic region
LRR	Leucine-rich repeat
M1	Matrix protein 1
M2	Matrix protein 2

m7G	7-methylguanosine
MDBK	Madin-Darby bovine kidney
MDBK	Madin-Darby Canine kidney
MEM	Minimum essential medium
$MgCl_2$	Magnesium chloride
mRNA	Messenger RNA
NA	Neuraminidase
NCR	Non-coding region
NaCl	Sodium chloride
NEP	Nuclear export protein
NES	Nuclear export signal
NLS	Nuclear localization signal
NP	Nucleoprotein
NPC	Nuclear pore complex
NS1	Non-structural protein 1 (influenza virus)
NT60	A/Northern Territory/60/1968 (H3N2)
NTP	Nucleoside triphosphate
OTG	Octylthioglucoside
PA	Polymerase acidic protein
PAGE	Polyacrylamide gel electrophoresis
PB1	Polymerase basic protein 1
PB2	Polymerase basic protein 2
PBS	Phosphate buffered saline
PCR	Polymerase chain reaction
PDB	Protein data bank
PEI	Polyethylenimine

PMSF	Phenylmethylsulfonyl fluoride
PNK	T4 polynucleotide kinase
Pol II	RNA polymerase II
poly(A)	Polyadenylic acid
Q	Glutamine
R	Arginine
Rab11	Ras-related in brain protein 11 family interacting protein
Ran	Ras-related nuclear protein
RdRp	RNA-dependent RNA polymerase
RNA	Ribonucleic acid
RNP	Ribonucleoprotein
rRNA	Ribosomal RNA
RT	Reverse transcription
S	Serine
s.e.m.	Standard error of the mean
SDS	Sodium dodecyl sulfate
SIM	SUMO interaction motif-like sequence
TBE	Tris-borate-ethylenediaminetetraacetic acid
TEMED	N,N,N′,N′-tetramethylethylenediamine
TEV	Tobacco etch virus protease
Tris	Tris (hydroxymethyl) aminomethane
vRNA	Viral RNA
vRNP	Viral ribonucleoprotein
WSN	A/WSN/33 (H1N1)
WT	Wildtype

CHAPTER 1

Introduction

1.1 Influenza Virus Biology

General background of influenza viruses

Influenza, caused by influenza viruses, is a contagious viral respiratory infection that affects the upper and lower respiratory tract (1). The first documented possible influenza outbreak by Thucydides can be traced back to 430 BC Athens, implying influenza viruses have eco-evolved with humans and animals throughout history (2). It was not until 1933 that the first human strain of influenza A virus (Influenza A/Wilson-Smith/1933 H1N1, WSN virus) was successfully isolated by Wilson Smith, Sir Christopher Andrews, and Sir Patrick Laidlaw of the National Institute for Medical Research in London, England (3). In 1940, the first strain of influenza B virus was isolated (4). Up until now, influenza still represents a major threat to public health due to its heavy health burden and pandemic potential. It is estimated that seasonal influenza alone causes approximately 3–5 million cases of severe illness and 290 000 to 650 000 respiratory deaths annually (5). Compared to seasonal influenza, influenza pandemics that occurred in the last century are catastrophic, with an example being the 1918 influenza pandemic that killed about 50 million people worldwide (6).

The most recent global outbreak of H5N1 avian influenza virus has affected at least 81 countries across five continents since 2022 (7). In addition to wild birds and poultry, the virus infected other mammalian species and caused infection among pigs, minks, cats, or even humans (8, 9) . The next influenza pandemic is believed to be inevitable. To improve influenza pandemic preparedness and management, it is important to understand the fundamental replication mechanisms of the influenza virus. This knowledge would allow

us to better predict the next pandemic strain and to develop more effective antiviral vaccines and antivirals.

1.1.1 Influenza virus taxonomy and nomenclature

Influenza viruses are part of the family of *Orthomyxoviridae* which are characterized with a negative-sense, single-stranded, and segmented RNA genome. There are seven different genera within the *Orthomyxoviridae* family: *Thogotovirus*, *Alphainfluenzavirus* (*influenza A virus*), *Betainfluenzavirus* (*influenza B virus*), *Gammainfluenzavirus* (*influenza C virus*), *Deltainfluenzavirus* (*influenza D virus*), *Quaranjavirus*, and *Isavirus*. Influenza A viruses have broad host tropism with wild aquatic birds as their natural reservoir (10). Influenza B viruses and influenza C viruses mainly infect humans and pigs (11); influenza D viruses mainly affect cattle and pigs (12, 13). According to the antigenicity of hemagglutinin and neuraminidase proteins, influenza A viruses are further classified into different subtypes. There are 18 HA subtypes (H1-H18) and 11 NA subtypes (N1-N18) that have been identified. The current nomenclature system for influenza viruses comprises the host of origin (omitted for human isolates), geographical origin, strain number, year of isolation, and description of HA and NA subtypes in parentheses. For instance, A/Northern Territory/60/1968 H3N2 represents a human influenza A virus isolated in Northern Territory in 1968 with a strain number of 60 and an H3N2 subtype. Influenza B viruses are divided into two linages (Victoria and Yamagata), while no subtypes and lineages are distinguished for influenza C viruses and influenza D viruses.

1.1.2 Influenza A virus virion structure

The pleomorphic influenza A virus can form spherical virions and filamentous virions (14). The morphology of influenza A virus virion is characterized by its distinctive spikes (HA

and NA) with lengths of approximately 10 to 14 nm **(Fig. 1.1A)**. As an enveloped virus, influenza A virus possesses a host-derived lipid membrane that harbours the hemagglutinin, the neuraminidase, and the M2 ion channel. Approximately, the ratio of HA trimer to NA tetramer is four (15), M2:HA ratio is about 1:10 to 1:100 (16). Beneath the envelope, the matrix (M1) protein forms an oligomeric layer to support the structural integrity of influenza virions (17). The core of influenza virion contains the viral ribonucleoprotein (vRNP) complex that is made up of the viral RNA (vRNA) segments, the nucleoprotein (NP), and the three polymerase subunits which are polymerase basic protein 2 (PB2), polymerase basic protein 1 (PB1), and polymerase acidic protein (PA). Other viral proteins such as non-structural protein 1 (NS1) and nuclear export protein (NEP) have been found within the virion as well (18-21). In addition to the viral proteins, proteomics studies have proven that numerous host proteins also make a substantial contribution to the structure of influenza virion (18, 22).

1.1.3 Influenza A virus genome structures

The genome of influenza A virus comprises eight viral RNA segments **(Fig. 1.1B)**. Each of these vRNA segments possesses noncoding regions at both the 3' and 5' ends containing a highly conserved sequences at the extreme ends followed by a segment-specific region (23). Notably, the highly conserved 12 nucleotides (nt) at 3' end and 13 nt at the 5' end are partially complementary and can form a panhandle structure which is recognized as the promoter region for influenza A viruses (24-26). The eight vRNA segments of influenza A virus genome with their lengths varying from 2.3 kb to 0.9 kb are numbered in order of decreasing length. The influenza A virus increases its genome coding capacity using alternative open reading frames or splicing. For instance, mRNAs of M and NS can be spliced to generate the M2 and NEP proteins (27-29). The PB1 segment encodes a PB1-

F2 protein using an alternative open reading frame, and PB1-N40 using a downstream start codon (29). PA-X protein is a frameshift product from the PA segment (30).

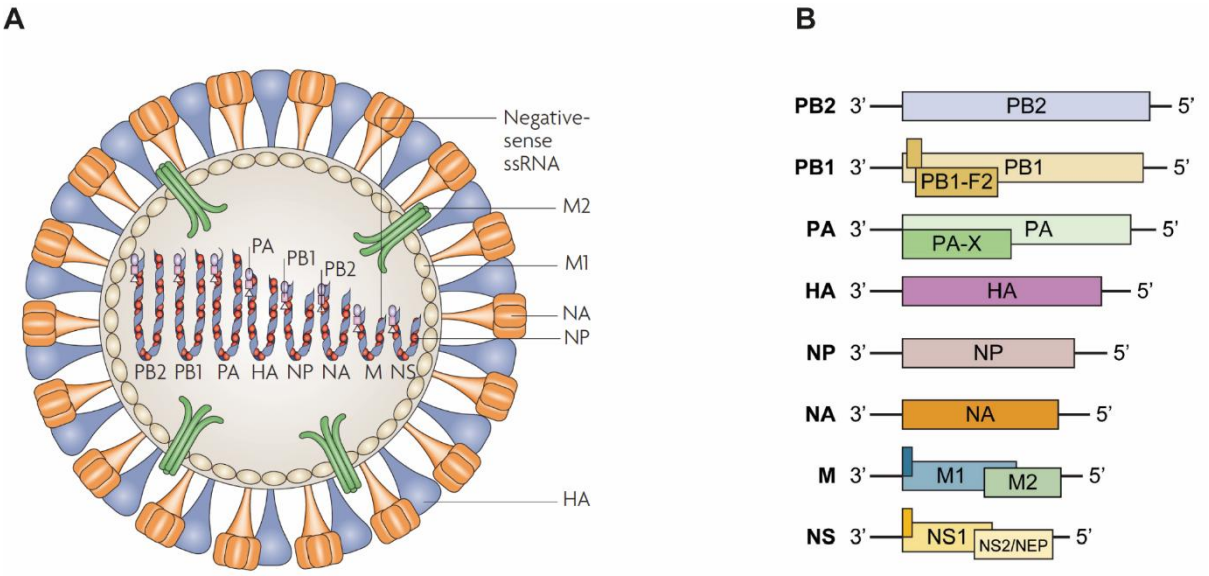

Fig. 1.1. Schematic diagram of influenza A virus virion and genome structure.

(A) Schematic diagram of influenza A virus virion with structural proteins labelled. The figure is adapted from (31). (B) Schematic of influenza A virus genome structure. The figure is adapted from (32). The eight vRNA segments (3' to 5') are arranged based on their length. NS2/NEP and M2 are translated from spliced mRNA of M and NS. PB1-F2 and PA-X are frameshift products from PB1 and PA segments.

1.1.4 Influenza A virus life cycle

The life cycle of influenza A virus is summarised in **Fig. 1.2**.

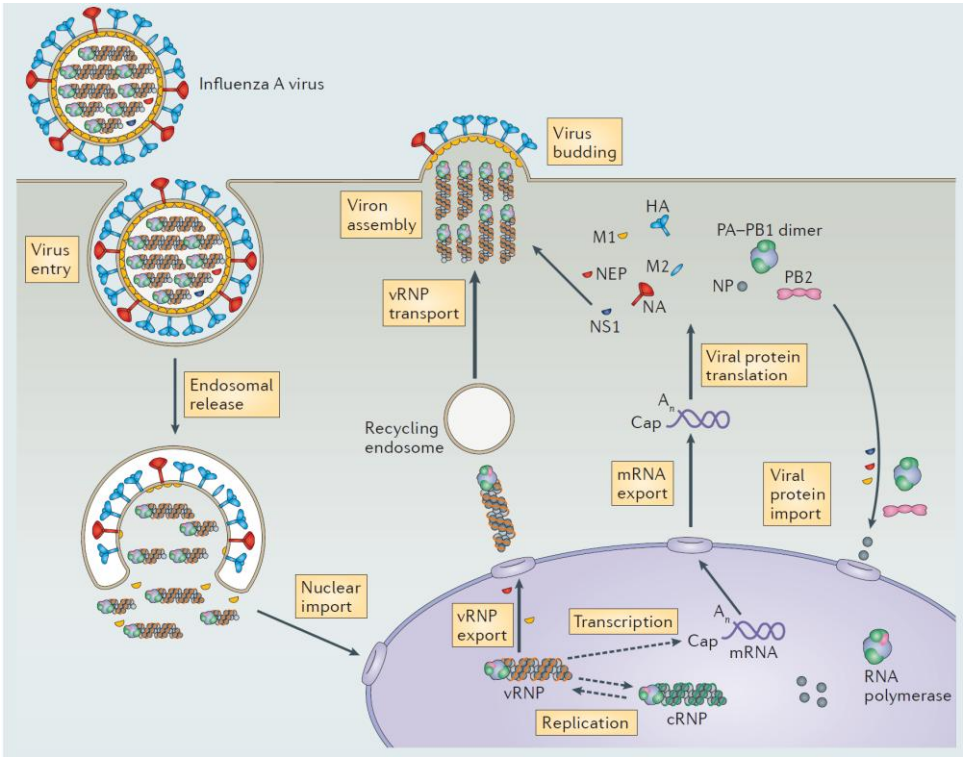

Fig. 1.2 Life cycle of influenza A virus.

Influenza A virus attaches to the host cell through its HA protein binding to the host sialic acid receptors. The virion enters the cells via endocytosis, and its low pH environment induces conformational changes in HA protein and eventually leads to membrane fusion. vRNPs are released into cytoplasm and subsequently imported into the nucleus, where viral transcription and replication occur. The incoming vRNPs synthesize mRNAs that are exported to the cytoplasm for translation of viral proteins. The newly synthesized viral polymerase and NP proteins are imported into nucleus and activate viral replication. Then vRNPs synthesize cRNA, replication intermediates, which are subsequently used as templates to synthesize progeny vRNA. vRNPs are exported from nucleus into the cytoplasm for selective packaging into the progeny virions together with other newly synthesized viral proteins at the plasma membrane. Progeny virions are released through budding with the assistance of NA. The figure is adapted from (23).

Attachment

Influenza A viruses (except bat influenza A viruses H17N10 and H18N11) attach to host cells through the binding of the viral HA protein to N-acetylneuraminic (sialic) acids on host cell glycoproteins and glycolipids (33). It has been shown that human strains preferentially bind to sialic acid conjugated with an α2, 6 linkage to galactose (SA α2, 6Gal), whereas avian strains bind to sialic acid with α2, 3 linkage (SA α2, 6Gal) (34-37). Indeed, SA α2, 3Gal are predominantly expressed in chicken and duck intestine (38), while human tracheal epithelial cells mainly contain SA α2, 6Gal (39). However, this species specificity is not absolute as both avian and human cells can contain both types of receptors (39, 40). Notably, bat-derived H17N10 and H18N11 viruses do not bind to the canonical sialic acid receptor; instead, these viruses rely on the major histocompatibility complex class II (MHC-II) human leukocyte antigen DR isotype (HLA-DR) for entry (41).

Entry

The clathrin-mediated internalization pathway, which is also used by Semliki Forest virus and vesicular stomatitis virus (42, 43), has traditionally been recognized as the entry mechanism for influenza viruses. Notably, influenza virus has been detected within the clathrin-coated vesicles during endocytosis (44). However, the use of a non-clathrin-dependent endocytic pathway by the influenza virus has also been reported (45). More recently, a dynamin-independent pathway that resembles macropinocytosis has been identified for the entry of influenza viruses, particularly for the filamentous influenza viruses (46, 47).

Fusion and uncoating

Prior to membrane fusion of influenza viruses, the HA0 precursor must be cleaved into HA1 and HA2. Upon endocytosis, the low pH environment of endosome dramatically changes the structure of the cleaved HA molecule (46). The fusion peptide at the N-terminus of the HA2 is exposed and inserts into the membrane of the endosome, bringing the endosome membrane into juxtaposition with the viral membrane (48, 49). Multiple HA molecules are orchestrated to undergo these conformational changes, resulting in the formation of a fusion pore through which the contents of the virion can enter the cytoplasm. M2 protein, which has ion channel activity, is also indispensable for effective uncoating process (50, 51). M2 protein conducts the influx of H^+ ions from the endosome into the virion and thereby facilitates the disruption of protein-protein interactions resulting in the release of free vRNPs without association of M1 (51).

Influenza virus transcription and replication

As RNA synthesis of the influenza virus occurs in the nucleus, the released vRNPs must be trafficked into the nucleus through an active nuclear import mechanism given the fact that vRNPs are too large to passively diffuse into the nucleus. All three polymerase subunits and NP possess nuclear localization signals (NLS) which can mediate their interactions with the cellular nuclear import machinery (52-56). Nevertheless, the NLS on NP is sufficient for the import of vRNA (57-61). The trafficking of vRNPs from cytoplasm to nucleus relies on the classical NLS-dependent nuclear import pathway in which importin-α interacts with the NLS of the cargo protein and thus recruits importin-β to form the trimeric complex (58, 62). Importin-α is also known to be determinant of the host range of the influenza A virus due to the differential use of importin-α isoforms by human versus avian influenza viruses (63-65). Once vRNPs are imported into nucleus, the resident

polymerase in vRNPs synthesizes mRNA. Transcription is a primer-dependent process which involves the binding of the carboxy-terminal domain (CTD) of host RNA polymerase II (Pol II) to viral polymerase and cap-snatching to generate the 5' capped primer (23). Viral mRNAs are exported outside of the nucleus for translation using the same pathway of as host mRNAs (66). As viral proteins accumulate in the infected cell, the resident polymerase in the incoming vRNPs starts the synthesis of the positive-sense cRNA which is the replication intermediate used for the subsequent synthesis of vRNA (10, 23) . **(Fig. 1.3)**. The detailed review of RNA synthesis by the viral polymerase will be discussed in chapter 1.2.

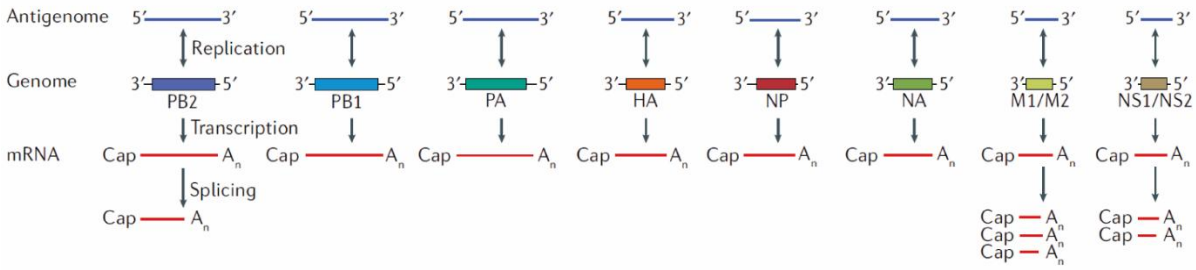

Fig. 1.3 Influenza A virus RNA synthesis.

Viral transcription starts at the 3' end of vRNA and terminates at a stretch of uracil residues near the 5' end of vRNA, generating 5' capped and 3' polyadenylated transcripts. Viral replication is a two-step process involving the synthesis of an antigenome intermediate (cRNA) and subsequent synthesis of progeny vRNA. The figure is adapted from (67).

Nuclear export of vRNPs

The newly synthesized vRNPs need to be transported from the nucleus into cytoplasm for virus assembly. CRM1 is an essential nuclear export factor, and it interacts with the GTPase Ran to perform the function of transporting cargo proteins through the nuclear

pore complex (NPC) (68). The directionality of nuclear transport is determined by the Ran-GTP gradient across the NPC (69, 70). The generally accepted model for vRNPs nuclear export is the so-called daisy chain model in which vRNP-M1-NEP (viral nuclear export protein) complex is formed for nuclear export (71). In the model **(Fig. 1.4A)**, CRM1 recognizes the two nuclear export signals (NES) in the N-terminus of NEP. The C-terminus of NEP interacts with the NLS in the N-terminus of the M1 protein that is associated with vRNPs using its C-terminal interaction with NP protein in vRNPs. Compared with the daisy chain model, a different model has been proposed with a difference that the C-terminus of NEP can directly interact with PB2 and PB1, and thus promote interactions between M1 and vRNPs (72) **(Fig. 1.4B)**. In either of these two models, both viral M1 and NEP proteins and host CRM1 are required for nuclear export of vRNPs. The role of CRM1 in vRNPs nuclear export has been confirmed by the observation that treatment with leptomycin B, a specific CRM1 inhibitor, abolishes vRNP export during virus infection (73-75). The requirement of NEP for vRNP nuclear export has been supported by the finding that injection of anti-NEP antibodies into the nucleus of infected cells inhibits vRNP export (76). Similarly, inhibition of M1 expression leads to the retention of vRNPs in the nucleus (77), which underlines the function of M1 in nuclear export of vRNPs. Both NEP and M1 have been suggested to prevent vRNPs from re-entering the nucleus following the export, which underlies their regulatory function in vRNP nuclear export (78, 79). After leaving the nucleus, vRNPs are trafficked to the plasma membrane for subsequent virus packaging in a Rab11a and microtubule-dependent mechanism (80-82).

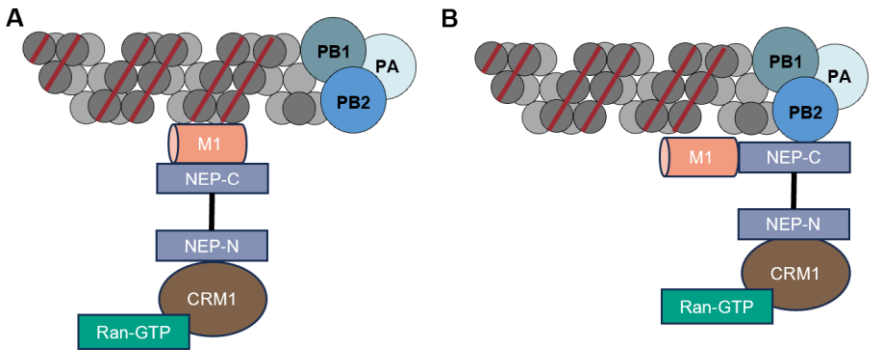

Fig. 1.4 Schematic diagram of vRNP nuclear export model.

(A) Daisy chain model of the nuclear export of vRNPs. The N-terminal domain containing NES of NEP interacts with CRM1, and its C-terminus interacts with M1 which is associated with vRNPs. (B) Alternative model of the vRNP nuclear export. The N-terminus of NEP interacts with CRM1, whereas its C-terminus directly interacts with the viral polymerase and thereby provides additional biding site to stabilize the vRNP-M1 complex. The figure is adapted from (83).

Virus assembly and budding

All the eight vRNPs must be correctly assembled and packaged into progeny virions. The selective incorporation model, in which each of the eight vRNPs is selectively packaged, is now widely accepted with accumulating evidence in recent years (84-90). Observations from electron microscopy and electron tomography reveal that the eight selected vRNPs are arranged in a specific "1+7" configuration with one vRNP in the centre and seven in the surrounding positions (84-86). Several studies have suggested that the selective packaging is achieved via RNA-RNA or protein-RNA interactions (88, 91-95).

HA, NA, and M2 are trafficked to the apical plasma membrane using their apical sorting signals (96-98). HA and NA accumulated at and are incorporated into lipid rafts within the plasma membrane (96, 99), while M2 is excluded from lipid rafts and may bridge several raft domains (100, 101). HA and NA stimulate membrane binding of the M1 protein (102). M2 has been reported to cause the membrane curvature at the neck of the budding virus, leading to membrane scission and the release of the progeny virion (103-105). Once budding is complete, the NA protein with its sialidase activity releases the progeny virus from the host cell thereby avoiding the aggregation of virus particles (106, 107).

1.1.5 Influenza pandemics

Influenza A virus represents a serious threat to public health due to its pandemic potential. Constant antigenic variation allows the virus to escape existing immunity among people and thus enables human-human transmission. The HA and NA proteins can change in two ways: antigenic drift and antigenic shift. Antigenic drift is a gradual process in which the accumulation of point mutations results in antigenic changes. This relatively slow process is also the reason that the vaccine for seasonal influenza needs to be updated annually.

Antigenic shift is a major antigenic change in which the HA or NA proteins that are not circulating in the human population are acquired by the virus via the swap of gene segments when different influenza viruses simultaneously infect a cell (reassortment). Reassortment is the driving force for the emergence of pandemic strains. Historically, three out of the four influenza pandemic strains in the past 100 years have emerged via reassortment (108-110).

In the past century, pandemic influenza viruses have emerged in 1918 (Spanish influenza, H1N1), in 1957 (Asian influenza, H2N2), in 1968 (Hong Kong influenza, H3N2), and in 2009 (swine influenza, H1N1) (111). The 1918 influenza pandemic is notorious for its extraordinary mortality, causing approximately 50 million fatalities across the world (6). The successful sequencing of the 1918 pandemic virus has revealed that this pandemic was trigged by an H1N1 virus that might have originated from an avian strain (112-115). The 1957 pandemic was caused by a reassortant H2N2 virus with its HA, NA, and PB1 genes of avian virus origin (116). It is estimated that this pandemic caused 1-2 million deaths worldwide (117). Similar to the 1957 pandemic strain, the 1968 pandemic influenza virus (H3N2) also emerged through reassortment, and its HA and PB1 genes originated from viruses of an Eurasian avian lineage (116). Globally, almost 4 million people were killed during this pandemic. This H3N2 virus is still circulating in the human population and is considered a seasonal strain nowadays. The most recent influenza pandemic outbreak was in 2009. The virus that is responsible for this pandemic is a swine-origin H1N1 virus named as A(H1N1) pdm09 virus. A(H1N1)pdm09 virus is a “triple” reassortant viruses with its genes inherited from avian, swine, and human strains: PB2 and PA genes of North American avian virus origin; NA and M genes of Eurasian avian-like swine virus origin; HA , NP, and NS genes of classical swine virus origin; PB1 gene of human H3N2 virus

origin. Intriguingly, this pandemic virus possesses neither an avian-origin PB1 nor the glutamic acid (E) to lysine (K) mutation at 627 residue of the PB2 protein (PB2 E627K) which is a hallmark of mammalian adapted virus (111). Indeed, alternative adaptive strategies deployed by this virus have been reported (118). A(H1N1) pdm09 virus has now become a seasonal influenza virus and is part of the seasonal influenza vaccine.

1.2 Influenza A virus RNA synthesis

1.2.1 Influenza A virus RNA synthesis machinery

1.2.1.1 Viral ribonucleoprotein complex (vRNP)

Each of the eight genomic RNA of the influenza A virus is packaged in vRNP, which is the most basic unit for viral RNA synthesis (119). The vRNP comprises the negative-sense vRNA bound by multiple copies of NP molecules and the viral RNA-dependent RNA polymerase complex (RdRp) at one end (23) **(Fig. 1.5)**. NP is an arginine-rich protein and maintains a net positive charge, giving it RNA-binding ability (120). The major function of NP during influenza virus replication is the encapsidation of nascent RNA products, which is mediated by electrostatic interactions between positively charged residues on NP and the negatively charged phosphate backbone of the RNA (121, 122) . Although RNA is bound by NP, the bases of RNA are exposed to the outside and the secondary structure of RNA is melted by the association of NP (121). Approximately, every NP monomer interacts with 24 nt of RNA (122). NP molecules can oligomerize in a manner such that the tail loop of one NP molecule is inserted into a binding site of the adjacent NP molecule (123, 124). Oligomerization of NP is important for maintaining the structure of the ribonucleoprotein complex (vRNP). Using cryogenic electron microscopy (cryo-EM) and negative-stain electron microscopy, several studies have shown that vRNPs display a twisted, anti-parallel double helical, rod-shaped structure (125-127). In these observed

RNP structures, NP can directly interact with the viral polymerase (128-130), which is required for genome replication, transcription, and packaging (131-133).

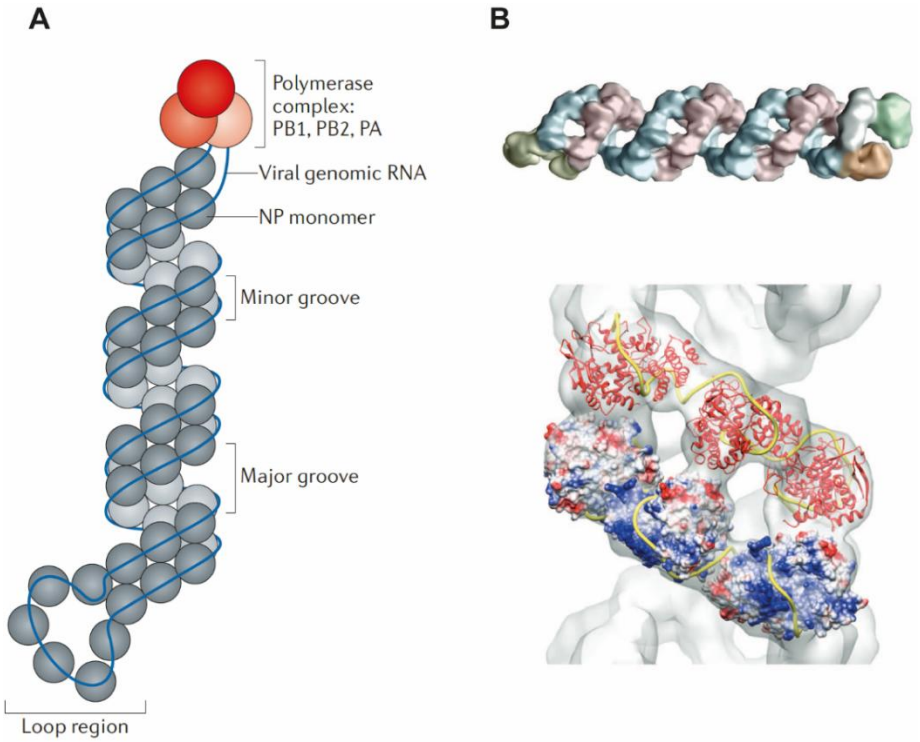

Fig. 1.5 The structure of the influenza A virus vRNP complex.

(A) Schematic diagram of viral ribonucleoprotein (vRNP). vRNP is made up of the heterotrimeric polymerase complex and a single-stranded, negative-sense genomic RNA coated with nucleoprotein. The 5' and 3' ends of vRNA are partially complementary and base pair to form a double-strand region that is bound by the viral polymerase complex at one end of the vRNP. A loop can be observed at the opposite end of the vRNP. The vRNP complex exhibits a double helical structure which is driven by the interaction among NP molecules. (B) Cryo-EM model for the structure of influenza A virus helical RNP. The viral polymerase (green and brown) and the terminal NP loop (yellow) in the helical structure of an RNP (Top panel). Model for the localization of the template RNA (yellow thread) in the RNP structure with one NP strand shown with surface potential and the opposite strand as a ribbon representation. Figures are adapted from (119, 126).

1.2.1.2 Viral RNA-dependent RNA polymerase complex

The viral heterotrimeric RdRp complex with a molecular weight of approximately 270 kDa consists of three polymerase subunits: PB2, PB1 and PA (23, 67) **(Fig. 1.6)**. High-resolution structures of different conformations of the influenza A virus polymerase have been resolved in recent years (134-138). The PB1 subunit is the centre of the viral polymerase complex, and it catalyses the RNA synthesis. Structurally, PB1 has the canonical right-hand-like fold and contains the fingers, palm and thumb subdomains which are characteristic of RdRp (139). A highly conserved SDD motif is found at 444-446 residues of PB1, which is essential for polymerase activity (139). The PB2 subunit comprises the N-terminal domain (PB2-N), the middle domain, the cap-binding domain, the 627-domain, and the C-terminal NLS domain with nuclear-localization signal. The cap-binding domain of PB2 binds to the 5′ cap of host pre-mRNAs, which is critical for the initiation of viral transcription(140). The PA subunit contains the N-terminal endonuclease (Endo) domain and the C-terminal domain (PA-C) which are connected by a long linker that wraps around the PB1 subunit (23). The endonuclease activity of the RdRp required to generate the capped primer for transcription resides in the PA Endo domain (137, 141, 142). The polymerase core is made up of PB1, PA-C, and PB2-N. The three polymerase subunits are tightly associated with each other to form a compact structure which can be viewed as a complex comprising of the polymerase core with flexible peripheral appendices that are formed by the PA Endo domain and the PB2 mid, cap-binding, linker, 627, and NLS domains (143).

The heterotrimeric RdRp of the influenza A virus displays a U-shaped structure. A large internal cavity formed by PB1 and PB2-N is found within the RdRp and the polymerase active site is at the edge of this cavity (136). A key feature of the polymerase active site is

the priming loop that is used for unprimed initiation of cRNA synthesis from vRNA template (144), which is a conserved anti-parallel β-loop that is made up of the residues 641-657 of PB1 protruding from the PB1 thumb domain towards the polymerase active site (137). Multiple channels with different functions are accessible to the polymerase active site (137). The template entry channel that leads from the 3' vRNA binding site to the polymerase active site is lined by conserved residues from all three subunits; the NTP entry channel consists of highly conserved PB1 basic residues and directly leads to the tip of priming loop; the template exit channel is on the same side of the polymerase as the template entry channel; the product exit channel is located along the PB1 finger domains and PB2 cap domain.

RdRp has multiple binding sites for the 3' and 5' ends of viral RNAs. The 5' end of vRNA and cRNA bind to a pocket near the template entry channel (135, 137). The 3' end of viral RNA has two binding sites (mode A site and mode B site) on the RdRp. Mode A site is near the template entrance channel, while mode B site is in a groove further away from the template entrance channel. The 3' end of vRNA has been found to bind both of these two sites (135, 138), whereas the 3' end of cRNA only binds to mode B site (135, 145).

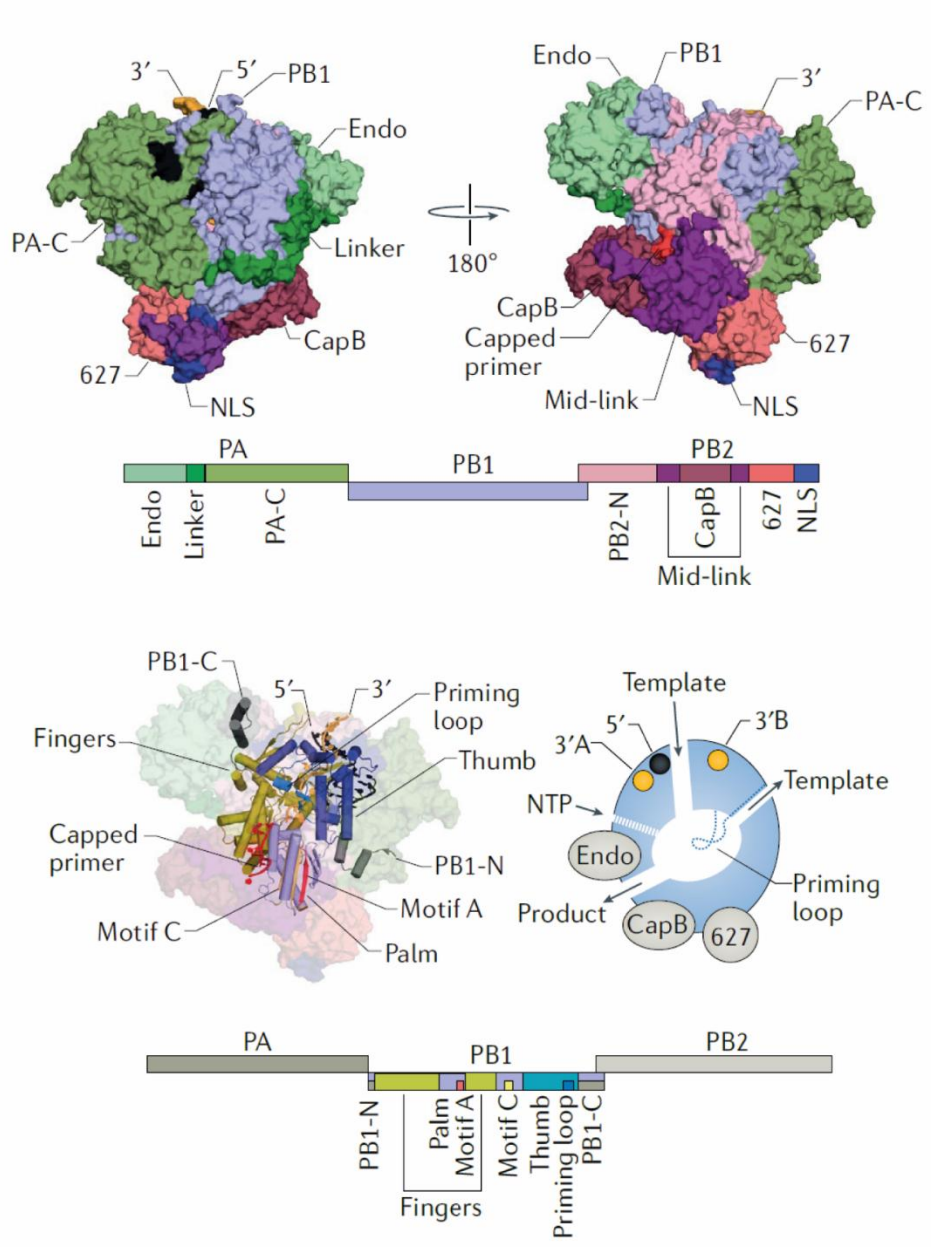

Fig. 1.6 Influenza A virus RNA polymerase structure.

Schematic diagram of different domains of the viral polymerase subunits and structure of the influenza A virus polymerase bound to vRNA and a capped RNA primer (PDB ID: 6RR7). The viral polymerase has a large internal cavity that is connected to the solvent via template and nucleotide triphosphate (NTP) entry channels, and template and products exit channels. The location of the priming loop, the 3′ and 5′ end-binding pockets are indicated. This figure is adapted from (67).

1.2.1.3 Promoter binding

All vRNA segments of the influenza A virus share a highly conserved 13 nt at the 5' end and 12 nt at the 3' end with their sequences displaying partial and inverted complementarity (146, 147) **(Fig. 1.7)**. These two regions form a non-canonical double helix, also known as panhandle (26), which is recognized as the promoter for the influenza A virus (25). Prior to the available structure of the influenza A polymerase bound to the viral RNA promoter (137), different models such as the 'corkscrew' model (148, 149) or the 'fork' model (150, 151) have been proposed. The resolved structure shows that the first 10 nt of 5' vRNA form a hook structure with two central canonical base pairs flanked by mismatching base pairs. The 1-9 nucleotides of 3' vRNA remain in a single-stranded form, and its distal 10-14 nucleotides, together with the 5' vRNA nucleotides 11-15, form a duplex region (**Fig. 1.6)**. cRNA also has a promoter region bound by the viral polymerase for vRNA synthesis. Although the cRNA promoter is complementary to the vRNA promoter (24, 152), its 5' end still resembles the hook-like structure of the 5' end of the vRNA promoter. The binding site of the cRNA 5' end by the influenza B virus polymerase is also same as that of the vRNA 5' end (153).

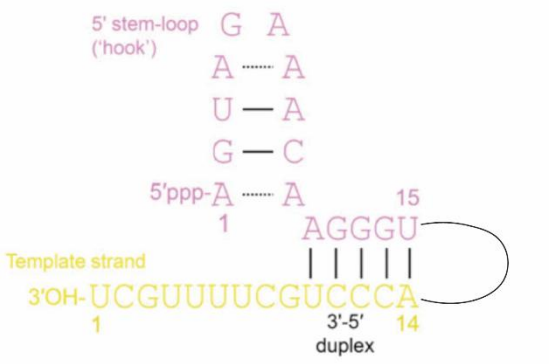

Fig. 1.7 Influenza A virus vRNA promoter.

The sequence and secondary structure of influenza A virus vRNA promoter showing the 5′ stem-loop ('hook') and the 3′-5′ duplex region. This figure is adapted from (154).

1.2.1.4 Nucleoprotein

The nucleoprotein (NP) of the influenza A virus is multi-functional viral protein (120, 155). As the component of RNPs, the major function of NP is encapsidation of nascent RNA products (119). Multiple structures of NP, in the absence or the presence of RNA, have been reported (123, 124, 156-158). The NP molecule displays a curved, crescent-like shape with a head domain (residues 150–276 and 429–452) and a body domain (residues 1–149 and 277–386) **(Fig. 3.5)**. NP can oligomerize by inserting the tail loop (residues 402 – 428) of one NP molecule into the groove of neighbouring NP molecule. A tail loop mutation (R416A) and an insertion groove mutation (E339A) can both abolish NP oligomerization (133, 156, 159). Two positively charged grooves (NP-G1, NP-G2) of NP have been identified (123, 156). Residues (R74/R75/R174/R175) in the NP-G1 and residues (R150/R152/R156/R162) in the NP-G2 are essential for the RNA-binding ability of NP. A recent study has proposed a model in which NP-G1 captures ambient RNA during replication, and displacement of the NP C-terminal tail exposes positively charged residues in NP-G2, allowing the 5' end of the RNA to shift into the NP-G2 groove (123). Notably, the translocation of NP to RNA is facilitated by different host factors such as UAP56 or ANP32 protein (160-162).

NP is recognized as an elongation factor during viral RNA synthesis. The dependency on NP can be removed when the length of the RNA template used for replication is shorter than 76 nt (159). NP greatly contributes to the accumulation of cRNA, although it is not essential for cRNA stabilization (163) as polymerase alone can stabilize certain amount of cRNA. Additionally, it is the RNA-binding ability, but not oligomerization, of NP that is required for stabilization of cRNA (164). A recent study also claims that NP has a direct

stimulatory effect on viral replication, implying that NP might serve as a switch for viral transcription and replication (165).

1.2.1.5 Nuclear export protein (NEP)/NS2 protein

Segment eight of the influenza A virus encodes two viral proteins: NS1 and NS2/NEP proteins (166, 167). NS2 was initially recognized as a non-structural protein. Later, NS2 was found in the virion and thus non-structural protein 2 is a misnomer (20, 21, 76). NEP consists of an N-terminal domain (residues 1-53) which interacts with CRM1 and a C-terminal domain (residues 54-121) that associates with M1 (71). Currently, only the C-terminal domain of NEP is structurally resolved and there is no available structure of the full-length NEP. Nevertheless, biochemical analyses have identified two nuclear export signals (NES) (**Fig. 1.9)**: NES1 (residues 12-21) comprising a stretch of hydrophobic residues and a leucine-rich NES2 (residues 31-40) located within the N-terminal region of NEP (76, 168, 169).

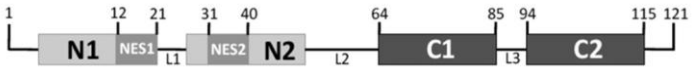

Fig. 1.9 The schematic diagram of influenza NEP.

The regions of two nuclear export signals are labelled. The N-terminal helices are in light grey; C-terminal helices are in dark grey; L1-L3 represent the unfolded linker regions. This figure is adapted from (72).

In addition to the well-defined function of NEP in nuclear export (review in section 1.1.4 nuclear export of vRNPs), there are increasing numbers of studies showing that NEP also plays a critical regulatory role during influenza virus RNA synthesis (170-176). NEP was initially found to alter RNA accumulation levels in the vRNP reconstitution assay (171). This study from our group shows that overexpression of NEP markedly enhances cRNA accumulation level but downregulates mRNA accumulation level in the vRNP reconstitution system. Notably, this regulatory function is not dependent on the NES of NEP. Surprisingly, adaptive mutations have been identified within NEP which can compensate for the lack of PB2 E627K mutation, the hallmark of mammalian-adapted viral polymerase (174), strengthening the regulatory role of NEP during influenza virus genome replication. NEP has been proposed to serve as a switch from viral transcription to viral replication by promoting the generation of 22-27 nt-long small viral RNA (svRNA) to promote genome replication in an allosteric manner (83, 175, 177). The most recent studies have shown that the last amino acid of NEP (residue 121) is important for the regulatory function of NEP and the hydrophobicity of this residue is essential for viral fitness (172, 173). However, the molecular mechanism underlying the polymerase regulatory function of NEP is still elusive.

1.2.2 Viral transcription

The transcription process of the influenza virus has been well elucidated by recent structural studies (134, 138, 178, 179) (**Fig. 1.10)**. Viral transcription is a primer-dependent process which requires the generation of 5' N7-methyl guanosine (m7G) capped primer for transcription initiation (180). The influenza virus cannot synthesize the 5' capped primer by itself and must steal it from nascent host RNAs such as small nuclear RNAs (snRNAs), small nucleolar RNAs, and promoter-associated capped small RNAs (181, 182),

which is known as the cap-snatching process. In this process, the serine-5-phosphorylated C-terminal domain (CTD) of Pol II interacts with PA-C, the 627 and NLS domains of PB2 in the resident viral polymerase, bringing vRNPs in close proximity to host 5' capped RNAs (138, 178, 179). Binding of Pol II CTD stabilizes the cap-binding domain of PB2 and Endo domain of PA in the transcription-ready conformation. The 5'cap of the nascent host RNA is bound by the PB2 cap-binding domain and cleaved by the PA Endo domain at the position approximately 10-14 nt from the 5' cap. After cleavage of capped nascent RNAs, the 3' end of the capped primer is transferred into the polymerase active site where it base pairs with the 3' end of the vRNA template at the penultimate or third base (183, 184). The priming loop, a loop structure that protrudes from the thumb subdomain towards the polymerase active site (144), is expelled outside the polymerase active site and remains extruded during elongation (134). Elongation of the capped primer generates a nine base-pair nascent strand-template RNA duplex that is maintained within the active site until the separation and following exit of template and transcription product via their respective exit channels (134). The nascent transcription product exits through the product exit channel and is bound by host mRNA-binding proteins (185), while the 3' end of the template exits through the template exit channel and is guided to the so-called mode B 3' binding site (134, 145). The viral transcription termination occurs when the viral polymerase stutters and slips on a uridine stretch starting at position 17 (U17) from the 5' end of vRNA. U17 flips in and out of the active site +1 position, generating a poly (A) tail (134, 186).

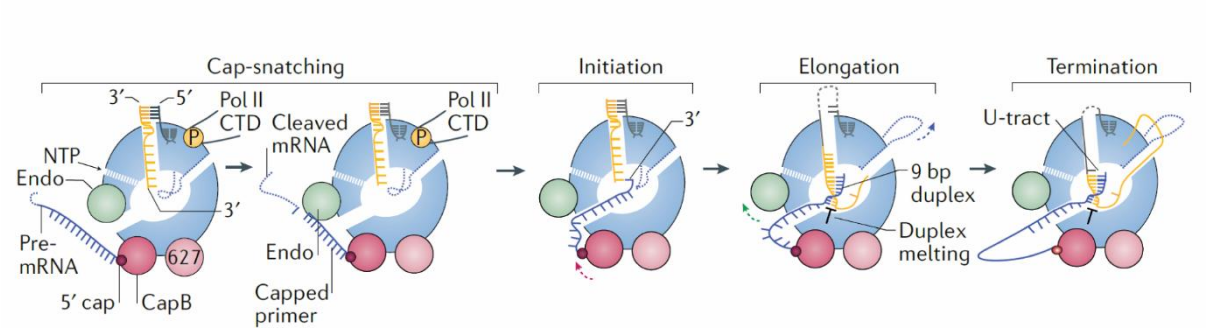

Fig. 1.10 Model for influenza A virus transcription.

The host capped pre-mRNA bound to the PB2 cap-binding domain (CapB) is cleaved by the PA endonuclease domain (PA-endo). The rotation of CapB allows the 3' end of the capped RNA primer to enter the polymerase active site through the product exit channel. The 3'end of the vRNA template inserts into the polymerase active site through the template entry channel. Transcription starts by the addition of NTP to the 3' end of the capped primer. During elongation, template and product are separated and exit via their own exit channels. Transcription is terminated when the viral polymerase stutters on a uridine stretch that leads to polyadenylation. This figure is adapted from (67).

1.2.3 Viral replication

Replication is a two-step, primer-independent process in which the incoming vRNPs synthesize cRNA that is subsequently used as a template for vRNA synthesis. A schematic diagram of viral replication process is depicted in **(Fig. 1. 11)**.

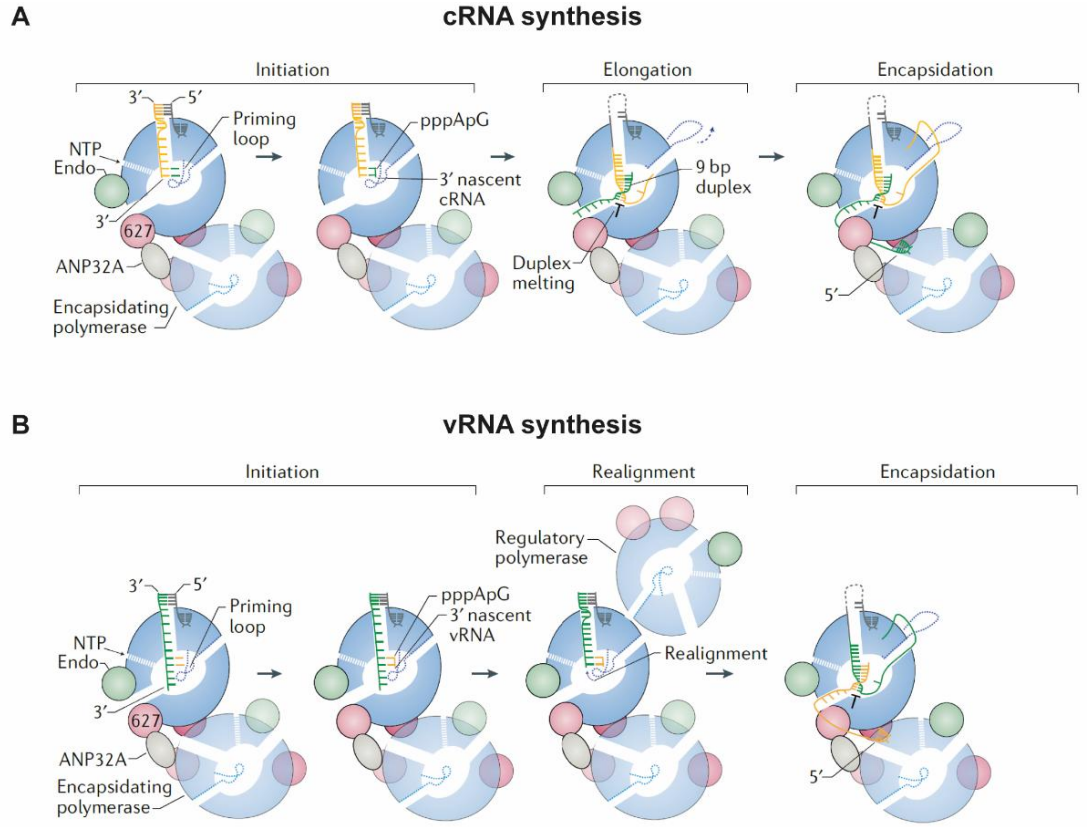

Fig. 1.11 Model for influenza A virus replication.

(A) Model for cRNA synthesis. The 3’ end of vRNA inserts into the polymerase activity site, and cRNA synthesis is initiated terminally. During elongation, template and product are separated and exit via their own exit channels. ANP32-mediated polymerase dimer ensures the co-replicative assembly of nascent cRNA into cRNP. (B) Model for vRNA synthesis. The 3’ end of the cRNA template inserts into the polymerase active site, and vRNA synthesis is initiated internally. In this step, a *trans*-activating polymerase is required. ANP32-mediated polymerase dimer is also needed to ensure the co-replicative assembly of nascent vRNA into vRNP. This figure is adapted from (67).

1.2.3.1 cRNA synthesis

The *de novo* (primer-independent) initiation of cRNA starts with the formation of pppApG dinucleotide opposite the residues U1 and C2 on the 3' end of vRNA, by a mechanism also known as terminal initiation (187). Priming loop is required for the cRNA synthesis initiation to stabilize the initiation complex, but not for the elongation step where the priming loop is extruded from the polymerase active to accommodate the extension of the nascent cRNA (144). The nascent cRNA is co-replicatively encapsidated by the newly synthesized RdRp (encapsidating polymerase) and NP to form the cRNPs, avoiding the degradation of cRNA (163). This process requires the formation of an asymmetrical polymerase dimer between the resident polymerase in vRNPs (replicating polymerase or replicase) and encapsidating polymerase, which is mediated by host factors called ANP32A or ANP32B proteins (188). The roles of ANP32 proteins during influenza virus replication will be reviewed in section 1.3. In addition to mediating dimer formation, ANP32 proteins possess a C-terminal low complexity acidic region (LCAR) that can recruit NP to the nascent RNA chain.

1.2.3.2 vRNA synthesis

The second step of viral replication is the synthesis of progeny vRNA. Unlike cRNA synthesis, the de novo initiation of vRNA involves internal initiation and realignment (187, 189). The vRNA synthesis is initiated at positions 4 and 5 of the 3' end of cRNA, resulting in the formation of pppApG dinucleotide which is realigned to the 3' end of cRNA through backtracking of the template (187, 189). This realignment process is facilitated by a conformational change in the priming loop which destabilizes the binding of the 3' cRNA (135, 144, 189). Structural analysis has suggested that this conformational change is induced by the dimerization of replicating polymerase and an additional regulatory

polymerase (135). In contrast to the asymmetric dimer mentioned above, this symmetric dimer formed between replicating and regulatory polymerase (transactivating polymerase) is required for vRNA synthesis from cRNA template, which aligns with previous findings from biochemical analysis that the binding of a second, regulatory polymerase is indispensable for vRNA synthesis (190, 191). The asymmetric dimer mediated by ANP32 is also required for vRNA synthesis to ensure the co-replicative assembly of nascent vRNPs (188, 192) .

1.3 The role ANP32 proteins in the influenza virus replication

ANP32 family proteins were identified in the 1990s (193-195) and were believed to have three members in mammalian species: ANP32A (also known as: PHAPI, pp32, I1PP2A, LANP, HPPCn, and Mapmodulin), ANP32B (also known as: SSP29, APRIL, and PAL31), and ANP32E (also known as: CPD1, LANP-L and PHAPIII) (196, 197). ANP32 proteins consisting of an N-terminal leucine-rich repeat (LRR) and a C-terminal low complexity acid region (LCAR) are multifunctional proteins. The cellular functions of ANP32 proteins include the regulation of transcription and chromatin architecture, activation of apoptosis pathways, and intracellular transport (196).

Prior to the discovery of the function of ANP32 proteins in influenza virus replication, the reported role of ANP32 proteins in virus replication mainly focused on their involvement in the CRM1-dependent nuclear export pathways. For instance, ANP32A and ANP32B have been reported to promote nuclear export of viral mRNA of human immunodeficiency virus (HIV) and foamy virus (198, 199). Additionally, ANP32B interacts with the M protein of Hendra virus, Nipah virus and other paramyxoviruses and thereby contributes to the nucleocytoplasmic trafficking of viral M proteins (199, 200).

1.3.1 The role of ANP32 protein in adaptation of the influenza A virus polymerase

1.3.1.1 Host restriction of the influenza A virus polymerase complex

The host restriction of the viral RdRp has long been recognized as one of the major barriers to the cross-species transmission of influenza A virus (10, 201, 202). A study published in 1977 has already reported that avian influenza virus cannot form plaques on mammalian cells due to the malfunction of its viral polymerase (203). In 1993, the PB2 E627K mutation, the hallmark of mammalian adaptation of the viral polymerase, was pinpointed (204). Ever since then, the molecular mechanism underlying host restriction of influenza A virus polymerase or RNPs has been extensively studied and several mechanisms have been postulated (65, 203, 205-208). Several studies have implied that the defect of avian influenza virus polymerase in human cells is in the vRNA synthesis step (174, 209). However, due to the independent nature of vRNA and cRNA synthesis, there is no direct evidence to prove this speculation. An increasing amount of evidence suggests that the incompatibility between the avian influenza virus replication machinery and host factors within mammalian cells leads to the restricted polymerase activity (205, 210). Until the identification of the role of the acidic leucine-rich nuclear phosphoprotein 32 kDa (ANP32) family in influenza virus replication, the molecular details of host restriction were not understood (211-213).

1.3.1.2 Species-specific differences in ANP32 proteins underlying host restriction of the influenza A virus polymerase complex

The ANP32 protein has been identified as a critical determinant of the influenza A virus species specificity (213). The chicken ANP32A (chANP32A) protein harbours an additional 33 amino acids (residue 176-208) insertion between its LRR and LCAR domains compared to human ANP32A (huANP32A) or human ANP32B (huANP32B). The

chimeric huANP32 protein with insertion of these 33 amino acids can support avian influenza polymerase (PB2 627E) in human cells (188, 213) **(Fig. 1.12)**. Notably, the interaction of viral RdRp with ANP32 proteins is not dependent on the signature of PB2 627 residues, as chANP32 exhibits stronger interactions to both human (PB 627K) and avian virus (PB2 627E) polymerases than its human cognates (214). A SUMO interaction motif-like sequence (SIM) identified in the unique avian insertion contributes to the stronger interaction between chANP32A with viral RdRp (214). The natural splicing variant of chANP32A with 29 amino acids insertion (chANP32$_{29}$) lacking the SIM still supports avian influenza polymerase, albeit to a lesser extent (215). Interestingly, a more recent study has shown that RdRp with PB2 E627K strongly favours the use of mammalian ANP32B protein due to the different sequences in the LCAR region of ANP32A and ANP32B proteins (216). Serial passages of influenza A virus in huANP32A and huANP32B double-knockout cells lead to the acquisition of compensatory mutations that allow the virus to use ANP32E, an ANP32 protein which is unable to support the wild type viral polymerase (217).

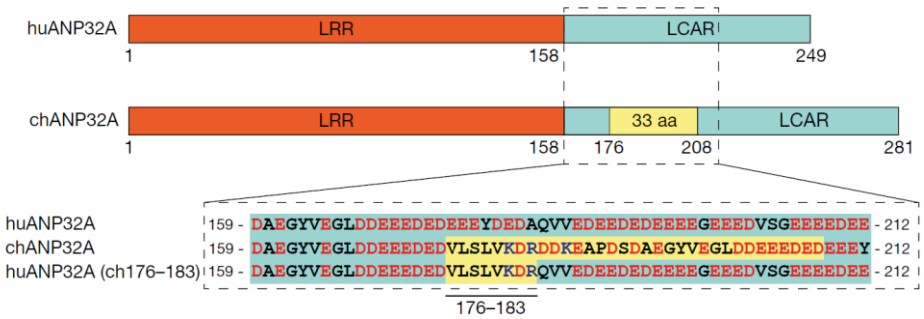

Fig. 1.12 Schematic of huANP32A and chANP32A.

Schematic of huANP32A, chANP32A, and a chimeric huANP32A in which residues 176–183 are replaced by those from chANP32A. The unique 33-amino-acid avian insertion (33 aa) is labelled in yellow. Acidic and basic amino acid residues are indicated in red and blue. This figure is adapted from (188).

1.3.2 ANP32 proteins mediate dimerization of influenza virus polymerases

Functionally, both vRNA and cRNA synthesis require ANP32-mediated polymerase dimerisation to ensure the co-replicative assembly of cRNPs and vRNPs (192). Recently, we also reported that ANP32 proteins have a second role during influenza virus replication, which is the recruitment of NP to nascent RNA products (161). Therefore, the ANP32-FluPol complex represents a replication platform for the genome of influenza virus. The recently resolved structure of ANP32 proteins in complex with the influenza C virus polymerase has revealed the molecular mechanism by which ANP32 proteins support influenza virus replication (188). ANP32 proteins bridge the asymmetric viral polymerase dimer of the encapsidating polymerase and replicating polymerase (reviewed in *1.2.3.1 cRNA synthesis*) via the PA-C domain, PB2 627 domain, NLS domain on the encapsidating polymerase and PB2-N, 627, linker domains of the replicating polymerase **(Fig. 1.13)**. The N-terminal LRR region of ANP32 mediates the formation of the asymmetric polymerase dimer. The N129 and D130 on ANP32A directly interact with the encapsidating polymerase, which accounts for the inability of chicken ANP32B harbouring I129 and N130 to support viral polymerase activity (218, 219). Although the C-terminal LCAR region of ANP32 is not fully resolved in the structure, the structural analysis has suggested that it contacts the PB2 627 domain of the replicating polymerase, agreeing with previous observations acquired using biochemical and NMR methods (220, 221). Particularly, the previously mentioned SIM sequence and its downstream region comprising a mixture of basic and acidic amino acid residues (176-VLSLVKDR-183) in chANP32A are respectively located next to positions equivalent to PB2 627 residue and 591 residue in influenza A virus where the two well-known adaptive mutations are (118, 188). Interaction of this region of chANP32A with the PB2 627 domain might be able to stabilize the asymmetric dimer. In contrast, this region in huANP32A/B is entirely acidic. The

difference of this region between chANP32A and huANP32A/B explains why chANP32A can support both avian virus polymerase (PB2 627K) and human virus polymerase (PB2 627K).

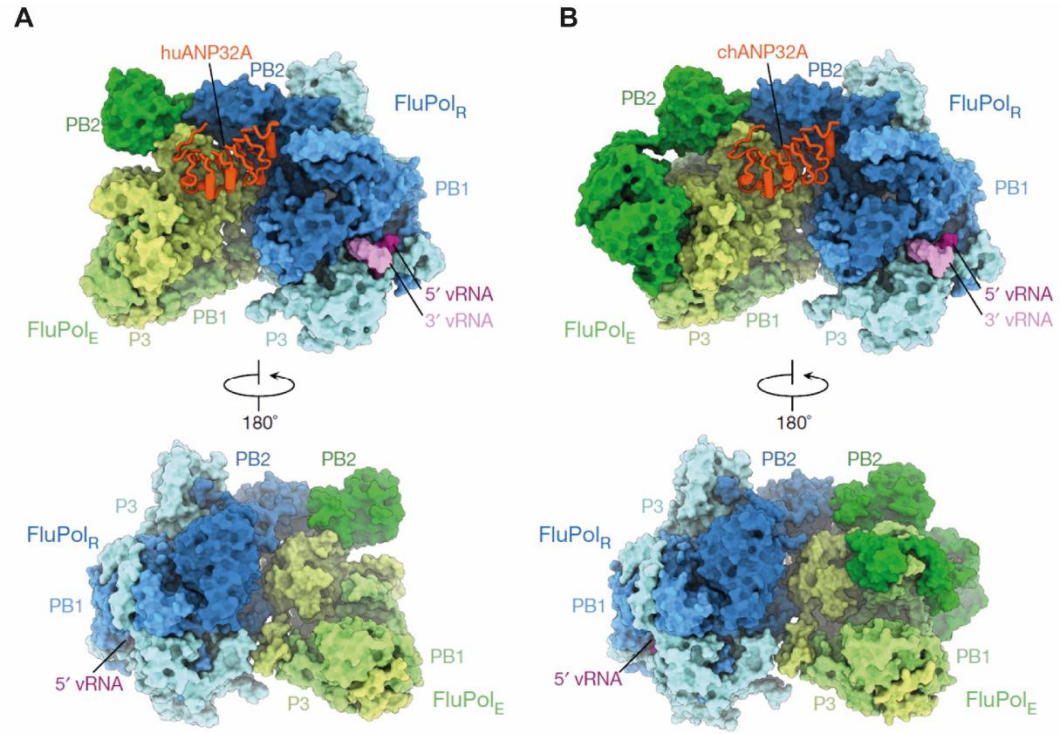

Fig. 1.12 Structures of dimers of FluPol heterotrimers with huANP32A and chANP32A.

Cryo-EM structures of dimers of FluPolC heterotrimers with huANP32A (A) or chANP32A (B). The FluPol serves as replicase is desigated as the FluPol replicase ($FluPol_R$). The FluPol molecule that encapsidated the nascent RNA products is designated as encapsidating FluPol ($FluPol_E$). This figure is adapted from (188).

1.4 Project objectives

Influenza A virus represents some of the major threats to public health and the next influenza pandemic is a certainty. However, the detailed mechanistic picture of influenza RNA replication is still unclear. The overarching goal of this DPhil project is to uncover the mechanisms by which key host and viral proteins regulate viral replication and transcription. I first functionally characterized the role of LCAR, a region that is not fully resolved in the structural analysis, in influenza virus genome replication (Chapter 3). Next, I explored the role of NP-C-terminal tail in influenza virus genome replication using a series of biochemical analyses (Chapter 4). To uncouple the two steps of replication process, I also set up an in vitro cRNP reconstitution system that can only measure the authentic vRNA synthesis without interference from ongoing replication (Chapter 5). Finally, I investigated the mechanism of NEP regulating viral replication and transcription through a structure-guided study (Chapter 6).

CHAPTER 2

MATERIALS AND METHODS

2.1 Molecular cloning

2.1.1 Oligonucleotide sequences

chANP32A 1-188_fwd	ATTTTGGCAAAGAATTGTGCGGC
chANP32A 1-188_rev	ACCACGCGGCCATGGTGGCCTCGAGTCAAGCTTCTTTGTCATCTCTGTCCTTC
chANP32A 1-208_rev	ACCACGCGGCCATGGTGGCCTCGAGTCAGTCCTCATCTTCCTCTTCATCATCCA
chANP32A 1-220_rev	ACCACGCGGCCATGGTGGCCTCGAGTCATTCCACCACCTGGGCATCG
chANP32A 1-235_rev	ACCACGCGGCCATGGTGGCCTCGAGTCAATCTTCCTCTTCCCCCTCTTCTT
chANP32A 1-250_rev	ACCACGCGGCCATGGTGGCCTCGAGTCAGCCGTCGTTGTAGCCTTCC
chANP32A 1-149_rev	ACCACGCGGCCATGGTGGCCTCGAGTCAGTCGTAGCCGTCCAGGTAG
huANP32A 1-235_rev	ACCACGCGGCCATGGTGGCCTCGAGTTACTGGCCTCTCTCTTCC
huANP32A 1-220_rev	ACCACGCGGCCATGGTGGCCTCGAGTTAGTCCACCTCGCCGTC
huANP32A 1-208_rev	ACCACGCGGCCATGGTGGCCTCGAGTTATTCTTCCTCCCCGGAC
huANP32A 1-188_rev	ACCACGCGGCCATGGTGGCCTCGAGTTAATCTTCCACCACCTGG
huANP32A 1-149_rev	ACCACGCGGCCATGGTGGCCTCGAGTTAGTCGTAGCCGTCCAG
huANP32B 1-235_rev	ACCACGCGGCCATGGTGGCCTCGAGTCACCCACCTTCTTCCTC
huANP32B 1-220_rev	ACCACGCGGCCATGGTGGCCTCGAGTCACTCGTCCAGGCCAAAC
huANP32B 1-208_rev	ACCACGCGGCCATGGTGGCCTCGAGTCACTCATCATCGTCTTC
huANP32B 1-188_rev	ACCACGCGGCCATGGTGGCCTCGAGTCACTCCTCCTCTCCATC
huANP32B 1-149_rev	ACCACGCGGCCATGGTGGCCTCGAGTCAATCGTATCCATCGAG
GST(huA, pCAGGAS)_fwd	ATTTTGGCAAAGAATTGTGCGGCCGCATGTCCCCTATACTAGGTTATTGG
GST(huA, pCAGGAS)_rev	CCATTTCCATGAATTCCGGGGATCCCAG

GST(NP, pcDNA)_fwd	CAGATATCCATCACACTGGCGGCCGCAT GTCCCCTATACTAGGTTATTGG
GST(NP, pcDNA)_rev	TGGTCGCCATGAATTCCGGGGATCCCAG
SLA-NP-fwd	TCTGGTGGGGGTGGGTCTGCGGCCGCCA TGGCGACCAAAGGCACC
SLA-NP-rev	AGGGCCCTCTAGATGCATGCTCGAGTTA ATTGTCGTACTCCTCTGCATTG
NP-SLA-fwd	TAAGCTTGGTACCGAGCTCGGATCCACC ATGGCGACCAAAGGCACC
NP-SLA-rev	CCAGATCCACCTCCACCGGCGGCCGCATT GTCGTACTCCTCTGCATTG
SLA-NEP-fwd	TCTGGTGGGGGTGGGTCTGCGGCCGCCA TGGATCCAAACACTGTG
SLA-NEP-rev	AGGGCCCTCTAGATGCATGC*TCGAG*TTAA ATAAGCTGAAACGAGAAAG
NEP-SLA-fwd	TAAGCTTGGTACCGAGCTCG*GATCCACC*A TGGATCCAAACACTGTG
NEP-SLA-rev	CCAGATCCACCTCCACCGGC*GGCCGC*AA TAAGCTGAAACGAGAAAG
SLA-huANP32A-fwd	TCTGGTGGGGGTGGGTCTGCGGCCGCCA TGGAAATGGGCAGACGG
SLA-huANP32A-rev	AGGGCCCTCTAGATGCATGCTCGAGTTA GTCGTCATCCTC
huANP32A-SLA-fwd	TAAGCTTGGTACCGAGCTCG*GATCCACC*A TGGAAATGGGCAGACGG
huANP32A-SLA-rev	CCAGATCCACCTCCACCGGC*GGCCGC*GT CGTCATCCTCGCCCTC
NP-SLA 491-498 deleted	CCAGATCCACCTCCACCGGC*GGCCGC*TCC GAAGAAATAAGATCCTTCATTACTCATG
NP-SLA (D491A, E495A, D497A)	CCAGATCCACCTCCACCGGC*GGCCGC*ATT GGCGTAGGCCTCTGC
Luc1-NP (491-498 deleted)	AGGGCCCTCTAGATGCATGC*TCGAG*TTAT CCGAAGAAATAAGATCCTTCATTACTCAT G
Luc1-NP (D491A, E495A, D497A)	AGGGCCCTCTAGATGCATGC*TCGAG*TTAA TTGGCGTAGGCCTCTG
PolI-NP C-terminus del Fw	GTAATGAAGGATCTTATTTCTTCGGATAA AGAAAAATACCCTTGTTTCTACT
PolI-NP C-terminus del Rev	AGTAGAAACAAGGGTATTTTTCTTTATCC GAAGAAATAAGATCCTTCATTAC
PolI-NP (D491A, E495A, D497A) Fw	AGAAACAAGGGTATTTTTCTTTAATTGGC GTAGGCCTCTGCATTAGCTCCGAAGAAA TAAGATCCTTCATTAC

PolI-NP (D491A, E495A, D497A) Rev	GTAATGAAGGATCTTATTTCTTCGGAGCT AATGCAGAGGCCTACGCCAATTAAAGAA AAATACCCTTGTTTCT
NP D491A Fw	AATTGTCGTACTCCTCTGCATTAGCTCCG AAGAAATAAGATCCTTC
NP D491A Rev	GAAGGATCTTATTTCTTCGGAGCTAATGC AGAGGAGTACGACAATT
NP E495A Fw	GGTATTTTTCTTTAATTGTCGTAGGCCTCT GCATTGTCTCCGAAGAA
NP E495A Rev	TTCTTCGGAGACAATGCAGAGGCCTACG ACAATTAAAGAAAAATACC
NP D497A Fw	CAAGGGTATTTTTCTTTAATTGGCGTACT CCTCTGCATTGTCTC
NP D497A Rev	GAGACAATGCAGAGGAGTACGCCAATTA AAGAAAAATACCCTTG
SLA-huANP32B Fw	TCTGGTGGGGGTGGGTCTGCGGCCGCCA TGGATATGAAACGCAGG
SLA-huANP32B Rev	AGGGCCCTCTAGATGCATGC*TCGAG*TCAG TCATCCTCTCCCTC
huANP32B-SLA-Fw	TAAGCTTGGTACCGAGCTCG*GATCCACC*A TGGATATGAAACGCAGGATTC
huANP32B-SLA-Rev	CCAGATCCACCTCCACCGGC*GGCCGC*GT CATCCTCTCCCTCGT
SLA-chANP32A Fw	TCTGGTGGGGGTGGGTCTGC*GGCCGCC*A TGGACATGAAGAAGCGG
SLA-chANP32A Rev	AGGGCCCTCTAGATGCATGC*TCGAG*TCAG TCATCCTCGTCGCC
chANP32A-SLA-Fw	TAAGCTTGGTACCGAGCTCG*GATCCACC*A TGGACATGAAGAAGCGG
chANP32A-SLA-Rev	CCAGATCCACCTCCACCGGC*GGCCGC*GT CATCCTCGTCGCCTTC
NEP-R15A Fw	CCCCAACTGCATTTTTGACATGGCCATCA GTATGTCCTGAAAGCT
NEP-R15A Rev	AGCTTTCAGGACATACTGATGGCCATGTC AAAAATGCAGTTGGGG
NEP-R42A Fw	TACTGCTTCTCCAAGCGAATCCGCGTAGA GTTTCAGAGACTCGAA
NEP-R42A Rev	TTCGAGTCTCTGAAACTCTACGCGGATTC GCTTGGAGAAGCAGTA
NEP-Q96A Fw	AATAGTTGTAAGGCTTGCATAAATGTTAT GGCCTCAAAACTATTCTCTGTTATCTTCA GTC
NEP-Q96A Rev	GACTGAAGATAACAGAGAATAGTTTTGA GGCCATAACATTTATGCAAGCCTTACAAC TATT
NEP-Q101A Fw	CTCCACTTCAAGCAATAGTTGTAAGGCG GCCATAAATGTTATTTGCTCAAAACTATT

NEP-Q101A Rev	AATAGTTTTGAGCAAATAACATTTATGGC CGCCTTACAACTATTGCTTGAAGTGGAG
NEP-Quadruple mutation Fw	CCACTTCAAGCAATAGTTGTAAGGCGGC CATAAATGTTATGGCCTCAAAACTA
NEP-Quadruple mutation Rev	TAGTTTTGAGGCCATAACATTTATGGCCG CCTTACAACTATTGCTTGAAGTGG
pcDNA-PB1-L364I Fw	GGTATTTGAGTTCTAATTTTCATACTCTT GCTCTCAAACATGTACC
pcDNA-PB1-L364I Rev	GGTACATGTTTGAGAGCAAGAGTATGAA AATTAGAACTCAAATACC
pHW2000-PB1-I364L-Fw	GGTATTTGAGTTCTAAGTTTCATACTCTT GCTCTCAAACATGTACC
pHW2000-PB1-I364L-Rev	GGTACATGTTTGAGAGCAAGAGTATGAA ACTTAGAACTCAAATACC
anchored oligo(dT)20	TTTTTTTTTTTTTTTTTTTTDVDN
NP47+	AAGCAGGGTAGACTAGTAAAGAAA
NP 47-	TTACTAGTCTACCCTGCTTTTGC
NA 1280	TGGACTAGTGGGAGCATCAT
NA160	TCCAGTATGGTTTTGATTTCCG
5S-100	TCCCAGGCGGTCTCCCATCC
NP_A_NT60_f	GGATCCATGGCTTCCCAGGGTAC
NP_A_NT60_r	GAATTCTTAGTTGTCGTATTCCTCAGC
NP_A_NT60_R74A_R75A_f	TTCTTCCAGGTACTTGTTAGCAGCCTCGT CGAAAGCGGACAGC
NP_A_NT60_R74A_R75A_r	GCTGTCCGCTTTCGACGAGGCTGCTAACA AGTACCTGGAAGAA
NP_A_NT60_R174A_R175A_f	CGCCAGCAGCACCAGAAGCAGCGGGCAG GGTGGAACCCT
NP_A_NT60_R174A_R175A_r	AGGGTTCCACCCTGCCCGCTGCTTCTGGT GCTGCTGGCG
NP_A_NT60_D402-428_f	CAACCAGCAAAGGGCTTTCACCGGCAAC ACCG
NP_A_NT60_D402-428_r	CGGTGTTGCCGGTGAAAGCCCTTTGCTGG TTG
NP_NT60_R150_152_156A_f	CACCACCTACCAGGCTACCGCTGCTCTCG TGGCTACCGGCATGGAC
NP_NT60_R150_152_156A_r	GTCCATGCCGGTAGCCACGAGAGCAGCG GTAGCCTGGTAGGTGGTG
NP_NT60_R162A_f	CGGCATGGACCCCGCTATGTGCTCCCTG
NP_NT60_R162A_r	CAGGGAGCACATAGCGGGGTCCATGCCG
NP_NT60_D491-498_f	GATCTTACTTCTTCGGCTAAGAATTCCCG GGTCG
NP_NT60_D491-498_r	CGACCCGGGAATTCTTAGCCGAAGAAGT AAGATC
huA_pGEX-pGEX-6p1_f	CCAGGGGCCCCTGGGATCCCCGGAATTC ATGGAAATGGGCAGACGG
huA_pGEX-pGEX-6p1_r	GTCAGTCACGATGCGGCCGCTCGAGTTA GTCGTCATCCTCGCC

huB_pGEX-6p1_f	CCAGGGGCCCCTGGGATCCCCGGAATTC ATGGATATGAAACGCAGG
huB_pGEX-6p1_r	GTCAGTCACGATGCGGCCGCTCGAGTCA GTCATCCTCTCCCTC
chA_pGEX-6p1_f	CCAGGGGCCCCTGGGATCCCCGGAATTC ATGGACATGAAGAAGCGG
chA_pGEX-6p1_r	GTCAGTCACGATGCGGCCGCTCGAGTCA GTCATCCTCGTCGCC
huA_pGEX-6p1_r 1-188	AGTCAGTCACGATGCGGCCGTCAATCTTC CACCACCTG
huB_pGEX-6p1_r 1-188	AGTCAGTCACGATGCGGCCGTCACTCCTC CTCTCCATC
chA_pGEX-6p1_r 1-188	AGTCAGTCACGATGCGGCCGTCAAGCTT CTTTGTCATCTC
chA_pGEX-6p1_r 1-208	AGTCAGTCACGATGCGGCCGTCAGTCCTC ATCTTCCTC
chA_pGEX-6p1_r 1-220	AGTCAGTCACGATGCGGCCGTCATTCCAC CACCTGGGC
chA_pGEX-6p1_r 1-235	AGTCAGTCACGATGCGGCCGTCAATCTTC CTCTTCCCC
chA_pGEX-6p1_r 1-250	AGTCAGTCACGATGCGGCCGGCCGTCGT TGTAGCCTTC
chA_189-220_f	AATTCCCCGACAGCGACGCCGAAGGATA TGTGGAAGGACTGGATGATGAAGAGGAA GATGAGGACGAAGAGGAATACGACGAC GATGCCCAGGTGGTGGAAGATC
chA_189-220_r	TCGAGATCTTCCACCACCTGGGCATCGTC GTCGTATTCCTCTTCGTCCTCATCTTCCTC TTCATCATCCAGTCCTTCCACATATCCTT CGGCGTCGCTGTCGGGG
huA_1-149_r	GTCAGTCACGATGCGGCCGCTCGAGTTA GTCGTAGCCGTCCAG
huA_1-158_r	GTCAGTCACGATGCGGCCGCTCGAGTTA AGAATCAGGGGCCTC
huB_1-149_r	GTCAGTCACGATGCGGCCGCTCGAGTTA ATCGTATCCATCGAGATAAG
huB_1-158_r	GTCAGTCACGATGCGGCCGCTCGAGTTA GGAATCAGGGGCCTC
chA_1-149_r	GTCAGTCACGATGCGGCCGCTCGAGTTA GTCGTAGCCGTCCAG
chA_1-158_r	GTCAGTCACGATGCGGCCGCTCGAGTTA AGAATCAGGGGCCTC
WSN_PB2_K627E_F	GCTGCTGCTCCTCCTGAGCAGTCCGGC
WSN_PB2_K627E_R	GCCGGACTGCTCAGGAGGAGCAGCAGC

2.1.2 Plasmids

2.1.2.1 Mammalian expression plasmids for viral and host proteins

Mammalian expressing plasmids	Notes
pCAGGS pcDNA	Empty mammalian expression vector
pcDNA-WSN-PB2 pcDNA-WSN-PB1 pcDNA-WSN-PA pcDNA-WSN-NP pcDNA-WSN-PB2 (627E) pcDNA-WSN-PB1a pcDNA-WSN-PB1 (I364L) pcDNA-WNS-GTS-NP pcDNA-WSN-NP (D491) pcDNA-WSN-NP (E495A) pcDNA-WSN-NP (D497A) pcDNA-WSN-NP (D491, E495A, D497A) pcDNA-WSN-NP (Δ 491-498)	Plasmids expressing viral polymerase and NP
pcDNA-NP-G1 (4)	RNA binding defective mutant NP
pcDNA-WSN-NEP pcDNA-WSN-NEP (R15A) pcDNA-WSN-NEP (R42A) pcDNA-WSN-NEP (Q96A) pcDNA-WSN-NEP (Q101A) pcDNA-WSN-NEP (4A, R15A, R42A, Q96A,Q101A)	NEP expressing plasmids
pGAGGS-GST-huANP32A pGAGGS-GST-huANP32B pGAGGS-huANP32A pGAGGS-huANP32B pGAGGS-chANP32A	ANP32 proteins expressing plasmids
pGAGGS-huANP32A 1-149 pGAGGS-huANP32A 1-188 pGAGGS-huANP32A 1-208 pGAGGS-huANP32A 1-220 pGAGGS-huANP32A 1-235	huANP32A proteins expressing plasmids

Mammalian expressing plasmids	Notes
pGAGGS-huANP32B1-149 pGAGGS-huANP32B 1-188 pGAGGS-huANP32B 1-208 pGAGGS-huANP32B 1-220 pGAGGS-huANP32B 1-235	huANP32B proteins expressing plasmids
pGAGGS-chANP32A 1-149 pGAGGS-chANP32A 1-188 pGAGGS-chANP32A 1-208 pGAGGS-chANP32A 1-220 pGAGGS-chANP32A 1-235	chANP32A proteins expressing plasmids
pcDNA-Mouse Pol II-CTD	Mouse Pol II-CTD expressing plasmid
pcDNA-M1	M1 expressing plasmid
pcDNA-CRM1	CRM1 expressing plasmid
pcDNA-WSN-PB2 (Δ55-679) pcDNA-WSN-PB2 (Δ111-679) pcDNA-WSN-PB2 (Δ154-679) pcDNA-WSN-PB2 (Δ213-679) pcDNA-WSN-PB2 (Δ248-679) pcDNA-WSN-PB2 (Δ535-667) pcDNA-WSN-PB2 (Δ248-759) pcDNA-WSN-PB2 (Δ680-759) pcDNA-WSN-PB2 (Δ739-759) pcDNA-WSN-PB2 (627-629AAA)	Plasmids expressing truncated PB2 proteins
pcDNA-PP7-Strep	Plasmids expressing PP7 coat protein

2.1.2.2 Plasmids for split-luciferase assays

Split-luciferase assay plasmids	Notes
pcDNA-Luc1 pcDNA-Luc2	Half of the *Gaussia* Luciferase
pcDNA-Luc1-PB2 pcDNA-PB2-Luc1 pcDNA-Luc2-PB2 pcDNA-PB2-Luc2	Split luciferase tagged PB2
pcDNA-Luc1-PB1 pcDNA-PB1-Luc1 pcDNA-Luc2-PB1 pcDNA-PB1-Luc2	Split luciferase tagged PB1
pcDNA-Luc1-PA pcDNA-PA-Luc1 pcDNA-Luc2-PA pcDNA-PA-Luc2	Split luciferase tagged PA
pcDNA-Luc1-NP pcDNA-NP-Luc1 pcDNA-Luc2-NP pcDNA-NP-Luc2 pcDNA-NP(D491, E495A, D497A)-Luc1 pcDNA-NP (Δ 491-498)-Luc1	Split luciferase tagged NP
pcDNA-Luc1-NEP pcDNA-NEP-Luc1 pcDNA-Luc2-NEP pcDNA-NEP-Luc2 pcDNA-NEP (R15A)-Luc1 pcDNA-NEP (R42A)-Luc1 pcDNA-NEP (Q96A)-Luc1 pcDNA-NEP (Q101A)-Luc1 pcDNA-NEP (4A)-Luc1	Split luciferase tagged NEP

Split-luciferase assay plasmids	Notes
pcDNA-Luc1-huANP32A pcDNA-huANP32A-Luc1 pcDNA-Luc2-huANP32A pcDNA-huANP32A-Luc2	Split luciferase tagged huANP32A
pcDNA-Luc1-huANP32B pcDNA-huANP32B-Luc1 pcDNA-Luc2-huANP32B pcDNA-huANP32B-Luc2	Split luciferase tagged huANP32B
pcDNA-Luc1-chANP32A pcDNA-chANP32-Luc1 pcDNA-Luc2-chANP32A pcDNA-chANP32A-Luc2	Split luciferase tagged chANP32A

2.1.2.3 Plasmids for reverse genetics

Plasmids used for reverse genetics	Notes
pHW2000-WSN-PB2 pHW2000-WSN-PB1 pHW2000-WSN-PA pHW2000-WSN-NP pHW2000-WSN-HA pHW2000-WSN-NA pHW2000-WSN-NP pHW2000-WSN-M pHW2000-WSN-NS	Plasmids used for reverse genetics of A/33/WSN (H1N1) virus
pPOLI-WSN-vRNA (NA) pPOLI-WSN-cRNA (NA)	Expression of vRNA or cRNA of NA segment
pPol-NP-47	Expression of 47-nt long vRNA like template
pHW2000-WSN-NP-(D491A) pHW2000-WSN-NP-(E495A) pHW2000-WSN-NP-(D497A)	Plasmids used for rescuing NP mutant viruses
pHW2000-WSN-PB1-(I364L)	Plasmids used for rescuing PB1 mutant virus
pPolI-vNA-PP7 pPolI-cNA-PP7	Plasmids used for rescuing PP7 tagged viruses

2.1.2.3 Plasmids for expressing recombinant proteins

Plasmids used for expressing recombinant proteins	**Notes**
pGEX-6p1-GST-chANP32A pGEX-6p1-GST-chANP32A 1-188 pGEX-6p1-GST-chANP32A 1-208 pGEX-6p1-GST-chANP32A 1-220 pGEX-6p1-GST-chANP32A 1-235 pGEX-6p1-GST-chANP32A 189-220 pGEX-6p1-GST-huANP32A pGEX-6p1-GST-huANP32A 1-188 pGEX-6p1-GST-huANP32B pGEX-6p1-GST-huANP32B 1-188	Recombinant ANP32 proteins
pGEX-6p1-GST-NP	
pGEX-6p1-NP R416A	
pGEX-6p1-NP G1	G1 (R74A/R75A/R174A/R175A)
pGEX-6p1-NP G2	G2 (R150A/R152A/R156A/R162A)
pGEX-6p1-NP ΔT	ΔT (residues 402–428 of the tail loop deleted)
pGEX-6p1-NP ΔC	ΔC (residues 491–498 of the C-terminal tail deleted)
pGEX-6p1-NP R416A/G1 pGEX-6p1-NP G1/ΔT pGEX-6p1-NP G1/ΔT/ΔC pGEX-6p1-NP G1/G2 pGEX-6p1-NP G1/G2/ΔT/ΔC	
pFL-NT60 pFL-NT60-PB2-627E pFL-NT60-PB1a pFL-NT60-PB2-627E-PB1	Recombinant FluPol of A/NT/60/1968 (H3N2)

2.1.3 Site-directed mutagenesis

Site-directed mutagenesis PCR was carried out using Pfu Turbo DNA Polymerase (Agilent) in 50 µl reaction mixtures containing: 1.5 µl DMSO (100%), 1 µl dNTPs (10 mM), 5 µl buffer (10 ×), 1 µl Pfu Tubo DNA polymerase, 1 µl plasmid template (100 ng/µl), 1 µl Forward Primers (10 µM), 1 µl Reverse Primers (10 µM), 38.5 µl H_2O. Thermocycling conditions were as follows: 95 °C 3 mins; 95 °C 30 s, 50°C 30s, 68°C (2 min/kb), 19 cycles; 68°C 5 mins. Reactions were treated with 1µl DpnI (NEB) at 37°C for 1 hour, then transformed into DH5α *E. coli* and spread on LB agar plates supplemented with 100 µg/mL ampicillin.

2.1.4 Gibson assembly

PCR primers were designed using NEBuilder Assembly Tool. PCR was carried out with Q5® High-Fidelity DNA Polymerase according to the manufacturer′s instructions. Reaction products were separated by 1% agarose gel electrophoresis pre-stained with SYBR Safe (Invitrogen), and target DNA fragments were excised and purified using the QIAquick Gel Extraction Kit (Qiagen) according to the manufacturer′s instructions. Gibson assembly was performed using Gibson Assembly® Master Mix – Assembly (E2611) as per manufacturer′s instructions, and reaction products were transformed into DH5α *E. coli* and subsequently spread on LB agar plates supplemented with 100 µg/mL ampicillin.

2.1.5 Transformation and plasmid preparation

5 µl of Gibson assembly reaction mixture was added to 50 µl of competent DH5α *E. coli* cells. The mixture of plasmid and competent cells was incubated on ice for 5 min and then heat shocked at 42°C for 90 s followed by another incubation on ice for 10 min. The

transformation mixture was subsequently mixed with 200 µl of LB and was incubated for recovery at 37°C for at least 30 mins. The competent cells were evenly spread on LB agar plates supplemented with 100 µg/mL ampicillin for overnight incubation at 37 °C incubator. Single colony was picked and inoculated into LB medium supplemented with 100µg/mL ampicillin for shaking incubation at 37 °C, 180rpm overnight. Plasmid DNA was prepared using Plasmid Maxi Kit (Qiagen) (25mL cultures) as per the manufacturer′s instructions. Plasmids were validated by Sanger sequencing (Source Bioscience).

2.2 Cells

All the mammalian cell cultures were obtained from cell bank of Sir William Dunn School of Pathology at the University of Oxford, except where stated otherwise by reference or acknowledgment. 293T, 293T-DKO, MDBK, MDCK cells were maintained in humified incubator at 37 °C and 5% CO_2. FreeStyle 293 expression system (293-F) cells were maintained on orbital shaker at in humified incubator at 37 °C and 8% CO_2.

Human Embryonic Kidney 293T (293T) were maintained in Dulbecco′s Modified Eagle Medium (DMEM) supplemented with 10% Fetal Calf Serum (FCS; Sigma-Aldrich). huANP32A and huANP32B double-knockout human Embryonic Kidney 293T (293T-DKO) cells were kind gift from Dr. Xiaojun Wang'a Lab (212). 293T-DKO cells were also maintained in DMEM with 10% FCS. Madin-Darby Bovine Kidney (MDBK) cells and Madin-Darby Canine Kidney (MBCK) cells were cultured in minimal essential medium (MEM, Sigma) supplemented with 10% FCS and 1x L-glutamine (200mM) (Gibco). 293-F cells were maintained in FreeStyle 293 Expression Medium (Gibco).

2.3 Viruses

2.3.1 Reverse genetics of WSN virus and its mutant viruses

Wildtype A/WSN/33 (H1N1) virus and its mutant viruses were rescued using the eight-plasmid reverse genetics system as previously described. Briefly, co-culture of 293T cells and MDCK cells were transfected with 500 ng of each of the eight bidirectional plasmids (pHW200-WSN) using Lipofectamine 2000 (Invitrogen) as per manufacture's protocol. 24 hpt, the cell culture medium (10% FCS) was replaced with virus growth medium (MEM with 0.5% FCS and 2 mM L-glutamine). The transfected cells were incubated for another 36 h and the supernatant was harvested for virus titration.

2.3.2 Virus infection or propagation

For virus infection, 60-70% confluent MDCKs cells were prepared prior to infection. Cell monolayers were rinsed DPBS twice and subsequently infected with virus at an MOI of 0.001 (WT virus) or 0.01 (WSN PB2-627E). Cell monolayers were incubated with virus inoculum at 37 °C for an hour to allow full absorption. The virus inoculum was then replaced with virus growth medium. The infected cells were incubated at 37 °C and 5% CO_2 for about 48 h. Supernatants were harvested when approximately 80% cells show cytopathogenic effect. The cell debris was removed by centrifugation at 4000 rpm for 10 mins. Virus titre was determined by plaque assay.

2.3.3 Growth kinetics

The viral growth kinetics was determined by multiple-cycle growth curve. The 70% confluent MDCK cells were infected by the virus at an MOI of 0.001 and supernatants were collected at 12, 24, 36, 48, 60 hpi and were stored at -80 °C. Viral titre of each time point was titrated in MDBK cells by plaque assay.

2.3.4 Plaque assay

90% confluent MDBK cells in 6-well plate were infected with serially diluted (×10) viruses in a volume of approximately 400 µL. After 1h of adsorption at 37 °C, the inoculum was aspirated, and cell monolayers were covered with 3 ml of agarose overlay (2% agarose dissolved in PBS diluted 1:1 in virus growth medium). The plates were incubated at 37 °C and 5% CO_2 for 72 h. The agarose overlay was gently removed, and cells monolayers were stained with 0.2% Coomassie Brilliant Blue dye in 7.5% glacial acetic acid and 50% methanol.

2.4 Viral RNA analysis

2.4.1 RNP reconstitution assay

For vRNP reconstitution with full-length vRNA template, 90% confluent 293T cells were transfected with 500 ng of plasmids expressing PB2, PB1, and PA subunits, 2000 ng of NP expressing plasmids, together with 100 ng of pPolI-vNA expressing vRNA of NA. The transfection was carried out using Lipofectamine 2000 as per manufacturer's protocol. Total RNA was harvest at 24 hpt except where stated otherwise.

2.4.2 NP-independent replication assay

Similar to vRNP reconstitution assay, 293T cells were transfected plasmids expressing PB2, PB1, PA, together with pPol-NP-47 expressing a 47- nt long vRNA-like template using Lipofectamine 2000. Total RNA was harvest at 24 hpt except where stated otherwise.

2.4.3 cRNA stabilisation assay

293T cells in 6-well plate were transfected with plasmids expressing indicated viral polymerase subunits or NP. 24 hpt (post hours transfection), the transfected cells were

infected with WSN virus at an MOI of 10 in the presence of cycloheximide (100 μg/ml). Total RNA was harvested at 4 hpi.

2.4.4 *In vitro* vRNP/cRNP reconstitution assay

The fractions from glycerol gradients containing vRNP or cRNP were selected using the primer extension analysis and silver staining analysis. Depending on the protein and RNA levels, 1-5 μl of isolated RNPs were incubated with 1 mM ATP, 0.5 mM GTP, 0.5 mM CTP, 0.5 mM UTP, 5 mM $MgCl_2$, 1 mM DTT, and 2 U RNasin (Promega), 1000 ng of recombinant polymerase, 130 ng of recombinant ANP32B, and 800 ng of recombinant NP in 20 μl of reaction system at 30 °C for 4 h. The recombinant proteins were diluted to desired concentration using vRNP buffer (100 mM HEPES-NaOH (pH 8.0), 150 mM NaCl, 10% glycerol, 1 × PMSF). The reaction mixture was then subjected to RNA extraction using TRI reagent. The extracted RNA was analysed by primer extension analysis.

2.4.5 Radiolabelling of oligonucleotides

To radiolabel the oligonucleotide, 10 pmol oligonucleotides were incubated in a 10 μl reaction containing 1 × kinase buffer A, 1 μl γ^{32}P-ATP (3000 Ci/mmol; Perkin Elmer), 10 U T4 Polynucleotide Kinase (NEP) at 37 °C for 1 h. Excess radionucleotide was removed using QIAquick Nucleotide Removal Kit (Qiagen) as per the manufacturer's protocol. The radiolabelled oligonucleotides were eluted in 30-50 μl dd $H2_O$ and were stored at -20 °C.

2.4.6 RNA extraction and primer extension

Total RNA was extracted from cells or reaction using TRI Reagent (Sigma-Aldrich) as per the manufacturer's instructions. 2000 ng (RNA samples from cells) or 3.5 μl (RNA samples from *in vitro* reactions) of total RNA was annealed with 0.25 μl of radiolabelled

primers in a 5 µl reaction system by heating at 95 °C for 3 mins and cooling on ice for 2 min. NA 160 and NA 1280 primers were used to detect the replication or transcription products from NA segment; NP 47+ and NP 47- primers were used to detect the products from short vRNA-like template (NP-47); 5S 100 primer was used to detect the cellular 5S rRNA which is used as an internal loading control. The RNA was then incubated with 5 µl reverse transcription master mix containing 2× First Strand Buffer (Invitrogen), 20 mM dithiothreitol (DTT), 1 mM, 50U SuperScript III Reverse Transcriptase (Invitrogen), 1mM dNTP mix (Themo Scientific) at 50 °C for 1 h. The reaction was heat inactivated at 70 °C for 10 min and then mixed with 10 µl loading dye (80% formamide, 1mM EDTA, bromophenol blue, xylene cyanol) and heated to 95 °C for 3 mins. Reaction products were resolved by 6% (for full-length NA segment template) or 12% (for NP 47 template) denaturing PAGE containing 7 M urea in TBE buffer and visualised by autoradiography.

2.4.7 Denaturing polyacrylamide gel electrophoresis

Radiolabelled RNA or DNA was resolved by 6% or 12% PAGE (AccuGel 19:1 acrylamide: bis-acrylamide; Geneflow) in 7M urea and 1× TBE (90 mM Tris, 90 mM boric acid, and 2.5 mM EDTA). Gels were polymerised by adding 0.1% of ammonium persulfate (APS) and 0.01% of N,N,N,N′-Tetramethylethylenediamine (TEMED) to 0.1%. Gels were run at 1250 V in 1×TBE buffer using vertical sequencing gel apparatus. Radiolabelled DNA products were visualised by exposure to phosphorimaging screens that were scanned on a Fujifilm FLA-5000 scanner. ImageJ was used to quantify cDNAs and values were normalized to the cDNA derived from the 5S rRNA control. The values for the ‘vector’ control were subtracted from the sample values. Data were analysed using Prism 10 (GraphPad).

2.4.8 Next-generation sequencing

For the next-generation sequencing of the viral genome, viral RNA from virus supernatant was extracted using TRI reagent. Reverse transcription and PCR were performed using SuperScript III reverse transcriptase as previously described (222). The PCR products were purified using QIAquick PCR Purification Kit (Qiagen) and were quantified using Qubit 4 Fluorometer (Invitrogen). Next-generation sequencing was performed using xGen NGS DNA Library Preparation Kits (IDT) and sequencing data was analysed using the CLC Genomics Workbench 9 software (Qiagen).

2.5 Preparation of recombinant proteins and PP7 tagged ribonucleoproteins

2.5.1 Purification of recombinant influenza A virus

The purification of FluPol from A/NT/60/1968 (H3N2) was carried out as previously described (135). 1 L of Sf9 insect cells at a density of 2×10^6 cells/ml were infected with recombinant baculoviruses expressing influenza virus polymerases at an MOI of 0.5-1 for 72 h at 27 °C. Cells were harvested by centrifugation at 800 g for 20 min at 4°C and were subsequently resuspended in 30 ml of resuspension buffer (50 mM HEPES-NaOH pH 7.5, 500 mM NaCl, 10% (v/v) glycerol, 0.05% (w/v) OTG, 1 mM DTT, 100 µg/ml ribonuclease A (RNaseA, Qiagen) and 1× cOmplete EDTA-free protease inhibitor (Roche)) at room temperature for 30 min. Resuspended cells were subsequently sonicated on ice at 15 µm oscillation for 4 × 30 s. The lysed cells were centrifuged at 35000 g for 45 min at 4 °C, and the supernatant from the lysate was incubated with 2 ml of pre-washed IgG Sepharose 6 fast flow beads (GE Healthcare) by rotating at 4°C for 3 h. After binding, beads were washed three times in 10 ml wash buffer (50 mM HEPES-NaOH pH 7.5, 500 mM NaCl, 10% (v/v) glycerol). The bound proteins were eluted by cleavage with home-made TEV protease in 7 ml wash buffer supplemented with 0.5 mg home-made TEV protease and

1mM final concentration of DTT. The cleavage reaction was performed by rotation overnight at 4°C. The eluted protein sample was concentrated using an Amicon Ultra centrifugal filter (Merck Millipore, 100 kDa MWCO) by centrifuging at 4000 g to a final volume below 500 µl. The concentrated protein samples were centrifuged for 3 min at 13000 g at 4°C to remove the precipitation and further purified by SEC on a Superdex 200 increase 10/300 gel filtration column (Cytiva) in FluPol SEC buffer (25 mM HEPES-NaOH pH 7.5, 500 mM NaCl, 10% (v/v) glycerol) connected to an ÄKTA fast protein liquid chromatography system (GE Healthcare). The peak fractions containing FluPol were combined and concentrated to the desired concentration. The concentrated proteins were then aliquoted and snap-frozen in liquid nitrogen and stored at -80 °C for future use.

2.5.2 Purification of recombinant huANP32B and NP

The purification of recombinant GST-huANP32B and GST-NP were carried out as previously described (161). Bacterial colonies were grown in 2 L of bacterial cultures supplemented with ampicillin at 37 °C. When OD_{600} is approximately 0.6–0.9, the culture was induced by 1 mM isopropyl β-d-1-thiogalactopyranoside (IPTG) for overnight incubation at 18 °C. The bacterial culture was harvested by centrifugation at 4000 g for 15 min at 4°C. The bacterial cell pellet was resuspended in 25 ml of lysis buffer (25 mM HEPES-NaOH pH 7.5, 150 mM NaCl, 5% (v/v) glycerol, 2 mM DTT, 100 µg/ml ribonuclease A (RNaseA, Qiagen) and 1× cOmplete EDTA-free protease inhibitor (Roche)) supplemented with 1 mg/ml lysozyme (Sigma Aldrich) by rotating at room temperature for 30 min. Resuspended cells were subsequently sonicated on ice at 15 µm oscillation for 4 × 30 s. The lysed cells were centrifuged at 35000 g for 45 min at 4 °C, and the supernatant from the lysate was incubated with 2 ml of pre-washed Glutathione Sepharose 4B beads (GE Healthcare) by rotating at 4 °C for 3 h. For NP purification, beads were washed 4 times with high salt washing buffer (25 mM HEPES-NaOH pH 7.5, 1.5 M NaCl, 5% (v/v)

glycerol, 2 mM DTT) and 1 time with the lysis buffer. For ANP32 purification, beads were wash 4 times with washing buffer (25 mM HEPES-NaOH pH 7.5, 150 mM NaCl, 5% (v/v) glycerol, 2 mM DTT). Proteins were eluted by incubation with 7 ml wash buffer supplemented with 1 mM final concentration of DTT, 0.5 mg home-made HRV 3C protease with rotation overnight at 4°C. The eluted protein samples were further concentrated using an Amicon Ultra centrifugal filter (Merck Millipore, 30kDa MWCO) by centrifugation at 4000 g to a final volume below 500 µl. The concentrated protein samples were centrifuged for 3 min at 13000 g at 4°C to remove the precipitation and further purified by SEC on a Superdex 200 increase 10/300 gel filtration column (Cytiva) in SEC buffer (25 mM HEPES-NaOH pH 7.5, 150 mM NaCl, 10% (v/v) glycerol) connected to an ÄKTA fast protein liquid chromatography system (GE Healthcare). The peak fractions containing NP/huANP32B were combined and concentrated to the desired concentration. The concentrated proteins were then aliquoted and snap-frozen in liquid nitrogen and stored at -80 °C for future use.

2.5.3 Isolation of PP7 tagged ribonucleoproteins

The method to isolate influenza virus vRNP and cRNP from infected cells were

The method to isolate influenza virus cRNPs and vRNPs from infected cells was modified based on the previously described protocol (191). Briefly, the PP7 tagged WSN viruses were rescued using reverse genetics. For isolation of ribonucleoprotein complex (vRNP and cRNP), 50 ml of 293-F cells at density of 1.5-2 million/ml were transfected with pcDNA-PP7-Strep (4 µg/ml of cell) using Polyethylenimine “Max” (PEI Max, Thermo Fisher). 24 hpt, the cells were infected with the indicated PP7 tagged viruses at an MOI of 5-10 for isolation of vRNP or cRNP with different PB2 627 identities respectively. 24 hpi, cells were harvested for isolation of RNPs using Strep-Tactin sepharose beads (IBA). The cell pellet was lysed in lysis

buffer (200 mM NaCl, 50 mM pH=8 Tris-HCl, 30% glycerol, 1mM DTT, 1 mM $MgCl_2$, 0.1% OTG) supplemented with BioLock (IBA). The isolated RNPs (eluate) were further purified using glycerol gradient ultracentrifugation (1ml each, 70%, 50%, 40%, 33%) at 45K RPM for 4 h. Fractions (250 µl/each) were collected dropwise from the bottom of the tube and analysed by SDS-PAGE and silver staining.

2.5.4 SDS polyacrylamide gel electrophoresis and silver staining

Protein samples were mixed with an equal volume of SDS loading dye (125mM Tris-HCl pH 6.8, 4% SDS, 20% glycerol, 10% β-mercaptoethanol, bromophenol blue) and heated at 95°C for 3mins. Protein samples were resolved by electrophoresis using a discontinuous PAGE system (Bio-Rad). Home-made gels were prepared with a 3.2% 29:1 acrylamide: bis-acrylamide (AccuGel; Geneflow) stacking layer (125mM Tris-HCl pH6.8, 0.1% SDS) and 8-12% 29:1 acrylamide: bis-acrylamide separating layer (375mM Tris-HCl pH 8.8, 0.1% SDS), and were polymerized by the addition of 0.1% APS and 0.01% TEMED. Gels were run at 150V in 1x SDS running buffer (25mM Tris, 250mM glycine,0.1% SDS) and proteins were visualised by silver staining using SilverXpress (Invitrogen) as per the manufacturer′s instructions.

2.5.5 Western blotting

After SDS-PAGE, proteins were transferred from the gel onto nitrocellulose membrane (BioRad) in transfer buffer (25 mM Tris, 190 mM glycine, 20% methanol) at 10 V and room temperature using the Trans-Blot Turbo Transfer system (Bio-Rad). Membrane was then incubated with 5% skimmed milk in PBS for 1 h at room temperature followed by incubation with primary antibody diluted in PBS (0.1% Tween-20) at 4 °C for overnight. After incubation with primary antibody, membrane was washed 3 times with PBS and then

incubated with the secondary antibody conjugated to horseradish peroxidase (HRP) for 1 h at room temperature. After washing for three times, membrane was visualised by chemiluminescence using Amersham ECL Western blotting detection reagents (GE Healthcare) as per the manufacturer's instruction. The developed membrane was exposed to X-ray film (Super RX Fuji Medical X-Ray film, Kodak). huANP32A, huANP32B, chANP32A and their truncated versions were probed with rabbit anti-huANP32A, rabbit anti-huANP32B, and rabbit anti-chANP32A antibodies, NP was probed with rabbit anti-NP, Beta-actin was probed with a mouse anti-beta-actin antibody. Goat anti-rabbit and anti-mouse antibodies conjugated to horseradish peroxidase (HRP) were used as secondary antibodies.

Antibodies	Dilution factor
rabbit anti-huANP32A (ab155148, Abcam)	1:1500
rabbit anti-huANP32B (ab200836, Abcam)	1:1500
rabbit anti-chANP32A (AV40203, Sigma)	1:2000
rabbit anti-NP (GTX125989, GeneTex)	1:3000
mouse anti-beta-actin antibody (sc-47778, SCBT)	1:4000
Goat Anti-Rabbit IgG H&L (HRP) (ab6721)	1:10000
Goat Anti-Mouse IgG H&L (HRP) (ab6789)	1:10000

2.5.6 Analytical size exclusion chromatography

Analytical size exclusion chromatography (SEC) was performed on a Superdex 200 Increase 10/300 GL column (GE Healthcare) in 25 mM HEPES-NaOH, pH 7.5, 150 mM NaCl, 5% (v/v) glycerol at 4°C.

2.6 Protein-protein interactions analysis

2.6.1 GST pull-down assays

The GST pull-down assay used for detecting ANP32-NP interactions were previously described (161). All pull-down assays were performed in 25 mM HEPES-NaOH, pH 7.5, 150 mM NaCl, 5% (v/v) glycerol at 4°C. Approximately 200 μg bait (GST tag alone or GST tagged ANP32 proteins) was incubated with 50 μl Glutathione Sepharose (GE Healthcare) for 2–3 h. The beads were then washed once with the same buffer as specified above before being loaded with 100 μg analyte (wildtype or mutant NP). If indicated, a 1.5 × or 4.5 × molar excess (over NP) of a 29-nt RNA (5′-AGUAGAAACAAGGCCGUAUAUGAACAGA-3′, Dharmacon) was added together with NP. The beads were then incubated for another 3–5 h and washed 3 times with the same buffer as above. GST tag was cleaved overnight with 50 μg PreScission protease in the presence of 1 mM DTT to release un-tagged bait from the beads. Protein samples were analysed by SDS-PAGE. To analyse binding of huANP32A and NP from cell lysates to purified GST-NP and GST-huANP32A, respectively, 293T cells in six-well plates were transfected with 3 μg of pCAGGS-huANP32A or pcDNA-NP. Forty-eight hours post transfection cells were lysed for 1 h at 37°C in 500 μl of cell lysis buffer (50 mM HEPES–NaOH, pH 8.0, 150 mM NaCl, 25% (v/v) glycerol, 0.5% NP-40, 1 mM β-mercaptoethanol, 2 mM $MgCl_2$, 1 mM PMSF, 1× cOmplete EDTA-free protease inhibitor cocktail tablet (Roche)) in the presence or absence of 250 U of Benzonase (Sigma). 400 μl of cell lysate was applied to the beads with bait bound as described above. The beads were then incubated for another 3–5 h and washed 3 times before eluting overnight with 25 mM reduced glutathione. Samples were analysed by western blotting.

2.6.2 Split-luciferase assays

The *Gaussia* split-luciferase assay was modified based on a previously reported method (223). Briefly, 293T cells were transfected with 200 ng of each plasmid expressing the *Gaussia*-luciferase tagged proteins along with other proteins depending on the purpose of detection. After transfection, cells were incubated at 37 °C for 24 h and subsequently were harvested and subjected to split-luciferase assay using *Renilla* Luciferase Assay system (Promega) as per the manufacture's protocol.

CHAPTER 3

The C-terminal LCAR of host ANP32 proteins interacts with the influenza A virus nucleoprotein to promote the replication of the viral RNA genome

Data from this chapter were published in:

Wang, Fangzheng, et al. "The C-terminal LCAR of host ANP32 proteins interacts with the influenza A virus nucleoprotein to promote the replication of the viral RNA genome." *Nucleic acids research* 50.10 (2022): 5713-5725 (161).

3.1 Introduction

Influenza A virus is a negative-sense single-stranded RNA virus with the viral genome comprising eight segments of viral RNA (vRNA) packaged within viral ribonucleoprotein (vRNP) complexes. During virus replication, vRNA acts as a template for the synthesis of complementary RNA (cRNA) which, in turn, serves as a template for the synthesis of progeny vRNA (23, 67). These two-steps of replication both occur in the context of ribonucleoprotein, which is the most basic replication unit of influenza virus. vRNP is composed of heterotrimeric RNA-dependent RNA polymerase (RdRp) and vRNA that is coated by multiple copies of nucleoprotein (NP) (67, 224). NP has been recognized to act as an elongation factor for virus replication (159). Following viral transcription, newly synthesized NP molecules are recruited to nascent vRNA or cRNA chains to ensure the co-replicative assembly of vRNP or cRNP. Despite this recognized role of NP in viral replication, the precise steps in NP recruitment process by influenza virus are less well understood. Notably, unlike non-segmented negative-strand RNA viruses, influenza virus lacks the acidic phosphoprotein (P) that recruits nucleoprotein (N) to the nascent RNA products, leaving the molecular details of NP recruitment elusive (67, 225, 226).

The acidic nuclear phosphoprotein 32 (ANP32) family proteins have been particularly well studied for influenza virus genome replication following the identification of their role in mediating viral polymerase dimerization (188, 211, 224). ANP32 proteins consist of an N-terminal leucine-rich repeat (LRR) domain and a C-terminal low-complexity acidic region (LCAR). Avian ANP32A proteins possess an additional 33-amino acid insertion compared to their human counterparts, rendering avian virus polymerase active activity in human cells (224). In our structure of ANP32-FluPol complexes, we found that LRR (residues 1-158) bridges an asymmetric dimer of influenza virus polymerases, whereas the LCAR could not be fully resolved due to its flexibility (188). Another observation from that structure is that the region (approximately 20-30 amino acid residues) extending from LRR of chANP32A is located in a groove formed by polymerase dimer, suggesting the involvement of N-terminal 180-190 residues of chANP32A in polymerase dimerization (188). In contrast, the remaining part of chANP32A that exclusively belongs to LCAR could be solvent accessible. We hypothesized that the acidic flexible LCAR could function similarly to the P protein encoded by non-segmented negative-strand RNA viruses, which is the recruitment of basic NP molecules to nascent replication products (67, 225). In this chapter, we aim to identify the role of ANP32 LCAR in influenza virus genome replication through a series of functional studies.

3.2 Results

3.2.1 ANP32 LCAR is critical to viral RNA synthesis during influenza virus replication

To elucidate the role of ANP32 LCAR during influenza virus replication, I first constructed a series of truncated mutants of huANP32A, huANP32B, and chANP32A with varying lengths of truncation in their LCAR region based on available structures and tested their

ability to support virus replication in 293T-DKO (huANP32A and huANP32B double-knockout) cells (188, 212). All these ANP32 constructs were expressed equally well in 293T-DKO cells **(Fig. 3.1)**.

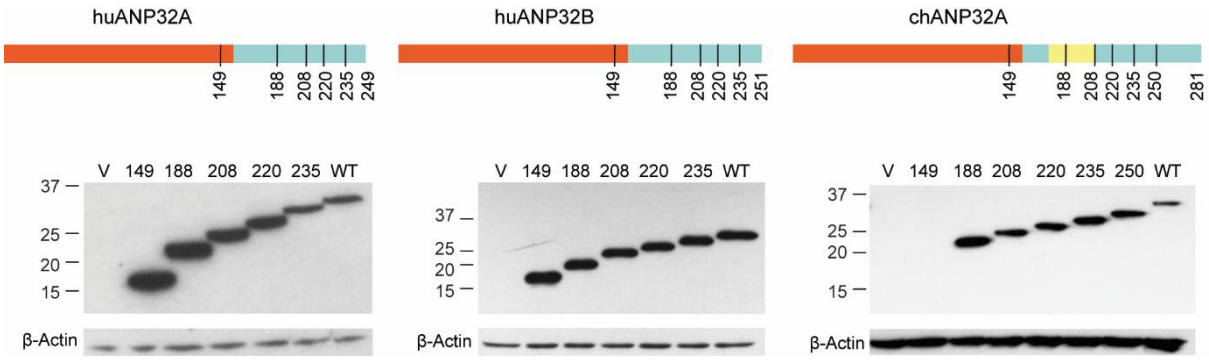

Fig. 3.1 Schematic representation and expression levels of huANP32A, huANP32B, and chANP32A with their corresponding truncated mutants.

ANP32 proteins consist of LRR (red) and LCAR (blue); chicken ANP32A protein possesses an additional 33-amino acid-insertion (yellow) in chANP32A. The number indicates the length of corresponding truncated ANP32 mutants. Expression levels of all these constructs were assessed by western blot in huANP32A and huANP32B double knockout 293T cells. Transfection of the empty vector (V) was set as the negative control. Molecular weight markers were labelled in kDa. Note that the antibody against chANP32A protein cannot recognize the 149 truncated mutant. The following antibodies were used: rabbit anti-huANP32A (ab155148, Abcam), rabbit anti-huANP32B (ab200836, Abcam), and rabbit anti-chANP32A (AV40203, Sigma) antibodies. Beta-actin was probed with a mouse anti-beta-actin antibody (sc-47778, SCBT). Goat anti-rabbit and anti-mouse antibodies conjugated to horseradish peroxidase (HRP) were used as secondary antibody.

293T-DKO cells were infected with influenza A/WSN/33 virus after pre-expression of truncated huANP32A or huANP32B and RNA accumulation at 8 hours post-infection was analysed by primer extension assay **(Fig. 3.2)**. Reconstitution of 293T-DKO cells with wildtype huANP32A led to robust viral genome replication, as demonstrated by the increased accumulation of mRNA, cRNA, and vRNA compared to the negative control (vector alone). Constructs with partial truncations in LCAR (1-209, 1-220, and 1-235) still retained the ability to support viral RNA synthesis, albeit with a slight decrease in RNA accumulation levels correlating with the reduced length of LCAR. Further truncation in LCAR (1-188) or complete removal of LCAR along with part of the LRR (1-149) profoundly dampened the RNA accumulation to a level similar to the negative control (vector). Similar trends were observed in 293T-DKO cells complemented with corresponding huANP32B constructs, with the difference of that huANP32B 1-188 construct can better support virus replication than its huANP32A counterpart. These results demonstrate that ANP32 LCAR plays a critical role in viral RNA synthesis during influenza virus replication, which is in line with other reports (192, 214, 220).

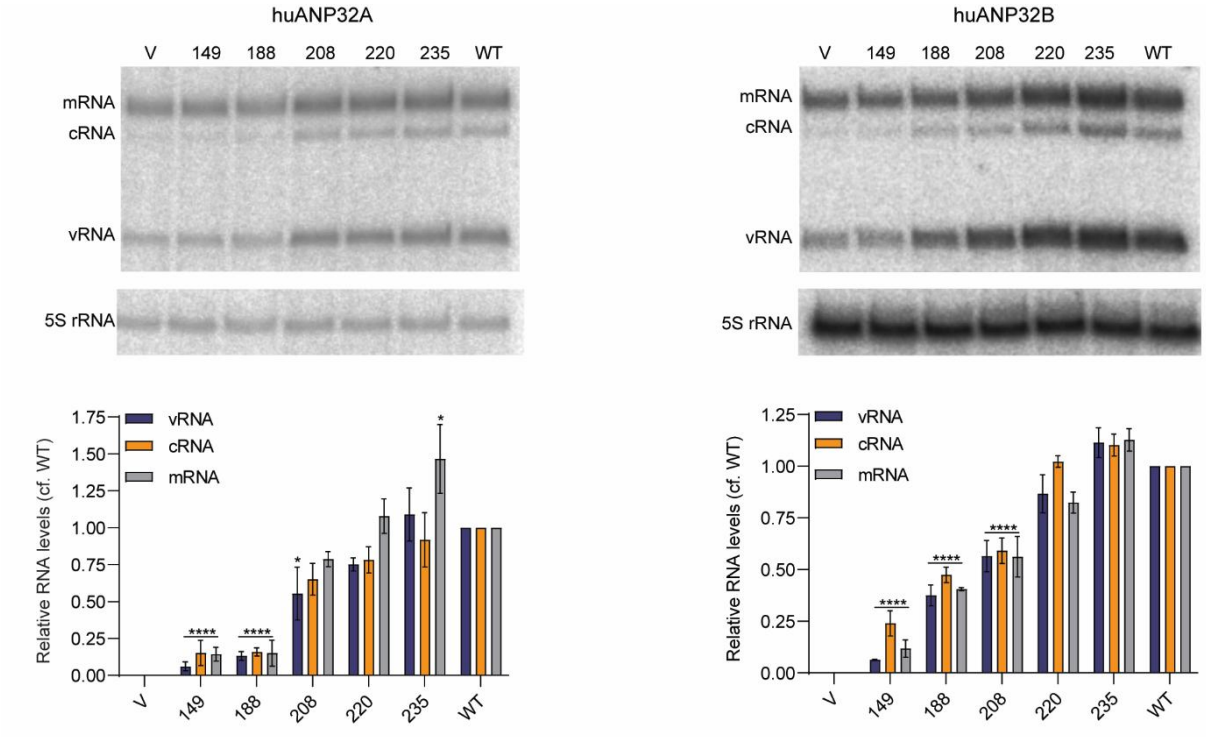

Fig. 3.2 Truncation of LCAR impairs viral RNA synthesis during infection.

293T-DKO cells were transfected with indicated plasmids expressing huANP32A or huANP32B and their truncated mutants. Twenty-four hours post-transfection, cells were subjected to infection with influenza A/WSN/33(H1N1) at an MOI of 5. Total RNA was isolated at 8 hours post-infection and was analysed by primer extension assay. The quantitative results show the mean signal intensity (with the activity of vector subtracted) relative to that of the infection in the presence of wild type ANP32 proteins from three independent experiments. Error bars represent the standard error of the mean (n=3). Significance was assessed using Ordinary Two-way ANOVA and asterisks indicate a significant difference as follows: *P<0.05; ****P<0.0001.

3.2.2 The LCAR of ANP32 proteins interacts directly with NP

ANP32 LCAR is acidic and could potentially facilitate the recruitment of basic NP to the nascent RNA chain during influenza virus genome replication. To test this hypothesis, we employed a GST pull-down assay using purified recombinant ANP32 proteins and NP from influenza A/NT/60/1968 (H3N2) virus (158) (Data from Dr. Haitian Fan). Since the purified NP can spontaneously oligomerize (124, 156), an R416A mutation was introduced to disrupt NP oligomerization and thereby maintain NP at monomeric status (157, 227). We found that monomeric NP can interact with N-terminally GST-tagged wildtype huANP32A, huANP32B, and chANP32A but not GST tag alone **(Fig. 3.3)**. In contrast, this ANP32-NP interaction was dampened when truncated ANP32 proteins (1-188), containing only the region that mediates influenza virus polymerase dimerization (192), were used in the pull-down assay. These results suggest LCAR accounts for the interaction between ANP32 proteins and NP.

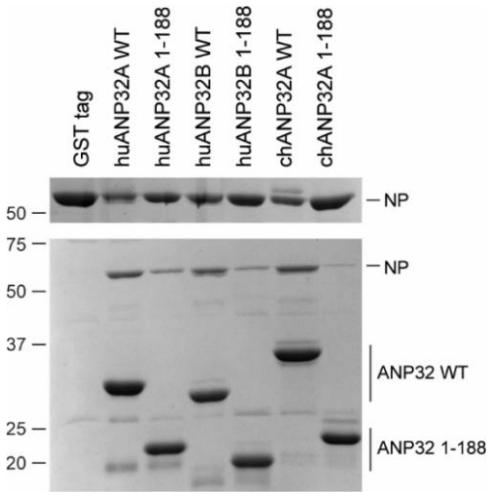

Fig. 3.3 ANP32 proteins interact with NP.

GST pull-down assay using GST-tagged ANP32 proteins and NP with a R416A mutation. Full-length huANP32A, huANP32B, chANP32A, and their truncated mutants (1-188) with a cleavable N-terminal GST tag were immobilized on glutathione Sepharose prior to the addition of NP (R416A). Bound proteins were released by addition of PreScission protease. The purified GST tag alone was set as negative control. Unbound proteins (upper gel) and eluates (lower gel) were separated by SDS-PAGE and staining with Coomassie Brilliant Blue. Molecular weight markers are indicated in kDa. (Figures from Dr. Haitian Fan)

To further verify the role of LCAR in ANP32-NP interaction, we assessed the NP binding affinity of a series of truncated chANP32A in the GST pull-down assay (Data from Dr. Haitian Fan). The amount of bound NP decreased as the full-length chANP32A protein was successively truncated to the 188 residue **(Fig. 3.4A)**. Remarkably, the ANP32-NP interaction was significantly compromised when chANP32A was truncated to a length shorter than 220-amino acid long, indicating that the region of 189-220 is important for NP binding. In support of this concept, we found that the recombinant peptide corresponding to region 189-220 of chANP32A pulled down a similar amount of NP as chANP32A (1-220) did in the GST pull-down assay **(Fig. 3.4B)**. The interaction between chANP32A with NP was further confirmed by size exclusion chromatography, where ANP32-NP complexes from both GST pull-down and pre-mixing of individually purified protein resulted in an earlier elution peak on a Superdex 200 column, compared with either chANP32A or NP alone **(Fig. 3.4C)**. These data indicate that ANP32-NP complex is stable in solution.

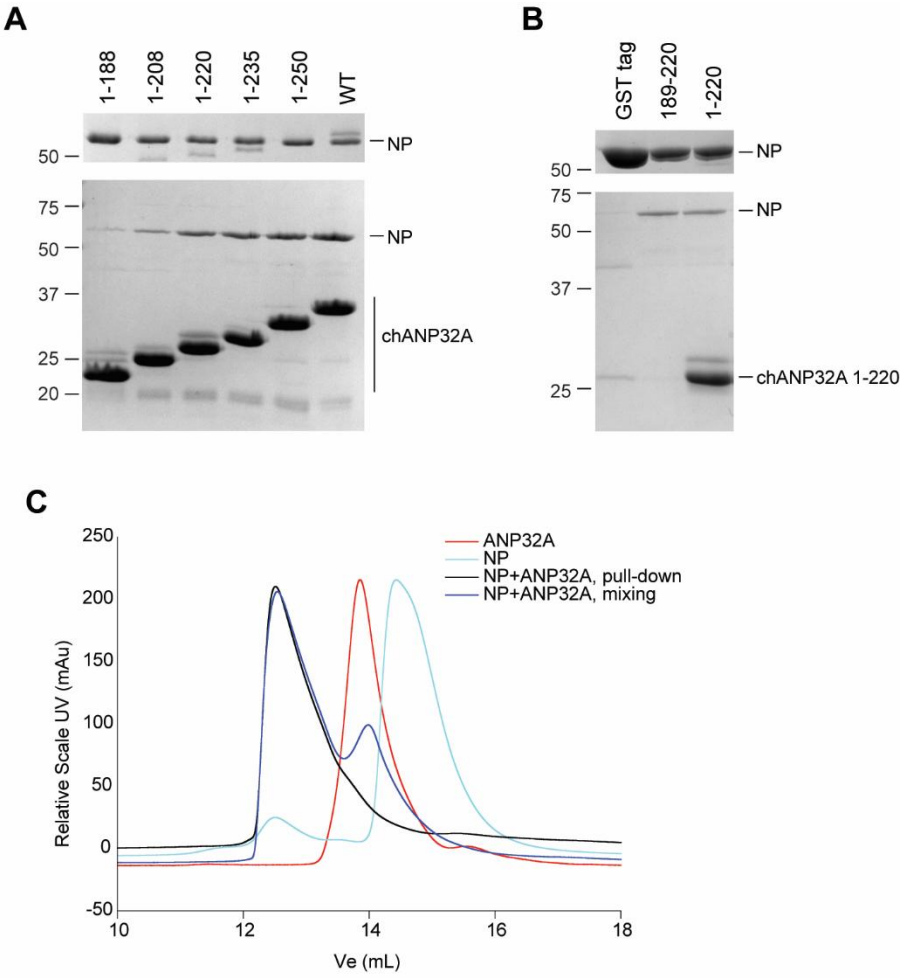

Fig. 3.4 ANP32 LCAR is essential for ANP32-NP interactions.

A series of chANP32A truncated mutants (A) and an chANP32 LCAR peptide (189-220) together with truncated chANP32A (1-220) (B) were immobilized on glutathione Sepharose prior to the addition of NP (R416A). Note that the 189–220 LCAR peptide cannot be captured on gel due to its small size. Bound proteins were released by addition of PreScission protease. The purified GST tag alone was set as negative control. Unbound proteins (upper gel) and eluates (lower gel) were separated by SDS-PAGE and stained with Coomassie Brilliant Blue. Molecular weight markers are indicated in kDa. (**C**) Size exclusion chromatography of chANP32A 1–220 and NP R416A complex formed by either using GST pull-down (pull-down) or mixing the two components (mixing). (Figures from Dr. Haitian Fan)

3.2.3 RNA binding grooves of NP contribute to ANP32-NP interactions

To identify the ANP32A binding site on NP, we designed various NP mutants based on available structures **(Fig. 3.5)** and subsequently used these NP mutants in the GST pull-down assay either in the absence or presence of a 29-nt RNA (5′-AGUAGAAACAAGGCCGUAUAUGAACAGA-3′, Dharmacon). The addition of RNA in the GST pull-down system significantly diminished the interaction between the monomeric NP (R416A) and chANP32A **(Fig. 3.6A)**, suggesting that RNA and ANP32 LCAR share the same binding site on NP. To further characterize the binding site of ANP32A on NP, four arginine to alanine mutations in the G1 RNA binding groove (known as the G1 (4) mutant) were introduced to monomeric NP (R416A) (124, 164). This mutant NP can no longer bind to chANP32A, irrespective of the presence or absence of RNA **(Fig. 3.6A)**. These results suggest that the G1 groove on NP plays a crucial role in mediating the interaction between chANP32A and NP.

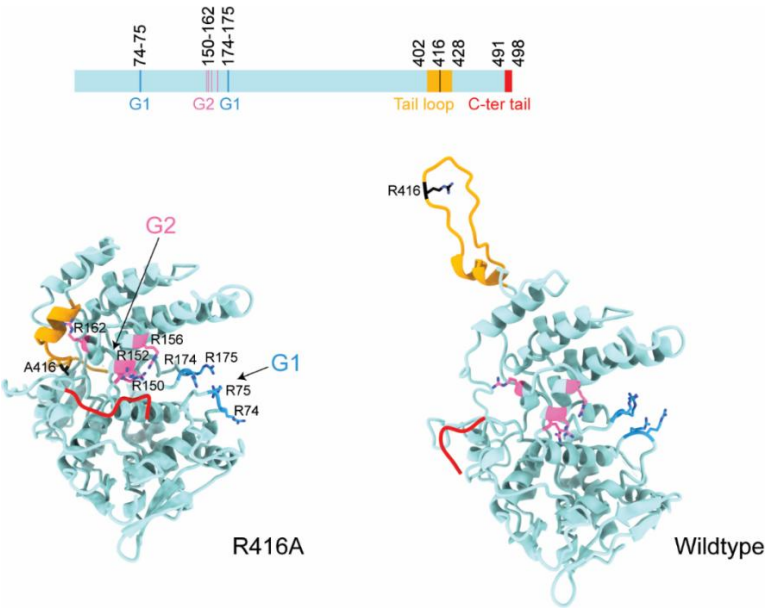

Fig. 3.5 Schematic diagram and structural models of influenza A virus NP.

Wildtype NP (PDB ID: 2Q06) and NP R416A (PDB ID: 3ZDP) with the G1 (blue) and G2 (pink) RNA binding grooves, tail loop (yellow), and C-terminal tail (red). Critical amino

acid residues in the RNA binding grooves and tail loop are shown in stick mode in structural models.

We also examined the binding capability of oligomeric wildtype NP and a G1 (4) mutant NP(R74A/R75A/R174A/R175A) in the GST pull-down assay (Data from Dr. Haitian Fan). As expected, wildtype NP bound to chANP32A, albeit very little binding to the negative control GST tag alone **(Fig. 3.6B)**. Based on band intensity, there were more oligomeric NP (wildtype) molecules bound to chANP32A compared to monomeric NP (R416A) **(Fig. 3.6B, lane 2 and lane 4)**. This discrepancy could be attributed to the fact that multiple oligomerized NP binds to a single chANP32A molecule. Intriguingly, the introduction of the G1 (4) mutation to wildtype NP did not abolish its interaction with chANP32A. However, addition of the 29-nt RNA still blocked the binding of both wildtype NP and G1 (4) mutant to chANP32A **(Fig. 3.6C)**. Collectively, these data suggest that multiple RNA binding sites on NP contribute to the ANP32A-NP interaction.

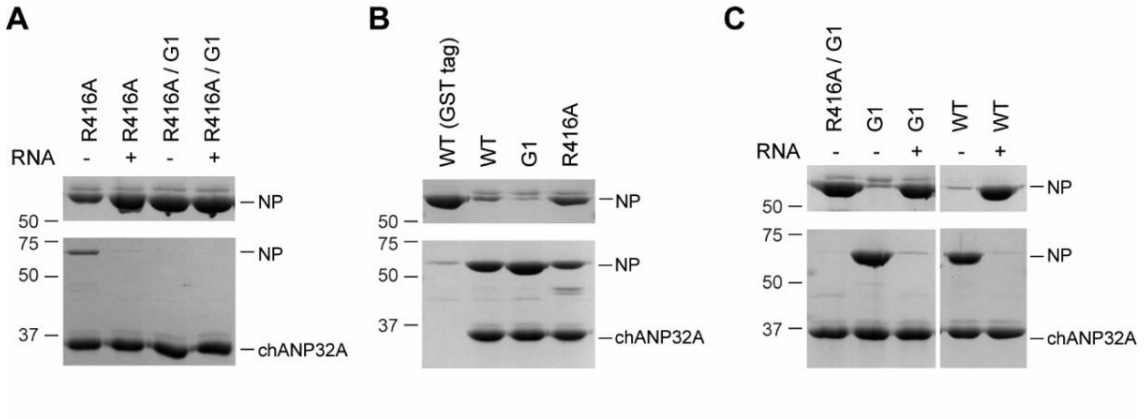

Fig. 3.6 LCAR binds to G1-RNA binding grooves on NP.

(A-C) GST pull-down assays using GST tagged chANP32A and mutant NP in the absence or presence of 1.5 × (+) molar excess of a 29-nt RNA. The G1 mutant NP (R416A) carries the following mutations other than R416A: R74A/R75A/R174A/R175A. The wildtype NP carries G1 (4) mutations: R74A/R75A/R174A/R175A. The purified GST tag alone was set as negative control. chANP32 protein with a cleavable N-terminal GST tag was immobilized on glutathione Sepharose prior to the addition of NP (R416A) or G1 mutant NP (R416A). Bound proteins were released by addition of PreScission protease. Unbound (upper gel) and eluates (lower gel) were separated by SDS-PAGE and staining with Coomassie Brilliant Blue. Molecular weight markers are indicated in kDa. (Figures from Dr. Haitian Fan)

NP possesses two RNA binding grooves, namely G1 and G2 (124). Available NP structures show that the G2 binding groove in monomeric NP (R416A) is partially obstructed by the NP tail loop (residues 402-428) and the C-terminal acidic tail (residues 491-498). The tail loop packs against a site adjacent to the G2 groove, closely located to R162; the C-terminal tail lies parallel to the G2 groove and is in proximity to R150 and R152 **(Fig. 3.5)**. In contrast, the tail loop in oligomeric NP (wildtype) extends toward to the neighbouring NP, forming an inter-molecular salt bridge between R416 and E330 on the adjacent NP protomer. The C-terminal tail is either missing or partially modelled in a position opposite the RNA binding grooves. Consequently, the critical residues such as R150, R152, and R162 in the G2 RNA binding groove could be spatially obstructed in the monomeric NP (R416A) but remain exposed in the oligomeric NP (wildtype). This disparity may account for the different binding affinities for chANP32A displayed by monomeric and oligomeric forms of the G1 (4) mutants.

To unravel the precise mechanistic details of the G2 binding groove in ANP32-NP interaction, we deleted the tail loop (ΔT) or the C-terminal tail (ΔC) and assessed their binding affinity to chANP32A in GST pull-down assay **(Fig. 3.7A)** (Data from Dr. Haitian Fan). Deletion of the C-terminal tail (residues 491-498) restored the binding of the monomeric G1 (4) mutant NP to chANP32. Given the fact that the tail loop is essential for NP oligomerization, removal of the tail loop (residues 402-428) abolished the binding affinity of G1 (4) NP to chANP32A, while further deletion of the C-terminal tail in this construct rescued the chANP32A binding affinity. These findings suggest that it is the C-terminal tail that blocks the G2 binding groove of monomeric NP during ANP32-NP interaction. To directly assess the contribution of G2 groove in NP-ANP32 interface, we introduced four arginine to alanine mutations in G2 groove together with G1 (4) mutation.

The mutant NP with G1/G2 grooves mutated exhibited a profound defect in binding to chANP32A as well as huANP32A or huANP32B compared with wildtype NP **(Fig. 3.7B)**. These results indicate that both G1 and G2 grooves of NP contribute to the ANP32-NP interaction.

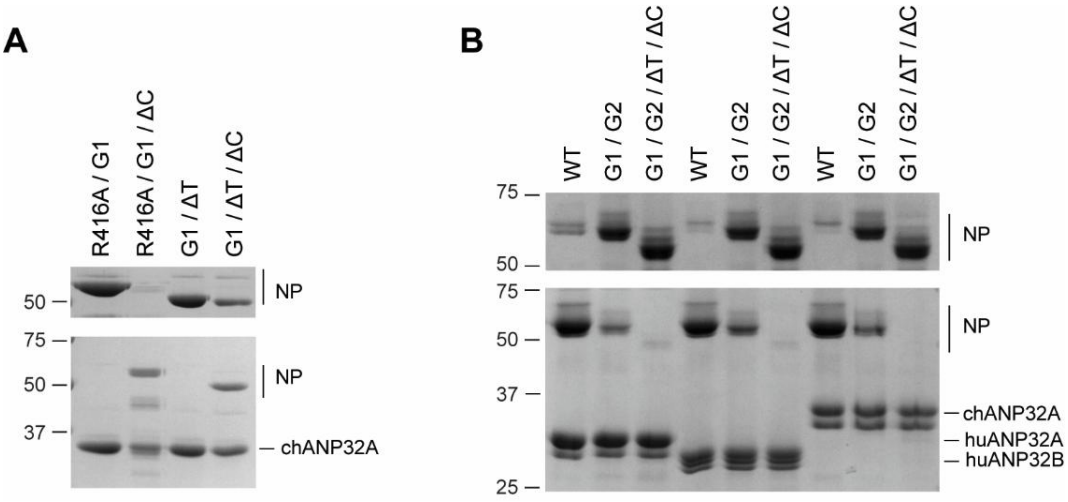

Fig. 3.7 G2-RNA binding groove on NP also contributes to the NP-ANP32 interaction. GST pull-down assay using GST-tagged chANP32A, huANP32A, and huANP32B together with the indicated wildtype or mutant NP. The following NP mutants were used: R416A, G1 (R74A/R75A/R174A/R175A), G2 (R150A/R152A/R156A/R162A), ΔT (amino acid residues 402–428 of the tail loop deleted), ΔC (amino acid residues 491–498 of the C-terminal tail deleted), and their combinations. Bound proteins were released by addition of PreScission protease. Unbound proteins (upper gel) and eluates (lower gel) were separated by SDS-PAGE and staining with Coomassie Brilliant Blue. Molecular weight markers are indicated in kDa. (Figures from Dr. Haitian Fan)

3.2.4 ANP32 proteins interact with NP within cells

To further confirm the ANP32-NP interaction within cells, we used a split *Gaussia* luciferase assay to directly monitor the ANP32-NP interactions (Luciferase assay results from Dr. Wendy Barclay's lab). The N-terminal half of the luciferase was tagged to the C terminus of NP and C-terminal half of the luciferase was tagged to the C-terminus of ANP32 proteins. The huANP32A (1-149) construct lacking the LCAR was set as negative control in this assay. The luminescence generated from lysates containing NP with huANP32A, huANP32B, or chANP32A is significantly higher than the negative control **(Fig. 3.8C)**, demonstrating that ANP32 proteins indeed interact with NP. Consistent with our GST pull-down assays results, RNase A treatment on cell lysates further enhanced the luciferase activity. Together, these data indicate that ANP32-NP interaction exists in cellular conditions and the presence of RNA interferes this interaction.

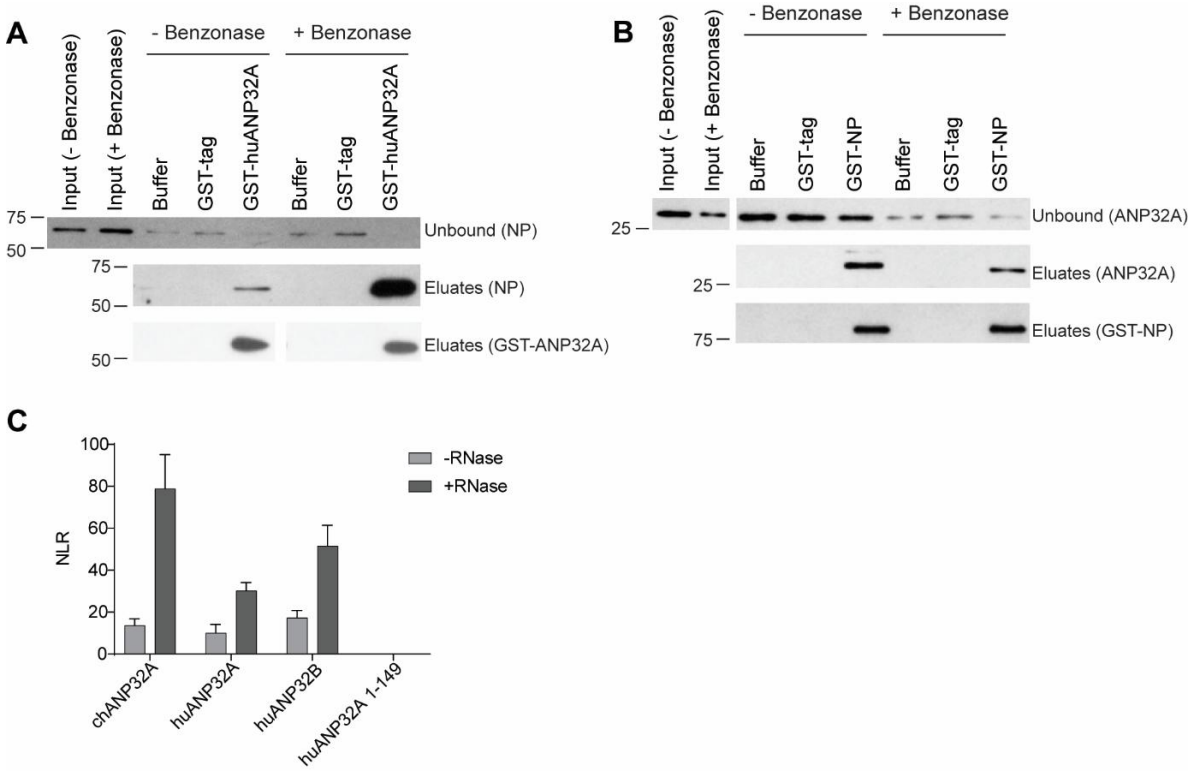

Fig. 3.8 ANP32 interaction with NP in cells.

Pull-down assays using bacterially expressed purified GST-tagged huANP32A and cell lysates from cells transfected with plasmids expressing NP (A) or vice versa (B). Cell lysates were treated with Benzonase. Input, unbound, and eluate samples were analysed by western blotting. Split-luciferase assay for measuring ANP32-NP interactions in 293T-DKO cells (C). Samples were treated with or without RNase prior to the measurement. Results shown are mean ± standard deviation from triplicate samples. NLR: normalized luminescence ratio. (Figure 3.8C from Carol Sheppard of Wendy Barclay's lab)

3.2.5 The LCAR of ANP32 proteins is required for efficient replication of a full-length influenza genome segment but not a short vRNA-like template

The observation of ANP32-NP interaction spurred our investigation on the role of this interaction during influenza virus genome replication. NP is regarded as an essential elongation factor for the replication of full-length viral genome. The dependency on NP can be mitigated when the full-length gene segment is replaced with a vRNA-like template that is shorter than 76-nts (159). Using viral ribonucleoprotein reconstitution assay with a full-length neuraminidase-encoding vRNA (1409-nt) or NP-independent replication assay with a 47-nt vRNA template in 293T-DKO cells, I respectively assessed the effect of LCAR truncations on the replication of full-length vRNA template or short vRNA template. Truncated huANP32A with part of the LCAR retained (1-220 and 1-235) supported the replication of both full-length and short vRNA template comparably to the wildtype huANP32A **(Fig. 3.9A)**. However, the shortest truncated huANP32A (1-149) with part of the LRR missing neither supported the replication of the full-length template nor the replication of the short vRNA template as LRR has been recognized to mediate the dimerization of polymerase, which is essential for replication (188). Crucially, huANP32A mutants (1-188 and 1-208) with most of LCAR deleted only supported the replication of short but not the full-length vRNA template. Similarly, truncations in LCAR of huANP32B and chANP32A also led to distinct consequences on the replication of templates with different lengths. **(Fig. 3.9B, C)**. These results indicate that NP-dependent replication of the full-length template is more sensitive to LCAR truncation compared with the replication of the short vRNA-like template in which NP is not required.

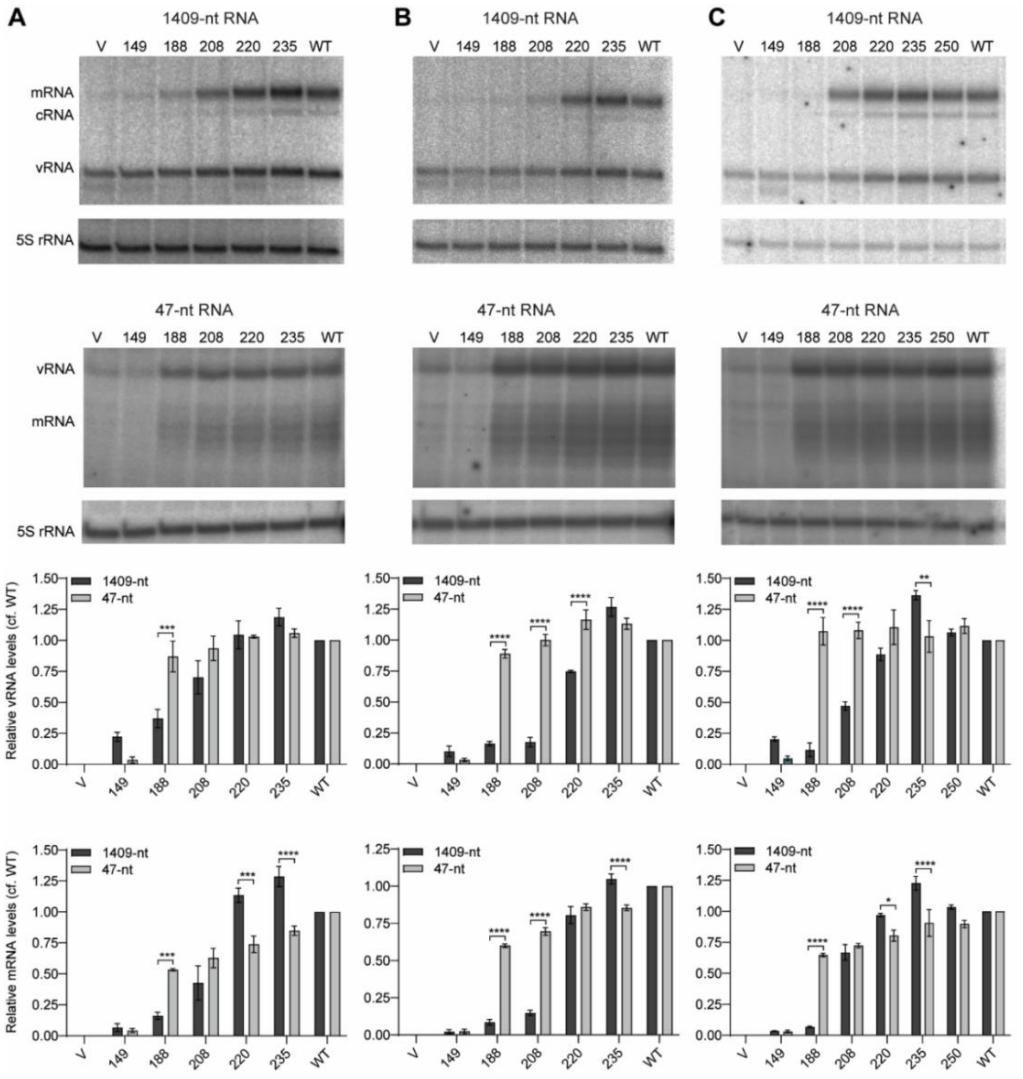

Fig. 3.9 ANP32 LCAR is required for the replication of a full-length influenza virus genome segment but not a short 47-nt vRNA-like template.

293T-DKO cells were co-transfected with plasmids encoding the indicated wildtype (WT) or truncation mutant huANP32A (A), huANP32B (B) and chANP32A (C) proteins together with plasmids expressing the PB1, PB2 and PA polymerase subunits, NP, and full-length NA vRNA (1409-nt) or a short vRNA-like template (47-nt) with the omission of NP expression plasmid. Transfection of an empty vector (V) was used as a negative control. Total RNA was extracted at 24 hpt and the accumulation of vRNA, cRNA, and mRNA was analysed by primer extension assay. The quantitation shows comparison of vRNA and mRNA accumulation for the full-length 1409-nt and short vRNA-like 47-nt

templates observed in the presence of truncated ANP32 proteins relative to that observed in the presence of wildtype ANP32 proteins (with the values for the vector subtracted) from three independent experiments. Error bars represent the standard error of the mean (n = 3). Significance was assessed using Ordinary Two-way ANOVA and asterisks indicate a significant difference as follows: *$P < 0.05$; **$P < 0.01$, ***$P < 0.001$, and ****$P < 0.0001$.

To scrutinize the function of LCAR during the replication of full-length or short vRNA template, I monitored the kinetics of viral RNA accumulation in 293T-DKO cells transfected with plasmids expressing either truncated ANP32 proteins (1-188) or wildtype ANP32 proteins. Throughout all tested time points, cells expressing truncated huANP32A (1-188) consistently exhibited markedly reduced replication of the full-length template compared to cells expressing wildtype huANP32A **(Fig. 3.10A)**. In contrast, replication of the short vRNA-like template was only impaired by truncation of LCAR at 12 hpt and then rapidly restored to levels comparable to those observed with wildtype huANP32A after 24 hpt. Similar trends were observed with huANP32B and chANP32A **(Fig. 3.10B and C)**. Together, our data suggest that the NP-dependent replication of full-length template critically relies on the function of LCAR, particularly for recruitment of NP to the nascent RNA during influenza virus replication.

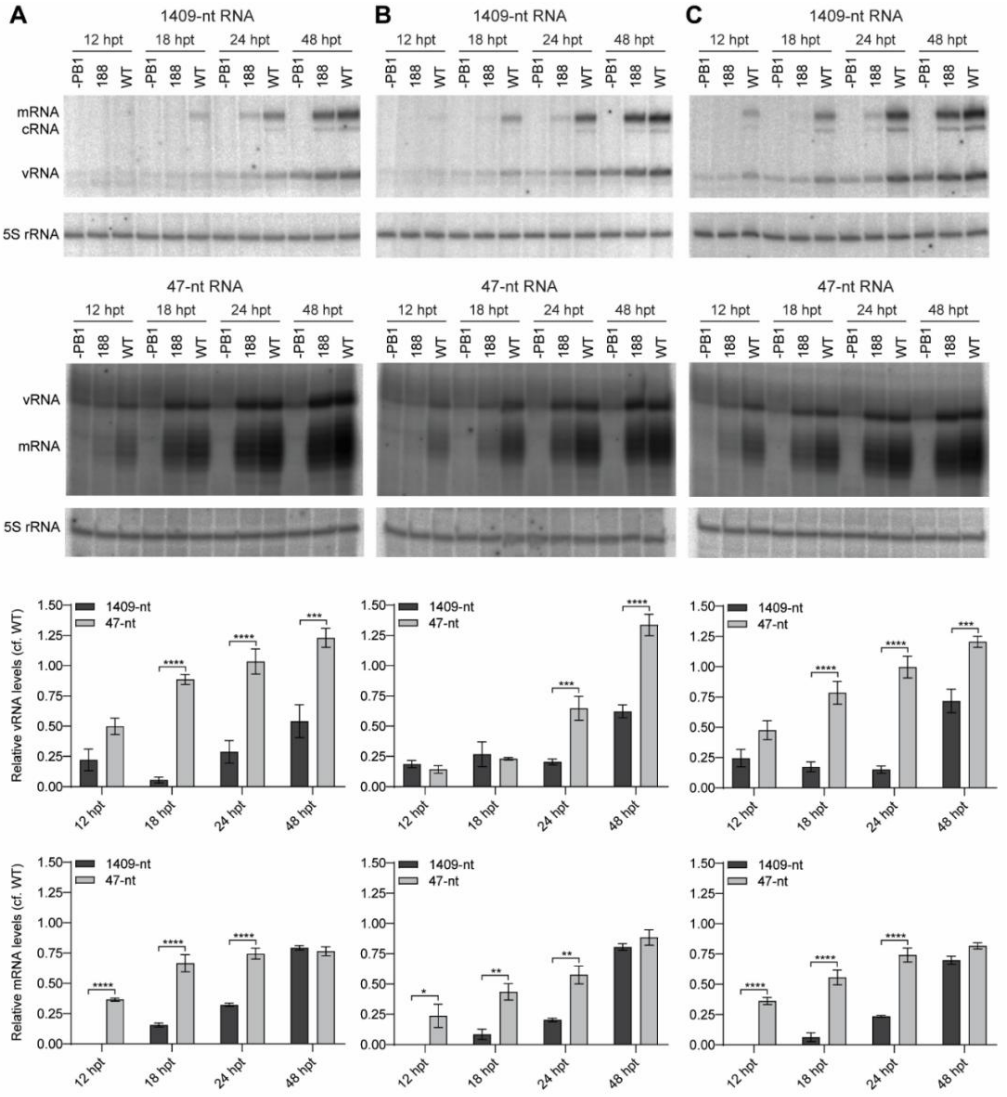

Fig. 3.10 Truncation of LCAR delayed the RNA accumulation during the replication of a full-length influenza virus genome segment compared to vRNA-like template.

293T-DKO cells were co-transfected with plasmids expressing the indicated wildtype (WT) or 1–188 truncation mutant huANP32A (A), huANP32B (B), and chANP32A (C) proteins together with plasmids to express the PB1, PB2 and PA polymerase subunits, NP, and full-length NA vRNA (1409-nt) or a short vRNA-like template (47-nt) with the omission of NP expression plasmid. The PB1 expression plasmid was omitted (–PB1) as a negative control. Total RNA was extracted at the indicated time points post transfection (hpt) and the accumulation of vRNA, cRNA, and mRNA was analysed by a primer extension assay. The quantitation shows ratios of vRNA and mRNA accumulation in cells expressing

wildtype and 1–188 ANP32 proteins for the full-length 1409-nt and short vRNA-like 47-nt templates from three independent experiments. Error bars represent the standard error of the mean (n = 3). significance was assessed using Ordinary Two-way ANOVA and asterisks indicate a significant difference as follows as follows: *P < 0.05; **P < 0.01, ***P < 0.001, and ****P < 0.0001.

3.3 Discussion

Our recent structural study has unveiled the critical role of ANP32 LRR in mediating the dimerization of influenza virus polymerase (188), which further corroborates the fact that ANP32 proteins are essential host factors co-opted by influenza virus for its genome replication (211-213, 220, 228). However, ANP32 LCAR remains largely unresolved in our structures, impeding the understanding of its function during virus replication. In this chapter, using different functional assays, we found that ANP32 proteins interact with NP and this interaction is mediated by the G1 and G2 RNA binding grooves in NP and LCAR in ANP32 proteins. Consistently, presence of RNA interferes with ANP32-NP interaction, or treatment with nuclease enhances this interaction, suggesting that NP shows higher binding affinity to nascent RNA product during virus replication. In the exploration of the role of ANP32-NP interaction in viral genome replication, we have found that ANP32-NP interaction is particularly important for the NP-dependent replication of full-length vRNA template, whereas the NP-independent replication of short vRNA-like template proves to be more resistant to the LCAR truncation in the scenario where ANP32-NP interaction is disrupted. Intriguingly, at early time point, the replication of short template was also adversely affected by truncation of LCAR, which warrants further investigation of the

function of LCAR beyond NP recruitment. Nevertheless, the overall higher levels of RNA accumulated during the replication of short template compared to the that of long template at all tested time points suggest the importance of the LCAR in NP recruitment.

Our previous study has shown that ANP32-FluPol complexes function as the replication platform for influenza viral genome (188). Here, we propose a model in which ANP32 LCAR recruits NP molecules to nascent RNA, ensuring the co-replicative assembly of RNPs during influenza virus replication. The N-terminal LRR of ANP32 proteins mediates the polymerase dimerization and thereby replication is initiated. The C-terminal LCAR captures monomeric RNA-free NP molecules and enriches them in regions spatially adjacent to nascent RNA products. As the nascent RNA strands extend, the higher binding affinity to RNA allows NP to dissociate from LCAR and binds to RNA via its RNA binding grooves, achieving co-replicative assembly of RNPs **(Figure. 3.11)**. Considering both vRNA and cRNA are packaged into RNPs, it is reasonable to speculate that the NP recruitment by ANP32 LCAR occurs during assembly of both vRNP and cRNP, which is in agreement with a recent report highlighting the requirement of ANP32 proteins for both vRNA and cRNA synthesis (192). While NP might be able to bind to nascent RNA products autonomously without the assistance of ANP32 LCAR, the efficiency of this binding could be notably less efficient **(Fig. 3.9)**. The length of the LCAR (100–130 amino acids) allows it to accommodate multiple NP monomers, suggesting that it could also act to increase local NP density and thereby enhancing the efficiency of NP recruitment to viral RNA. A fully resolved structure of ANP32-FluPol complexes could provide molecular details of NP recruitment by LCAR. In conclusion, in addition to the known role of ANP32 proteins in mediating dimerization of viral polymerases, we identify that NP

recruitment is another important function of ANP32 proteins during influenza virus genome replication.

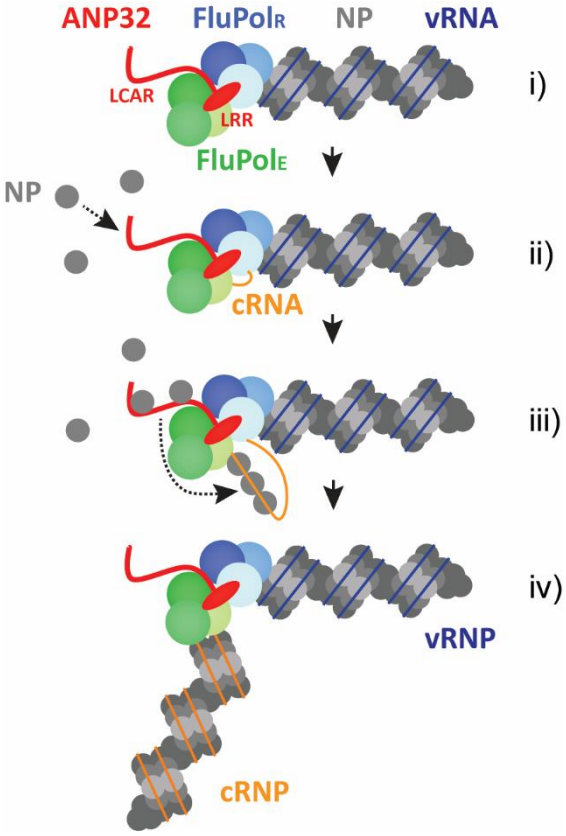

Fig. 3.11 Model of influenza virus RNA genome replication.

(i) ANP32 proteins mediate polymerase dimerization through their N-terminal LRR domain (red oval). The newly synthesized free influenza virus polymerase (encapsidating polymerase, $FluPol_E$) is recruited to the resident polymerase within the vRNP (replicating polymerase, $FluPol_R$). (ii) $FluPol_R$ initiates cRNA synthesis and the 5' end of the nascent cRNA (orange) is captured by $FluPol_E$. The ANP32 LCAR (red line) recruits newly synthesized NP molecules, increasing the density of NP locally. (iii) ANP32 LCAR facilitates the transfer of NP to nascent cRNA. Due to the higher binding affinity between NP and RNA, NP dissociates from ANP32 LCAR. (iv) cRNA is assembled into cRNP and released from the template vRNP complex.

CHAPTER 4

The functional analysis of the Influenza A virus nucleoprotein C-terminal tail

4.1 Introduction

The double-helical ribonucleoprotein (RNP) complexes of influenza virus consist of a trimeric polymerase complex, vRNA/cRNA, and a scaffold of nucleoprotein (NP) (67). NP has been recognized as an elongation factor for viral genome replication, and it is essential for the replication of full-length viral genome segments (159). During influenza virus replication, NP binds to nascent vRNA and cRNA through its two RNA binding grooves, G1 (defined by R74, R75, R174 and R175) and G2 (defined by R150, R152, R156 and R162) (123, 124). NP molecules can interact with each other and homo-oligomerize by NP inserting its tail-loop into a groove of the neighbouring NP molecule (124, 156). This tail-loop-mediated NP interaction is believed to maintain the association between adjacent NP molecules in the same direction on the RNA strand **(Fig. 4.1)**. Additionally, NP molecules can also form a dimer, a crucial process for forming the double-helical structure of RNPs, involving two polypeptide regions (residue 149-167 and 482-498) (229). This dimer interaction occurs between antiparallel NP molecules that are associated with two antiparallel RNA strands. Oligomerization of NP molecules is particularly important for maintaining the structure and biological activities of RNPs, as evidenced by the observation that decreased or increased oligomerization adversely affects viral transcription or replication (227, 229).

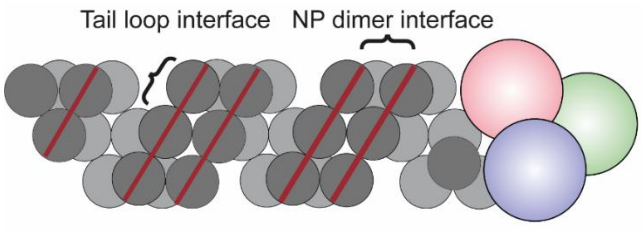

Fig. 4.1 Schematic diagram of double-helical RNP with indicated NP-NP interface. NP molecules are labelled in grey, the RNA molecule is red, and the trimeric polymerase complex with three subunits labelled in pink, green, and purple.

The biological functions of NP C-terminal tail (490-498) have not been extensively studied, although different NP structures containing this region have been resolved (123, 156, 227, 229). The NP C-terminal tail contains four acidic amino acids (D491, E494, E495, and D497) and other neutral amino acids, rendering this region acidic. Intriguingly, the acidic nature of this C-terminal tail is a conserved feature for all members of the *Orthomyxoviridae* family. Functionally, the C-terminal tail has been demonstrated to play a role in regulating NP oligomerization and RNA binding (227, 229). Previous studies have reported that the deletion of the NP C-terminal tail increases its RNA binding affinity and NP dimer formation (229). Consistently, in chapter 3, our data also showed that the NP C-terminal tail blocks the G2 binding groove in monomeric NP and deletion of it can promote ANP32-NP interaction. It has been found that NP dimerization mediated by the NP C-terminal tail can be disrupted by NP D491A mutation. Using a luciferase reporter assay, the authors also claimed that NP D491A mutation on the C-terminal tail impairs RNA synthesis, suggesting the NP dimer required for maintaining the double-helical structure is important for viral RNA synthesis (229). However, the relevant functional studies of NP

C-terminal tail are very limited, hindering the understanding of the biological relevance of this region.

In this chapter, I aim to investigate the molecular details of NP C-terminal tail during influenza virus replication. The results from a series of functional assays could provide us more insight into the function of the NP C-terminal tail.

4.2 Results

4.2.1 C-terminal tail of NP is essential for viral RNA synthesis

To elucidate the role of the NP C-terminal tail (491-498 residues) in influenza A virus replication, I first introduced mutations or deletion into the NP C-terminal tail based on the structure of NP (123) and subsequently assessed their impact on viral RNA synthesis **(Fig. 4.2A)**. There are conserved acidic residues at position 491, 495, and 497; I therefore respectively mutated these acidic residues to alanine. In the vRNP reconstitution assay, RNA accumulation levels in cells expressing the truncated NP with deletion of the C-terminal tail (ΔC) were markedly reduced compared with those in cells expressing wildtype NP **(Fig. 4.2B)**. The triple mutant NP with the three acidic residues substituted with alanine (3A) also exhibited reduced RNA accumulation levels, albeit to a lesser extent compared to truncated NP (ΔC). Intriguingly, single-site mutations in NP led to moderate reduction (NP D491A) or had almost no effect (E495A and D497A) on the RNA accumulation levels, implying a single mutation in the NP C-terminal is insufficient to abolish its function in the vRNP reconstitution system. Together, these results indicate that the C-terminal tail of NP is critical for the optimal viral RNA synthesis.

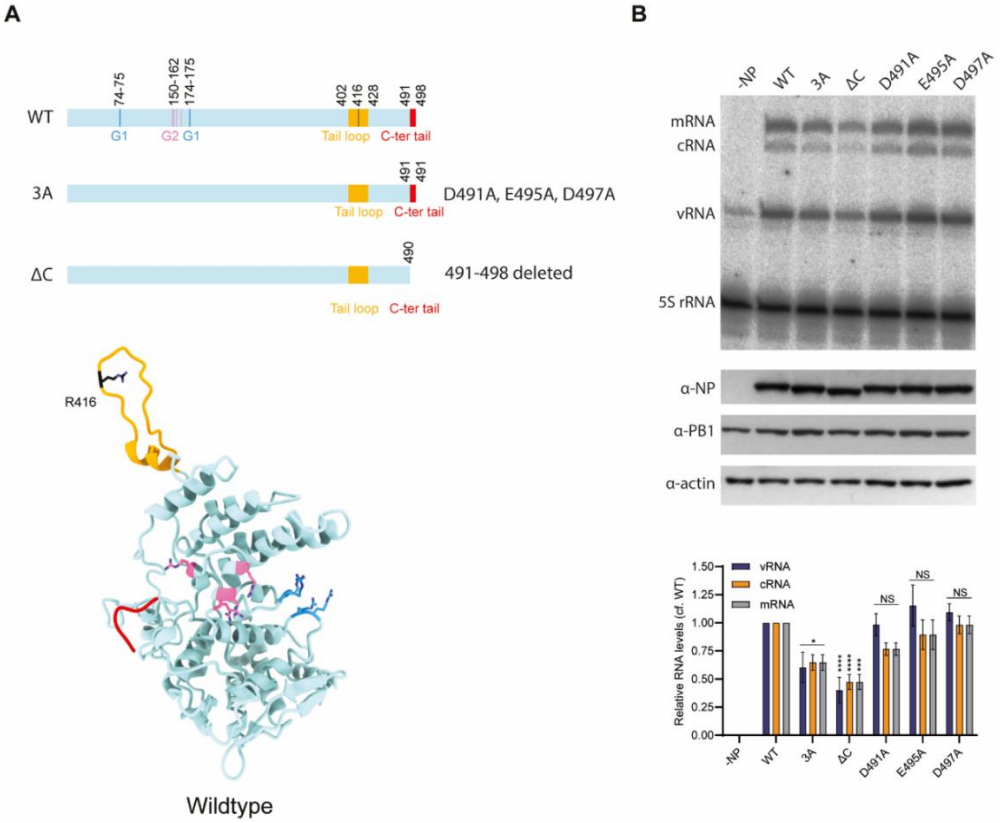

Fig. 4.2 NP C-terminal tail is essential for accumulation of viral RNA.

(A) Schematic diagram and structural model of NP (PDB ID: 2Q06) and mutant NP with mutations (D491A, E495A, D497A, or triple mutation, 3A) or deletion (491-498 residues deleted, ΔC). (B) vRNP reconstitution assay in 293T cells. 293T cells were transfected with plasmids expressing PB2, PB1, PA and the indicated NP together with pPolI-NA plasmid expressing NA segment of A/WSN/1933(H1N1); transfection of an empty vector instead of NP expressing plasmid was used as a negative control. Total RNA was harvested at 16 hpt and the accumulation of vRNA, cRNA, and mRNA was analysed by a primer extension assay. The quantification shows the relative RNA levels in the presence of the indicated NP compared to that observed in presence of wildtype NP (with the values for the vector subtracted) from three independent experiments. Error bars represent the standard error of the mean (n = 3). Significance was assessed using Ordinary One-way ANOVA and asterisks indicate a significant difference as follows: *P < 0.05; ***P < 0.001, and, ****P < 0.0001. NS, not significant.

4.2.2 NP C-terminal tail is required for accumulation of cRNA during replication.

NP has been reported to play an important role in cRNA stabilization (163). Therefore, I next tested the effect of NP C-terminal deletion or mutations on the accumulation and replication of cRNA using a cRNA stabilization assay. As previously described (163), preexpression of NP and the catalytically inactive viral polymerase complex (PB1a: D445A/D446A) prior to viral infection in the presence of cycloheximide, an inhibitor of protein translation, could result in the linear accumulation of cRNA without synthesis of progeny vRNA. Omission of NP substantially reduced the cRNA accumulation level compared with that in presence of wildtype NP **(Fig. 4.3)**, consistent with previous findings that viral polymerase, instead of NP, is the essential component for cRNA stabilization, although the presence of NP could greatly increase the cRNA accumulation level. In agreement with our observations in the vRNP reconstitution assay **(Fig. 4.2B)**, deletion (ΔC) or triple mutation (3A) of the C-terminal tail of NP greatly diminished the amount of cRNA being stabilized. In contrast, D497A single-site mutant showed comparable cRNA stabilization ability to wildtype NP, whereas the D491A/E495A mutant NP had a greatly reduced cRNA stabilization ability, which was almost as strong as that of the NP (3A) and NP (ΔC). Collectively, these results suggest that the C-terminal tail is particularly important for cRNA accumulation during viral RNA synthesis.

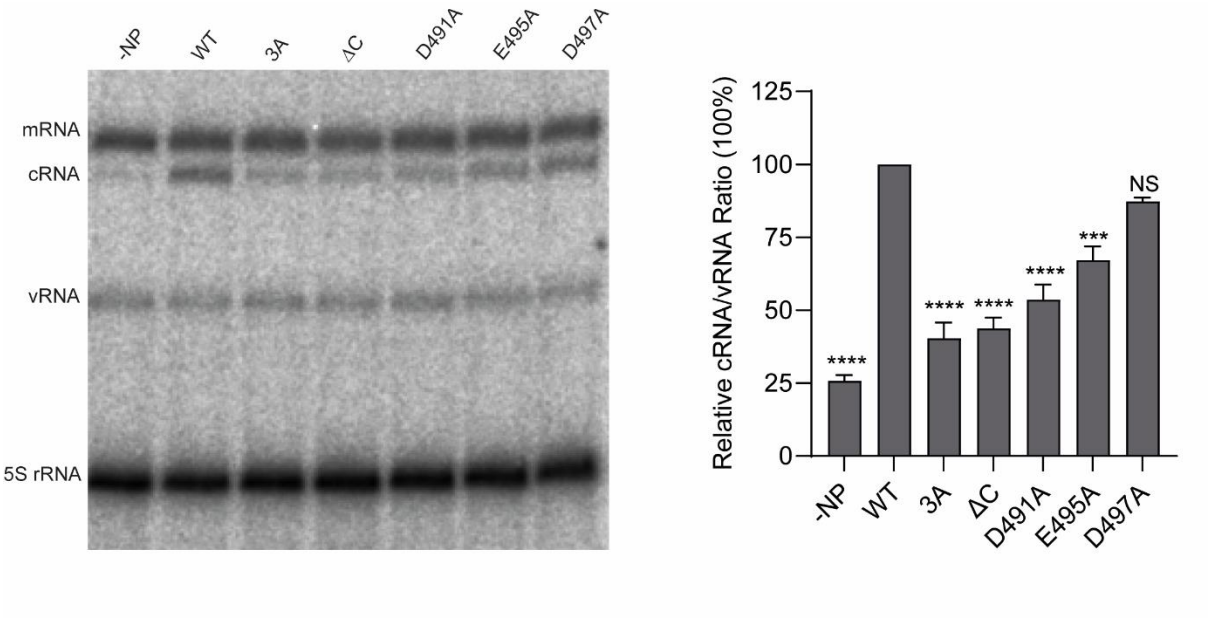

Fig. 4.3 NP C-terminal tail is required for accumulation of cRNA during replication. PB2, PB1, PA, and the indicated NP were expressed in 293T cells for 24 hours prior to infection with influenza A/WSN/33 virus at an MOI of 10 in the presence of cycloheximide; transfection of an empty vector instead of NP expressing plasmid was used as a negative control. Total RNA was harvest at 4 hpi and was subsequently subjected to primer extension analysis. The quantification shows the relative cRNA/vRNA levels in the presence of the indicated NP compared to that observed in presence of wildtype NP from three independent experiments. Error bars represent the standard error of the mean (n = 3). Significance was assessed using One-way ANOVA and asterisks indicate a significant difference as follows: ***$P < 0.001$ and ****$P < 0.0001$. NS, not significant.

4.2.3 NP C-terminal tail is required for robust FluPol-NP interactions.

I next sought to identify the molecular details by which the NP C-terminal tail is essential for viral RNA synthesis. To evaluate the role of NP C-terminal tail in FluPol-NP interaction, I first established a split-*Gaussia* luciferase assay to measure FluPol-NP interactions **(Fig. 4.4A)**. I found that the polymerase subunits with C-terminally tagged Luc2 and NP with C-terminally tagged Luc1 can generate strong luminescence in the context of the full polymerase complex **(Fig. 4.4B)**. Omission of any two of the three polymerase subunits resulted in greatly diminished FluPol-NP interaction, although a relatively stronger residual interaction was observed when PB2 was used as probe for monitoring the interaction, which was probably due to the direct interaction between PB2 and NP as reported by other studies (132, 230). Using a series of previously described PB2 truncated mutants in this split-luciferase assay for FluPol-NP interactions (231), I found that deletion of the PB2-N domain and cap-binding domain, the regions that have been previously reported for mediating PB2-NP interaction, markedly abolished the FluPol-NP interaction **(Fig. 4.5)**, suggesting that these two domains also contribute to FluPol-NP interactions. However, these data need to be interpreted with caution as no western blots have been performed to address whether all PB2 fragments are expressed equally well.

To directly examine the role of the NP C-terminal tail in FluPol-NP interactions, I introduced the triple mutation or deletion in the NP C-terminal tail in the NP construct with tagged Luc1 and assessed their effects on FluPol-NP interactions. Both NP (3A) and NP (ΔC) significantly reduced the FluPol-NP interactions, regardless of whether the Luc1 was tagged on C-terminus **(Fig. 4.6A)** or N-terminus **(Fig. 4.6B)** of NP. Taken together, these results indicate that NP C-terminal tail is required for robust FluPol-NP interactions.

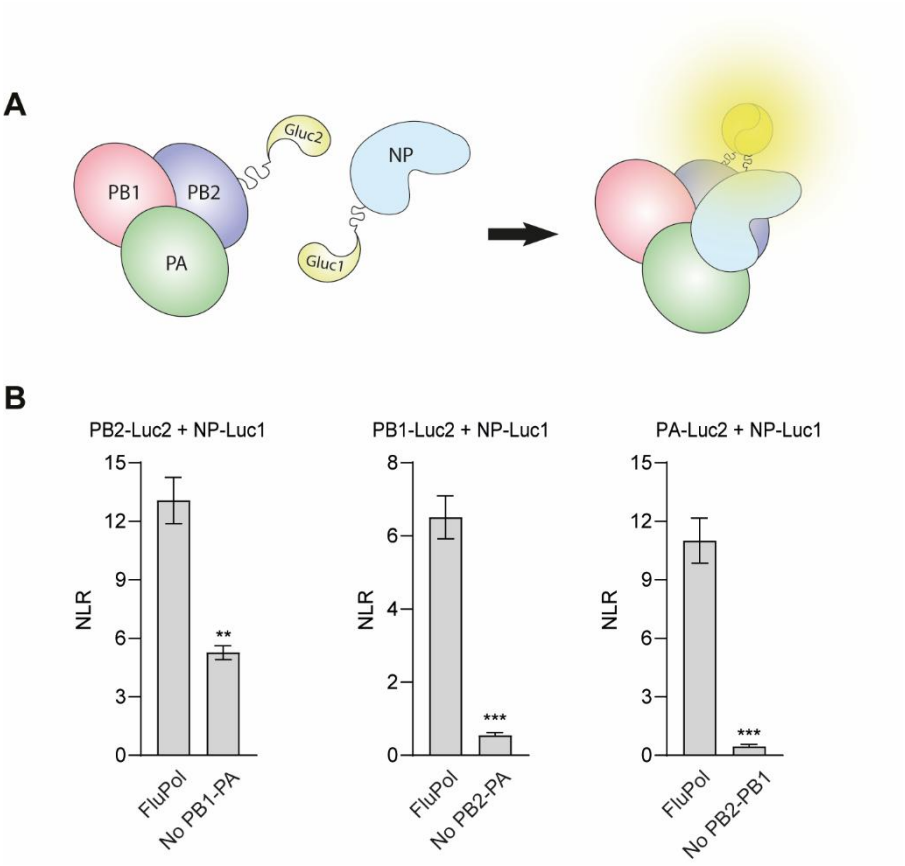

Fig. 4.4 Establishment of split-*Gaussia* luciferase assay for measuring FluPol-NP interactions.

(A) Schematic diagram of split-Gaussia luciferase assay to measure FluPol-NP interactions. One of the influenza A virus polymerase subunits (PB2, PB1, or PA) was C-terminally tagged in frame with Gluc2 and NP was C-terminally tagged in frame with Gluc1. If FluPol and NP interact, luciferase is reconstituted and its activity is measured using a luciferase assay. (B) 293T cells were transfected with the indicated luciferase-tagged polymerase subunit and NP together with the remaining two polymerase subunits. As negative controls, two of the three polymerase subunits were omitted in each setting. Luminescence was measured from cell lysate at 24 hpt. Normalised luciferase ratio (NLR) was calculated as described in the Materials and Methods chapter. Data represent three independent experiments performed in technical duplicates (mean ± SEM of n=3 biological replicates) $^{**}P < 0.01$, $^{***}P < 0.001$ (two-tailed, unpaired Student's *t*-test).

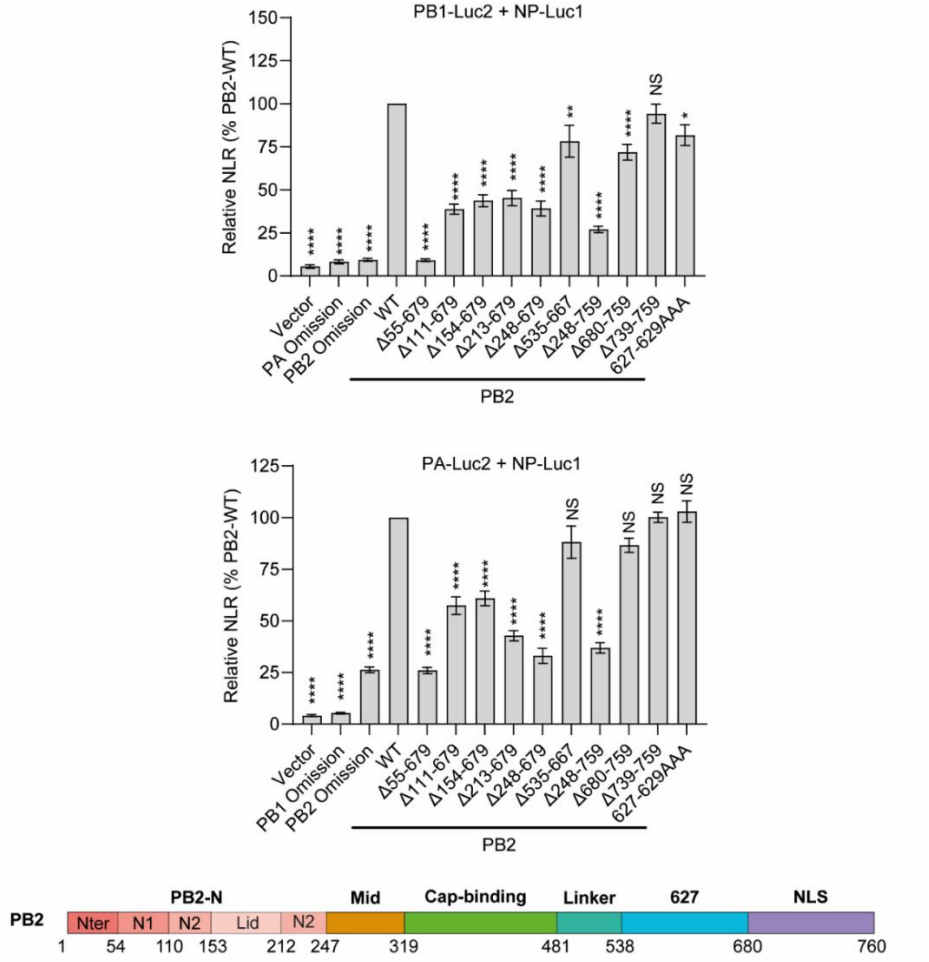

Fig. 4.5 The N-terminal domain and Cap-binding domain of PB2 are important for FluPol-NP interactions.

293T cells were transfected with the indicated PB2 truncated mutants with the split-luciferase constructs to measure FluPol-NP interactions. PB1-Luc2 and NP-luc1 combination was used in the upper panel; PA-Luc2 and NP-Luc1 combination was used in the bottom panel. The setting with the omission of two polymerase subunits (Vector) was set as negative control. Luminescence from cell lysates was measured at 24 hpt. The luciferase activities are presented as percentage of NLR changes relative to the NLR for assay with wildtype PB2 (set as 100%). Data represent at least four independent experiments performed in technical duplicates (mean ± SEM of n=4 biological replicates) *P < 0.1, **P < 0.01, ****P < 0.0001 (One-way ANOVA; Dunnett's multiple comparisons test). NS, not significant.

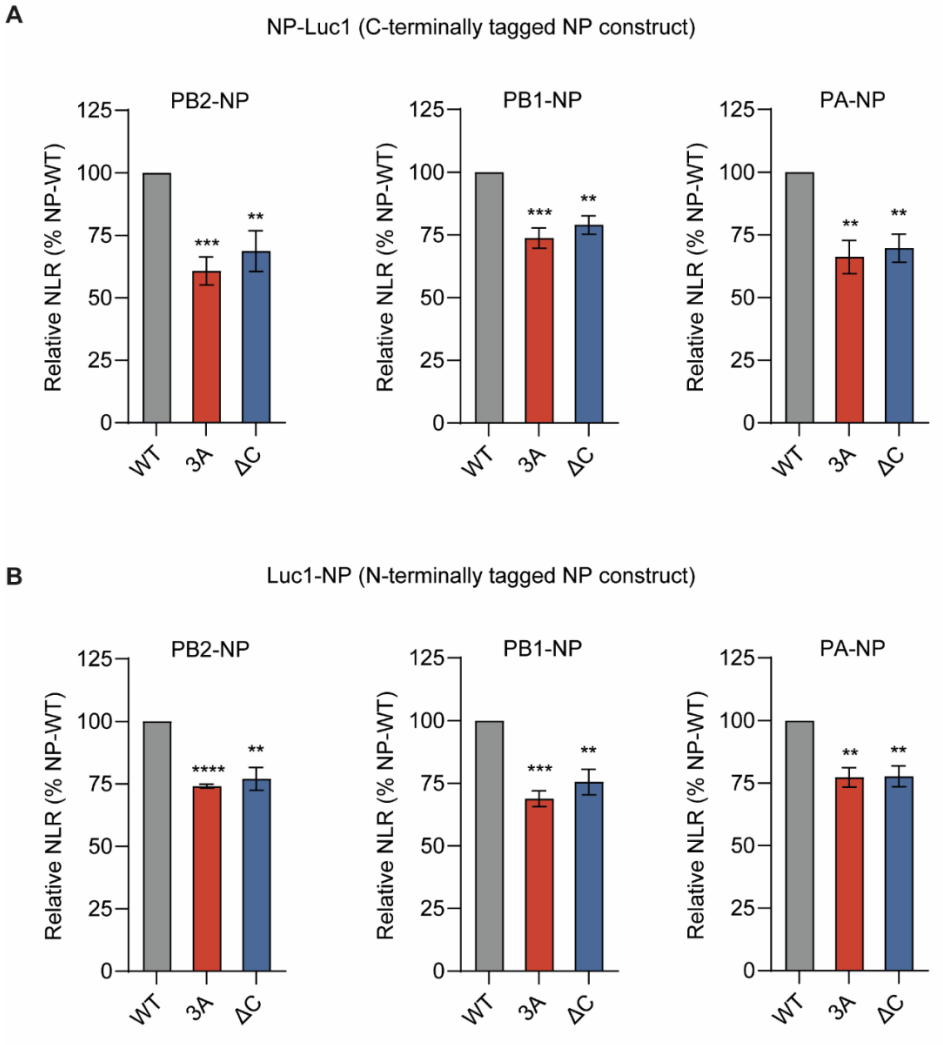

Fig. 4.6 Deletion or mutations of the NP C-terminal tail dampens FluPol-NP interactions.

293T cells were transfected with the indicated constructs used in the split-luciferase assay to measure FluPol-NP interactions. The Luc1 was tagged to either the C-terminus of NP (A) or the N-terminus of NP. 3A represents the Luc1-tagged NP carrying D491A, E495A, D497 mutations; ΔC represents the Luc1-tagged NP with deletion of NP C-terminal tail (residues 491-498). Luminescence from cell lysates was measured at 24 hpt. The luciferase activities are presented as percentage of NLR changes relative to the NLR for wildtype NP (set as 100%). Data represent at least three independent experiments performed in technical duplicates (mean ± SEM of n=3 biological replicates) $^{**}P < 0.01$, $^{***}P < 0.001$, $^{****}P < 0.0001$ (One-way ANOVA; Dunnett's multiple comparisons test).

4.2.4 NP D491A attenuates the virus

To substantiate our findings from the vRNP reconstitution assay and cRNA stabilization that NP C-terminal tail is important for viral RNA synthesis, I next rescued mutant WSN with either mutations or deletions in the NP C-terminal tail. In agreement with the above findings from the functional assays, neither the virus with triple mutation in the NP C-terminal tail nor the one with the entire NP C-terminal tail deleted could be rescued using reverse genetics (data not shown), probably due to the profound defect in cRNA stabilization. In contrast, mutant WSN viruses carrying single-site mutations in the NP C-terminal tail were all successfully rescued. Of note, the plaque size of D491A virus was noticeably smaller, and the virus titer was reduced by almost 3 logs compared with the wildtype WSN virus **(Fig. 4.7)**. Judging from the plaque phenotype and growth kinetics, the NP E495A mutation only moderately attenuated the virus, and the NP D497A mutation had almost no effect on the virus. The different cRNA stabilization ability of NP mutants probably accounts for this distinct fitness of these mutant viruses as their trends were well matched. These data suggest that the NP C-terminal tail, in particular residue 491, is crucial for viral fitness.

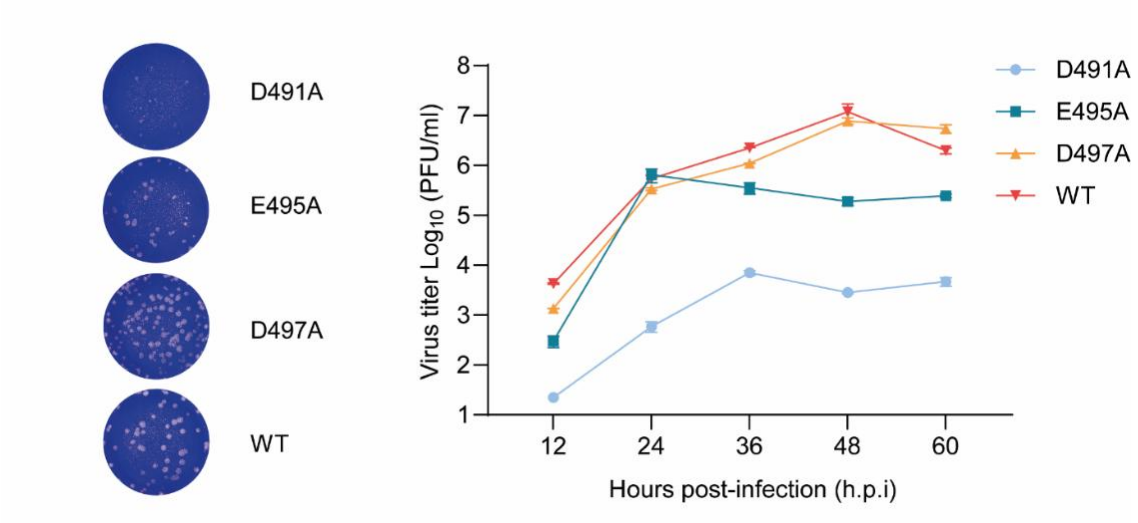

Fig. 4.7 The NP D491A virus is highly attenuated.

Growth kinetics and plaque phenotypes of WSN wildtype virus and its indicated NP single mutant viruses (D491A, E495A, D497). MDCK cells were infected with indicated viruses at an MOI of 0.01 and were incubated at 37 ℃. Supernatants were collected at 12, 24, 36, 48, and 60 hpi. Virus titers were measured by plaque assay using MDBK cells.

4.2.5 NP D491A virus reverts to wildtype fitness

In an exploration of the underlying mechanism behind the attenuation of the NP D491A virus, I investigated whether this attenuated virus could regain its original fitness through the acquisition of compensatory mutations. The NP D491A virus rapidly restored its fitness after three passages in MDCK cells, as evidenced by the emergence of large plaques alongside the small plaques formed by the original attenuated NP D491A virus **(Fig. 4.8)**. By the fourth passage (P4), the virus had fully recovered, with the large-plaque virus becoming the dominant phenotype. Indeed, growth kinetics also demonstrated that the P4 virus replicated as well as the wildtype WSN virus, indicating the viral fitness was fully restored to a level comparable to wildtype WSN virus.

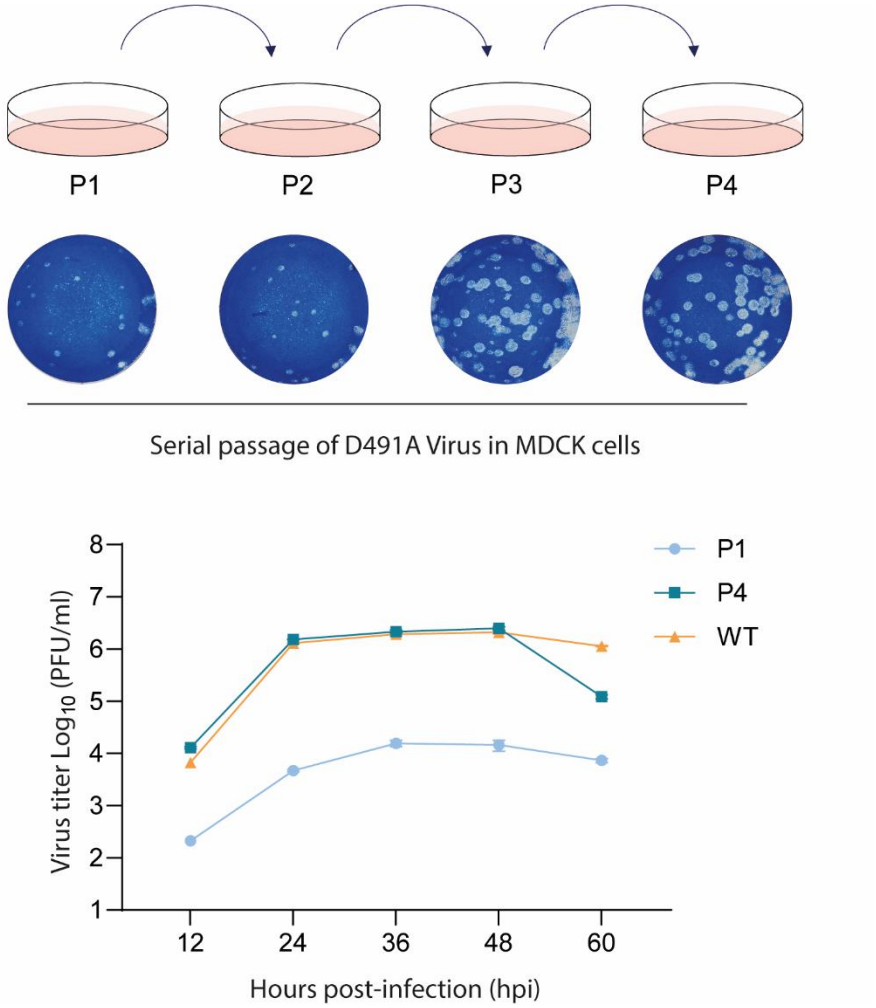

Fig. 4.8 The replication fitness of NP D491A virus rapidly reverted to the level of the wildtype virus after serial passages in MDCK cells.

NP D491A virus was serially passaged using MDCK cells for four passages (P1 to P4). Plaque phenotypes of P1, P2, P3, and P4 are shown in the upper panel. The growth kinetics of P1, P4, and WT were measured in parallel using MDCK cells at an MOI of 0.01 at 37 ℃. Supernatants were collected at 12, 24, 36, 48, and 60 hpi. Virus titers were measured by plaque assay using MDBK cells.

Subsequent NGS analysis of viral RNA from P1 to P3 viruses (performed by Kung-Yu Chen) revealed that the P3 virus acquired only three mutations, either in PB1 or NP **(Table. 4.1)**. Notably, the reversion of alanine to aspartic acid at residue 491 occurred in approximately 2% of P3 viruses, which is unlikely to account for the significant proportion of the reverted plaque phenotype shown in the P3 virus. The percentage of PB1 I364L mutation rapidly increased from 23% to 97%, suggesting that this mutation might be associated with the reversion of P3 virus. To address this question, I rescued the double mutant virus carrying both NP D491A mutation and PB1 I364L mutation. However, this double mutant virus displayed similar plaque phenotype as the NP D491A virus (**Fig. 4.9)**, indicating that PB1 I364L mutation alone is not responsible for the reversion of the NP D491A virus. It is worth noting that I have not yet tested the effect of NP I33M mutation on viral fitness due to time constraints.

Mutations	P1	P2	P3
NP A491D	1%	1%	2%
NP I33M	4%	5%	6%
PB1 I364L	23%	81%	97%

Table. 4.1 Identified mutations from P1 to P3 viruses by NGS analysis.

Total RNA was harvested from NP D491A and its P1, P2, and P3 viruses. RNA was subjected to NGS analysis (performed by Kuang-Yu Chen). The ratios of the indicated mutations are shown in the table.

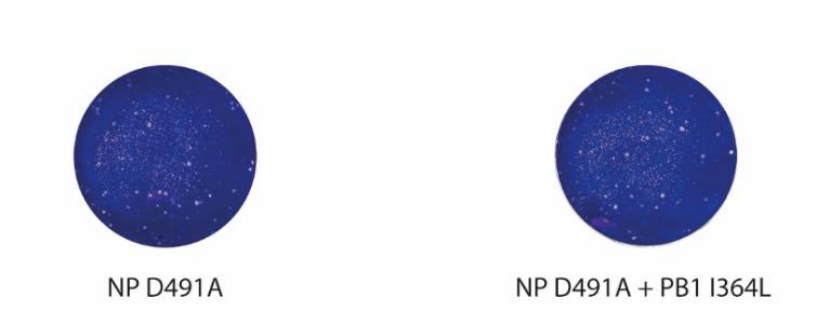

Fig. 4.9 Plaque phenotypes of NP D491A virus and NP D491/ PB1 I364L virus.

Plaque phenotypes of NP D491A virus and double mutant virus NP D491/ PB1 I364L virus were determined on MDBK cells.

4.3 Discussion

NP is one of the most critical viral factors in regulating RNA synthesis during influenza virus genome replication and transcription (119, 159). The critical functions of various domains in NP have been revealed with the assistance of multiple available crystal structures of NP (123, 124, 156, 158). However, the C-terminal tail of NP, which has been structurally shown to mediate NP-NP dimerization and to block the G2 binding groove (123, 229), is poorly characterized for its biological functions. In this chapter, I demonstrated that NP C-terminal tail is essential for replication of the full-length vRNA template **(Fig. 4.2)**. Using cRNA stabilization assay, I showed that the C-terminal tail of NP is required for replication and stabilization of cRNA, and mutation of acidic residues at 491 and 495 resulted in reduced cRNA stabilization ability **(Fig. 4.3)**. Furthermore, I established a split-luciferase assay which allows to monitor transient FluPol-NP interactions in cellular conditions **(Fig. 4.4)**. Using a series of truncated PB2 constructs, I mapped critical domains in PB2 that contribute to FluPol-NP interactions **(Fig. 4.5)**. The

split-luciferase assay results indicate that NP C-terminal tail is important for robust FluPol-NP interactions in addition to the formation of NP dimer **(Fig. 4.6)**. In agreement, by rescuing mutant viruses harbouring mutations in the NP C-terminus, I found that the mutant virus carrying NP D491A, a previously reported NP-NP dimer defective mutation, was profoundly attenuated **(Fig. 4.7)**. Intriguingly, the attenuated NP D491A virus rapidly reverted to wildtype-phenotype **(Fig. 4.8)**, suggesting the lost function of the NP C-terminal tail was quickly restored.

Our finding that the NP C-terminal tail, particularly residue 491, is important for cRNA stabilization ability, agrees with a previous study showing that the D491A mutation decreases luciferase signal in the mini-replicon luciferase reporter assay (229). Here, I elucidated that this defect in RNA synthesis occurs in the cRNA stabilization process. Although NP is not the most essential component for stabilizing cRNA, its presence markedly increases the amount of cRNA being stabilized (164). Deletion of the NP C-terminal tail enhances the RNA binding affinity of NP (123, 229), which is a change that should not account for the defective cRNA stabilization ability. Structurally, NP C-terminal tail deletion or NP D491A mutation disrupts the NP dimer (229). While NP homo-oligomerization has been deemed dispensable for cRNA stabilization, it is important to note that the oligomerization-deficient mutations (R416A or E339A) tested in these studies were used to disrupt the tail-loop mediated oligomerization, but not the NP dimer mediated by the NP C-terminus (164). Further investigation is warranted to determine the role of NP dimer in cRNA stabilization.

I observed that the C-terminal tail of NP is required for robust interactions between viral polymerase and NP. It is possible that the diminished FluPol-NP interactions resulting

from mutations or deletion in NP C terminal tail led to the dampened cRNA stabilization ability. Proper FluPol-NP interactions have been implicated in host adaptation and switch from transcription to replication (132, 165, 232); however, most of these studies are controversial and the molecular details of FluPol-NP interactions remain elusive. NP has also been shown to individually interact with different polymerase subunits (132), which was also observed in our data that PB2 can interact with NP in the absence of PB1 and PA. It is worthwhile to explore the effect of NP C-terminal tail deletion or mutations on the interactions between NP and individual polymerase subunits. As we have shown in chapter 3, deletion of the NP C-terminal tail exposes the G2 binding grooves which, in turn, could result in a stronger NP-ANP32 interaction. The abnormally stronger NP-ANP32 interactions may impede the binding of NP to nascent RNA products, leading to impaired cRNA stabilization. Reduced NP availability also has been reported to promote host immune recognition (233). Therefore, ascertaining the antiviral responses in presence of these mutant NP can also provide us insights into the molecular mechanisms of how NP C-terminal is involved in viral RNA synthesis.

I also validate the impact of NP D491 mutation in the scenario of virus infection. I demonstrated that NP D491A mutant virus is highly attenuated, in agreement with previous findings that this mutation diminishes viral RNA synthesis (229). Intriguingly, NP D491A virus rapidly reverted to wildtype phenotype after three passages, although 98% of the P3 viruses still retained the D491A mutation, suggesting the virus might regain its fitness via the other two potential compensatory mutations identified by NGS analysis. Due to time constraints, I have not yet tested the effect of all these mutations on viral fitness. Further studies on this will provide us with a comprehensive understanding of the role of the NP C-terminus in influenza A virus replication.

CHAPTER 5

Development of a cRNP replication reconstitution system for uncoupling vRNA and cRNA synthesis of influenza A virus

5.1 Introduction

The replication of the influenza A virus genome involves a primer-independent, two-step RNA synthesis catalysed by the heterotrimeric RNA-dependent-RNA polymerase (23, 67). The replication process starts with the synthesis of complementary RNA (cRNA) from incoming vRNP (vRNA → cRNA). The newly synthesized cRNA is co-replicationally assembled into cRNP for the downstream synthesis of progeny vRNA (cRNA → vRNA) (119). It has been well demonstrated that the avian influenza polymerase cannot function well in mammalian cells due to species-specific differences in ANP32 proteins, essential host factors mediating influenza virus polymerase dimerization (204, 206, 213). Several mechanistic studies have implied that this host restriction only impedes vRNA synthesis (cRNA → vRNA) by avian virus polymerase while leaving cRNA synthesis (vRNA → cRNA) unaffected (174, 209). A previously reported cRNA stabilization assay measuring cRNA synthesis/accumulation alone by blocking progeny vRNA synthesis allows separate investigation of the step of vRNA → cRNA (163). However, due to the interdependency of vRNA synthesis and cRNA synthesis, there is currently no direct method to uncouple these two steps of viral replication and to evaluate vRNA synthesis independently.

Numerous endeavours have been undertaken to recreate RNA synthesis process by influenza viral polymerase in a test tube, although most of these methods were proven to be technically challenging or inefficient due to the limited understanding of the fundamental replication mechanism of influenza virus at that time (228, 234-236).

Recently, our group has established an *in vitro* vRNP replication reconstitution system that could recapitulate viral transcription and the full cycle of genome replication in a test tube using virion-derived vRNPs and recombinant viral and host factors (165). Drawing inspiration from this system and a previously reported method for isolation of cRNPs of influenza A virus (191), I aim to develop a cRNP replication reconstitution system that could be used to explore the molecular details of vRNA synthesis from cRNP without the interference of vRNA synthesis.

5.2 Results

5.2.1 Isolation of vRNPs or cRNPs

To develop an *in vitro* cRNP replication reconstitution assay, I first isolated cRNPs of influenza A virus using a previously described RNA-based affinity purification strategy from infected cells (191). This strategy takes advantage of the robust binding affinity of the coat protein of *Pseudomonas aeruginosa* bacteriophage 7 (PP7) to an optimized RNA affinity tag composed of a hairpin stem-loop **(Fig. 5.1A)** (237). Using reverse genetics, the recombinant influenza A/WSN/33 virus and its avian cognate WSN (PB2 627E) virus, with the insertion of PP7 RNA tag in their neuraminidase (NA) segment, were successfully rescued and grown to high titers. The inserted RNA tag enables the separation and isolation of vRNP and cRNP complexes **(Fig. 5.1B)**. These viruses were subsequently used to infect cells expressing strep-PP7 coat protein, leading to the generation of viral RNP complexes bound by strep-PP7 coat protein for the downstream affinity purification. To improve the yield and quality of vRNPs and cRNPs, I made several modifications of the previously published method (191). First, I replaced the adherent 293T cells with the suspension FreeStyle 293 expression system (293-F cells) for the large-scale purification of vRNPs and cRNPs. Furthermore, BioLock, a commercially available biotin blocking solution

containing avidin, was added during the strep purification step to reduce the non-specific binding of biotin/biotinylated proteins to Strep-Tactin beads.

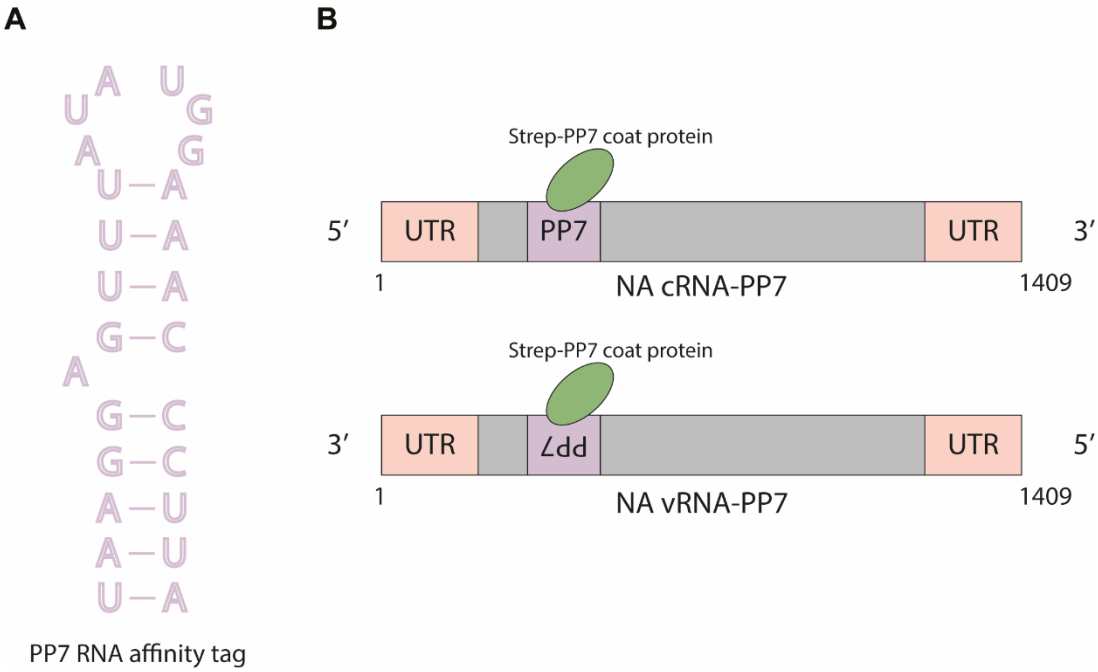

Fig. 5.1 RNA tag-based affinity purification of influenza A virus vRNPs and cRNPs

(A) Sequence and schematic diagram of PP7 RNA tag that binds to PP7 coat protein. (B) PP7 tag was inserted into the NA segment of influenza A/WSN/33 virus for the generation and isolation of vRNPs and cRNPs. The coding sequence of NA segment was labelled in grey, the untranslated terminal sequences (UTR) were labelled in pink. The PP7 coat protein is strep-tagged for purification purpose.

Results of primer extension analysis and silver staining of glycerol gradient fractions containing RNPs confirmed the presence of vRNA, cRNA, polymerase complex, and NP, indicating that both vRNPs and cRNPs have been successfully isolated **(Fig. 5.2 and Fig. 5.3)**. Although the bands for polymerase complex were not distinctly visible in the silver staining results of the wildtype (627K) vRNP and cRNP fractions **(Fig. 5.2)**, probably due to the relative low yield from a small scale of preparation and high background of the gel, primer extension analysis showed distinct vRNA and cRNA bands which were indicators used for the selection of fractions containing vRNPs and cRNPs. Similarly, the avian (627E) vRNP and cRNPs were also successfully isolated judging from the presence of polymerase complex and NP along with vRNA and cRNA bands observed by primer extension analysis (**Fig. 5.3)**. The cRNP preparation was slightly contaminated by vRNP, which was also observed by others in our lab, suggesting that the specificity of the tag is not perfect. However, the proportion of this vRNA contamination is minimal and thereby the potential interference from it is considered negligible in our downstream functional analysis.

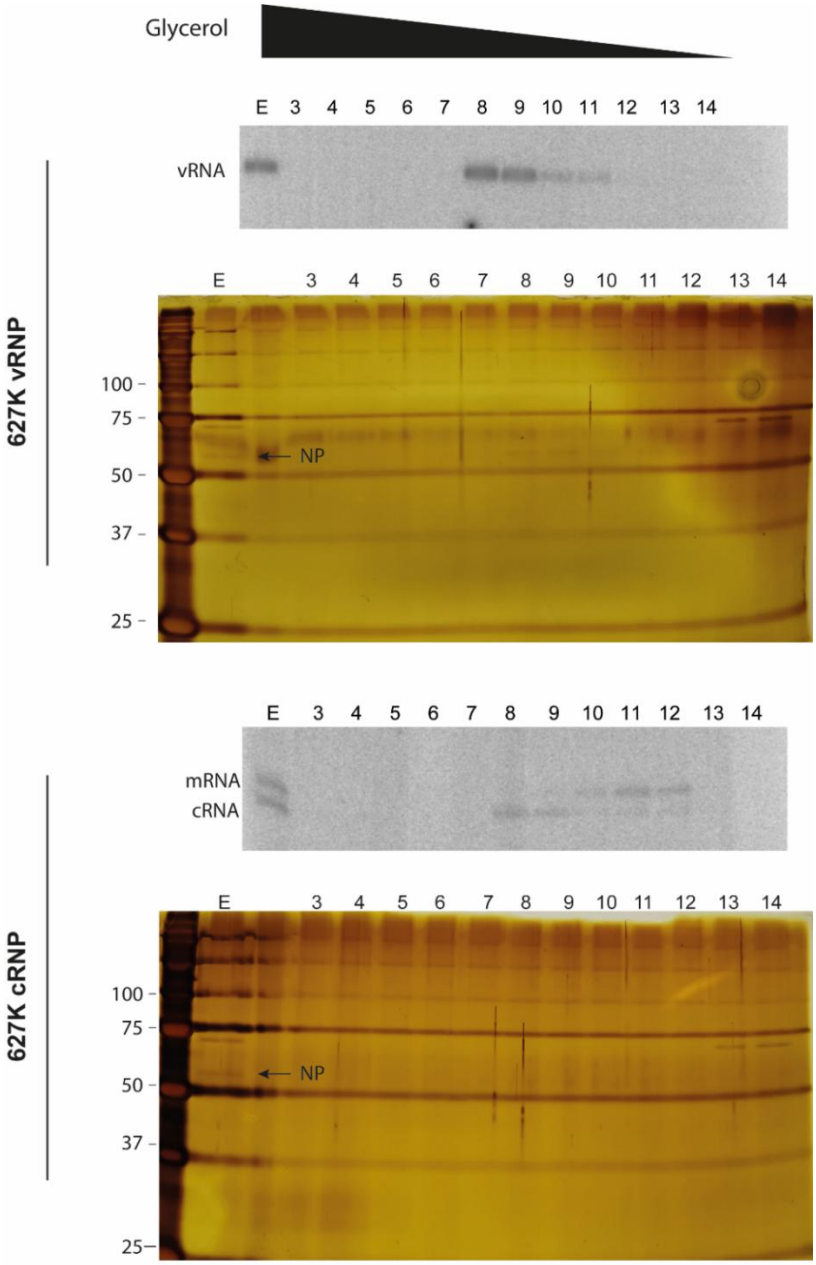

Fig. 5.2 Primer extension analysis and silver staining analysis of glycerol gradient fractions containing vRNPs or cRNPs (627K).

RNA from each glycerol gradient fraction was analysed by primer extension assay using NA primers that anneal to the NA segment. Protein samples from each fraction were separated by SDS-PAGE and silver stained. E represents the eluate after strep-tag purification; The position of NP band is labelled with an arrow; the number indicates the order of fractions collected after glycerol gradient centrifugation; molecular weight markers are indicated in kDa.

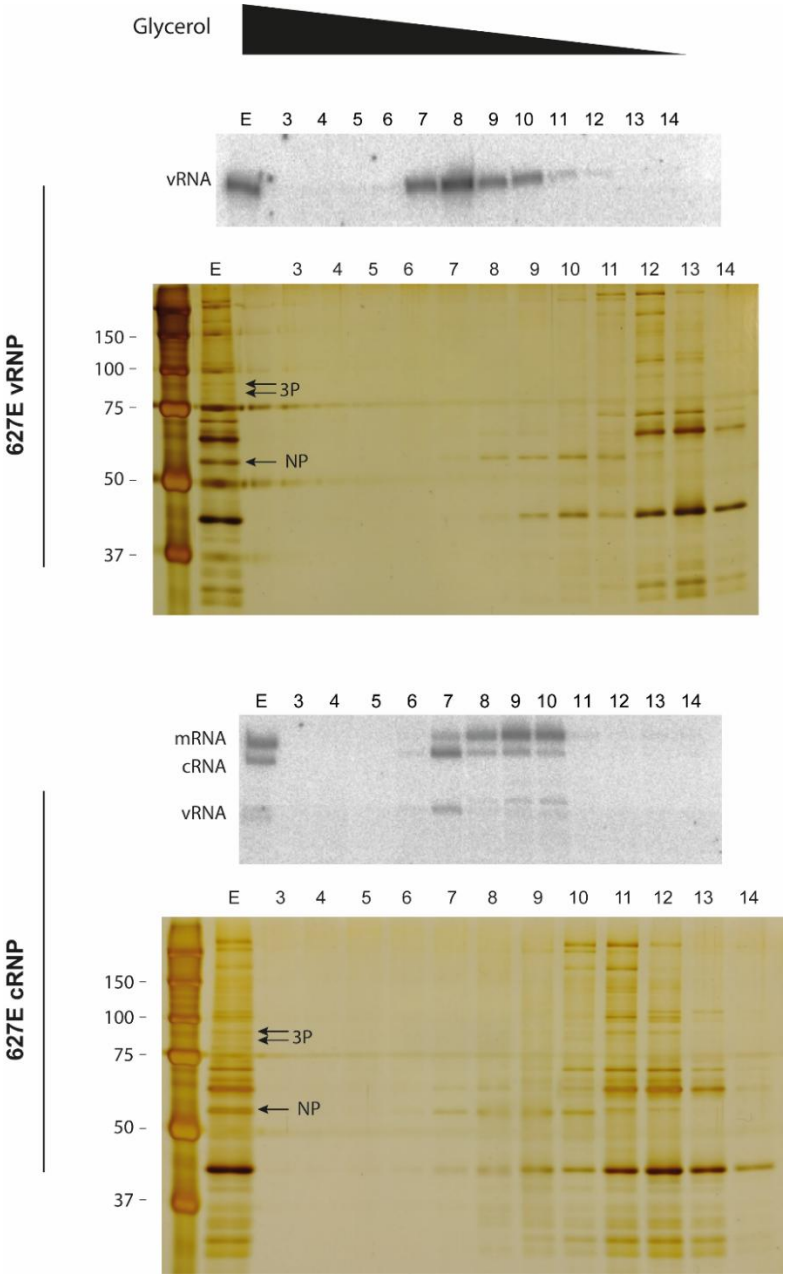

Fig. 5.3 Primer extension analysis and silver staining analysis of glycerol gradient fractions containing avian-like vRNPs or cRNPs (627E).

RNA from each glycerol gradient fraction was analysed by primer extension assay using NA primers that anneal to the NA segment. Protein samples from each fraction were separated by SDS-PAGE and silver stained. E represents the eluate after strep-tag purification; 3P represents the polymerase complex; the position of NP band is labelled with an arrow; the number indicates the order of fractions collected after glycerol gradient centrifugation; molecular weight markers are indicated in kDa.

5.2.2 Preparation of recombinant FluPol, NP, and human ANP32B

The Fodor lab's recent study has highlighted that the minimal components required for *in vitro* replication from virion-derived vRNPs includes viral polymerase, NP, and ANP32 proteins (165). Therefore, I purified recombinant viral polymerase complex expressed in insect cells, as well as ANP32 protein and NP protein expressed in *E. coli* **(Fig. 5.4)**. It should be noted that the recombinant polymerase complex is from influenza A/NT/60/1968 (H3N2) virus instead of the WSN virus due to the technical difficulties in protein expression and purification of the WSN viral polymerase. Both the wildtype NT60 (PB2 627K, designated as K) polymerase and its avian cognate NT60 (PB2 627E, designated as E) were expressed and purified. The corresponding catalytic inactive version of NT60 polymerases with double mutations in its active site (PB1a: D445A/D446A, designated as Ea or Ka depending on the signature of PB2 627 residue) were simultaneously expressed and purified.

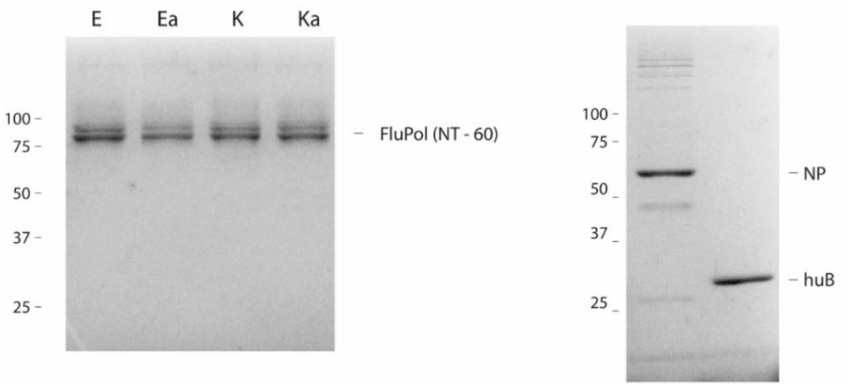

Fig. 5.4 Analysis of purified recombinant viral polymerase (FluPol), NP, and huANP32B by SDS-PAGE and staining with Coomassie Brilliant Blue.

The wildtype NT60 viral polymerase (K) and its avian-like mutant NT60 (E) as well as the corresponding catalytically inactive (PB1a) mutants: NT60 (PB1a, designated as Ka) and avian-like NT60 (PB1a, Ea) were purified from insect cells. NP of NT60 virus and huANP32B protein purified from *E. coli*. Proteins samples were separated by SDS-PAGE and stained with Coomassie Brilliant Blue. Molecular weight markers are indicated in kDa.

5.2.3 *In vitro* vRNP or cRNP reconstitution assay

To validate the previously reported minimal components for *in vitro* replication (165), I used the PP7-vRNP (PB2-627E) or PP7-cRNP (PB2-627E) in the replication system with the indicated omission of huANP32B, NP, viral polymerase (K polymerase), or ribonucleotide triphosphate (rNTPs) substrates in each condition **(Fig. 5.5)**. In the absence of rNTPs, only input vRNA **(lane 5)** and cRNA **(lane 10)** from the purified PP7-RNPs were detected. The faint vRNA band observed in cRNPs in the absence of rNTPs represents vRNP contamination mentioned earlier. In the presence of ANP32 protein, viral polymerase, and NP, the isolated vRNP generated newly synthesized cRNA and the cRNP generated progeny vRNA **(lanes 1 & 6)**, indicating these isolated PP7-RNPs are catalytically active and can be used for setting up the *in vitro* replication reconstitution system. Omission of huANP32B greatly dampened the replication for both vRNP and cRNP **(lanes 2 & 7)**, highlighting the crucial role of ANP32 protein in influenza virus genome replication (188). Surprisingly, the exclusion of NP resulted in enhanced RNA synthesis **(lane 3 & 8)**, which could be attributed to the depletion of ANP32B by the high level of NP in the system. As expected, the absence of additional viral polymerase completely abolished the replication for both vRNP and cRNP **(lane 4 & 9)**, reaffirming the indispensable noncatalytic role of viral polymerase during replication. Overall, these results demonstrate that the vRNPs and cRNPs isolated through RNA-based affinity purification are catalytically active and could be used to set up the *in vitro* vRNP and cRNP replication reconstitution system for the recapitulation of vRNA synthesis and cRNA synthesis in a test tube.

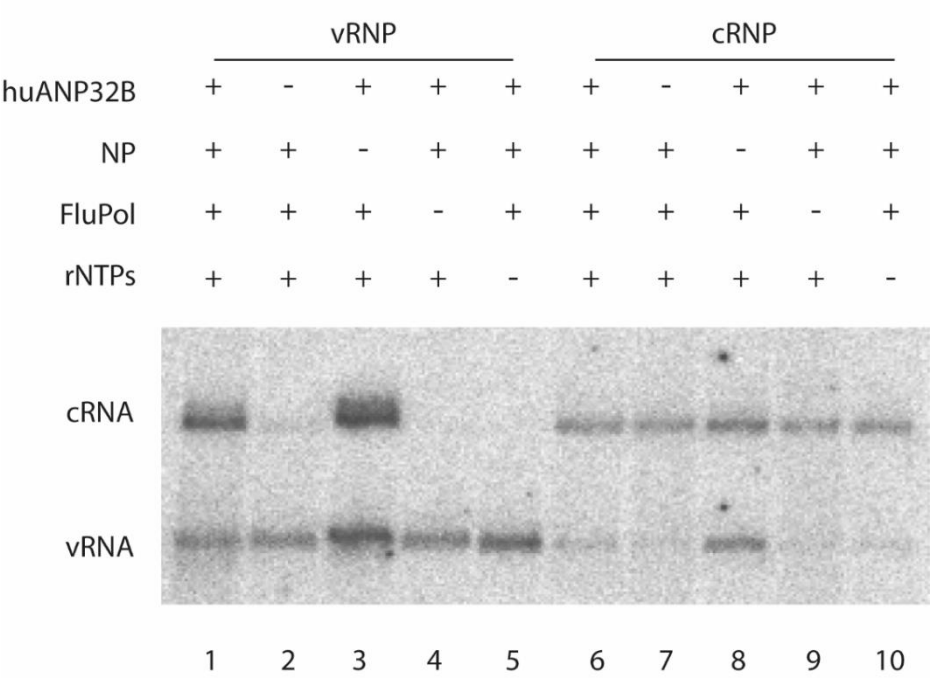

Fig. 5.5 *In vitro* vRNP or cRNP replication reconstitution assay.

The isolated vRNPs or cRNPs were respectively incubated with the indicated viral or host factors at 30 °C for 4 hours in the presence or absence of rNTPs. The RNA was extracted from each reaction and subjected to primer extension analysis with primers annealing to NA segment of WSN virus.

5.3 Discussion

By combining our recently reported *in vitro* RNP replication reconstitution system with an improved influenza A virus cRNPs isolation technique (165, 191), I managed to achieve *in vitro* replication starting from cRNPs. Meanwhile, I also successfully expressed and purified recombinant viral polymerase carrying different mutations at the 627 residue of the PB2 protein, which could be used to explore the molecular details of how the signature of PB2 627 residue influences viral RNA synthesis, particularly vRNA synthesis, a step believed to be defective during avian influenza virus replication in human cells.

The experiment using cRNPs (627E) marks the first instance of using cRNPs carrying PB2 627E, a distinctive feature of avian influenza virus polymerase which cannot use human ANP32 proteins (188, 213). In this *in vitro* cRNP replication reconstitution system, this avian-like cRNP (PB2 627E) can be used to ascertain whether the adaptation status of the replicating polymerase on cRNP affects vRNA synthesis. Conversely, using the recombinant viral polymerase with PB2 627E, I can address the question of whether the adaptation status of the encapsidating polymerase influences vRNA synthesis. The results from these experiments could resolve this long-standing puzzle in the field of influenza virology. However, it should be noted that the currently available results for this chapter are preliminary due to time constraints, and more optimization and replicates are needed for this replication system.

CHAPTER 6

The dynamic interplay between nuclear export protein (NEP) and factors involved in influenza virus replication

6.1 Introduction

As a negative-sense RNA virus, influenza A virus packages its eight segments of viral RNA in viral ribonucleoproteins (vRNPs) comprising the RNA-dependent RNA polymerase (FluPol) and nucleoprotein (NP) (23, 67). The life cycle of influenza A virus centers on vRNPs which serve as the template for both transcription and replication (119). Viral transcription is a primer-dependent process which requires capped RNA primers snatched from nascent RNA polymerase II (Pol II) transcripts (66). Binding of Pol II C-terminal domain (CTD) to viral polymerase represents a hallmark of viral transcription as it induces the viral polymerase transcriptase conformation (178). Replication of influenza A virus is a *de novo* process which involves cRNA synthesis and vRNA synthesis (238). The distinct mechanisms used in viral transcription and replication have led to the "switch model" in which the viral polymerase needs to undergo transition from transcriptase to replicase (165, 176). Alternatively, a stabilization model has been proposed that synthesis of mRNA or cRNA are regulated in a stochastic manner but cRNA is degraded by host nucleases until it is stabilized by sufficient amounts of newly synthesized viral RdRp and NP (163).

The 121-amino acids-long NEP is a multifunctional protein translated from a spliced mRNA derived from segment 8 (NS segment) (71). One of the well-demonstrated functions of NEP is nuclear export of vRNPs (72, 76, 169). NEP contains two nuclear export signals (79, 169), which allow it to facilitate nuclear export of vRNP by hijacking

the cellular CRM1 nuclear export *machinery* (72). In addition to the nuclear export function, recent studies have found that NEP can regulate mRNA (transcription), vRNA and cRNA (replication) accumulation levels (83, 171-173), pointing to the regulatory function of NEP in RNA synthesis by the viral polymerase. This regulatory function has been linked to the switch from transcription to replication, given the observation that NEP level reaches a plateau at late stage of infection and overexpression of NEP in the vRNP reconstitution assay enhances vRNA and cRNA accumulation (171, 173, 177). Additionally, mutations in NEP have been shown to compensate for the defective replication by avian influenza virus polymerase, in agreement with the regulatory role of NEP in viral replication (174). Interestingly, the most recent studies have linked the replication-enhancing effect of NEP to the last residues of NEP (residue I121) and found that the hydrophobic nature of this residue is essential for viral fitness (172, 173). Nevertheless, the molecular mechanism for this regulatory function of NEP in viral RNA synthesis remains elusive, although different mechanisms such as svRNA (small viral RNAs)-mediated regulation or modulating of FluPol dimerization have been proposed (172, 173, 175, 176). Moreover, it is also unclear whether the regulatory function and the vRNP nuclear export function of NEP are interdependent or not, as evidenced by the observation that the absence of NEP nuclear export signal does not affect the regulatory function of NEP (171).

In this chapter, I aim to reveal the molecular details of the regulatory function of NEP in viral RNA synthesis. Particularly, I will address this question based on the first available structure of FluPol-NEP complex as recently resolved in the Fodor lab.

6.2 Results

6.2.1 NEP regulates viral RNA synthesis in a dose-dependent manner

The regulatory function of NEP in viral RNA synthesis (replication and transcription) has been reported by different groups (83, 171-176). These studies consistently demonstrate a stimulatory effect on viral replication with a low amount of NEP. However, discrepancies arise in observations on the inhibitory effect on viral RNA synthesis, particularly vRNA synthesis, caused by a high-dose of NEP. Additionally, adaptive mutations on NEP have been shown to restore the restricted activity of avian virus polymerase in human cells (174). To elucidate the regulatory function of NEP in viral RNA synthesis, I first performed vRNP reconstitution assay in the absence or presence of NEP in the huANP32A and huANP32B double-knockout 293T cells (293T-DKO). Replication was abrogated when ANP32 proteins, key factors supporting viral replication (188, 211), were missing in the system despite the presence of NEP **(Fig. 6.1A)**. Complementation of 293T-DKO cells with huANP32A restored the replication, and overexpression of NEP further enhanced viral RNA synthesis, demonstrating that the stimulatory effect on viral RNA synthesis by NEP cannot bypass the critical function of ANP32 proteins. I next examined the effect of NEP on viral RNA synthesis in a dose-dependent manner using vRNP reconstitution assay in 293T cells. Low amounts of NEP markedly increased vRNA, cRNA, and mRNA accumulation levels in the system, consistent with previous reports that NEP stimulates viral RNA synthesis **(Fig. 6.1B)** (171, 173). Nevertheless, overexpression of a high-dose of NEP still elevated vRNA and cRNA levels , albeit to a lesser extent compared to that in cells expressing a low-dose of NEP. In contrast, mRNA level was moderately reduced in the presence of a high-dose of NEP compared with that in vector-expressing cells where no NEP was expressed (vec, no NEP), suggesting a role of NEP in switching the viral polymerase from transcription to replication. It should be noted that there was still a robust

level of viral RNA synthesis occurring even in the presence of a high-dose of NEP, contradicting previous observations that a high-dose of NEP could fully suppress RNA synthesis or transcription alone (83, 174), probably due to different origins of viral polymerase and NEP used in these studies or different replication efficiency of the vRNP reconstitution assay. Overall, these results confirmed the regulatory function of NEP in viral replication and transcription.

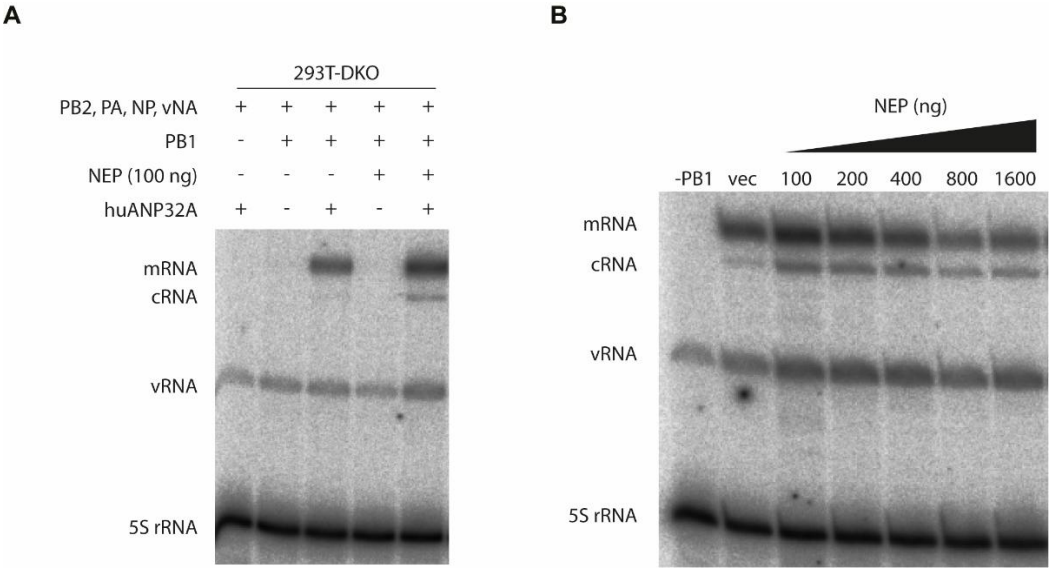

Fig. 6.1 NEP regulates viral RNA synthesis in a dose-dependent manner.

(A) vRNP reconstitution assay in 293T-DKO cells. 293T-DKO cells were transiently transfected with the indicated plasmids expressing PB2 (500 ng), PB1 (500 ng), PA (500 ng), NP (2000 ng), NEP (100 ng), huANP32A (1000 ng) proteins and a pPolI-vNA plasmid (100 ng) expressing the NA segment of the WSN virus. (B) vRNP reconstitution assay in 293T cells with increasing amounts of NEP. 293T cells were transiently transfected with 500 ng of plasmids expressing PB2, PB1, PA, 2000 ng of plasmid expressing NP, 100 ng of pPolI-vNA plasmid expressing the NA segment of the WSN virus along with the indicated amounts of plasmids expressing NEP from WSN virus. PB1 was omitted in the negative control. Total RNA was harvested at 24 hpt. and analysed by primer extension assay.

6.2.2 NEP interacts with FluPol

To uncover the molecular basis for the regulatory function of NEP on viral polymerase, I established a split-*Gaussia* luciferase assay to measure FluPol-NEP interactions **(Fig. 6.2A)**. I found that the viral polymerase subunits, particularly PA subunit, with C-terminally tagged Luc2 and NEP with C-terminally tagged Luc1, generated strong luminescence in the context of the full polymerase complex **(Fig. 6.2B)**. Exclusion of any two out of the three polymerase subunits resulted in reduced FluPol-NEP interactions.

6.2.3 FluPol-NEP interactions are mainly contributed by PB1 and PA.

I extended our study to the previously described PB2 truncated mutants and measured their effects on FluPol-NEP interactions in this split-luciferase assay (231). Intriguingly, the omission of PB2 did not completely disrupt the FluPol-NEP interactions as the omission of PA did when PB1-Luc2 and NEP-Luc1 were used as probes **(Fig. 6.3)**. In contrast, the FluPol-NEP remained almost unaffected when PA-Luc2 and NEP-Luc1 were used as probes. Notably, the deletion of major parts of PB2, including the cap-binding domain or 627 domain, did not affect or even stimulated FluPol-NEP interactions, further suggesting that PB2 might not contribute to the major interface for FluPol-NEP interactions. However, these data need to be interpreted with caution as no western blots have been performed to address whether all PB2 fragments are expressed equally well.

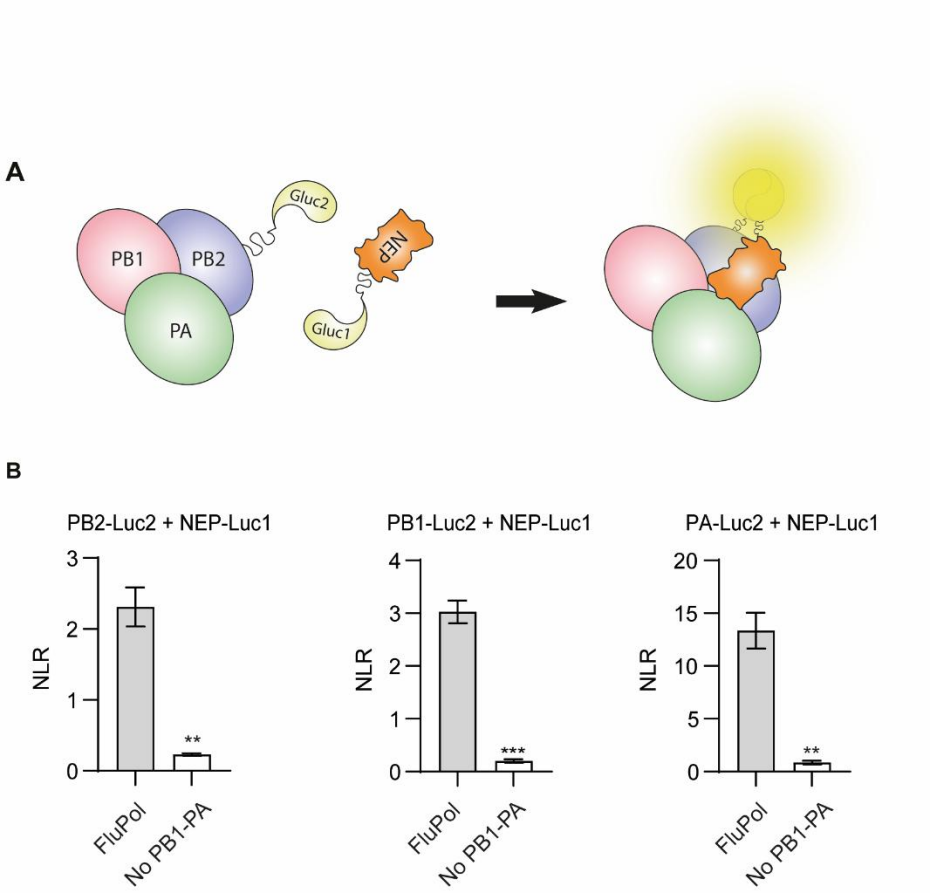

Fig. 6.2 Establishment of split-*Gaussia* luciferase assay for measuring FluPol-NEP interactions.

(A) Schematic diagram of the split-*Gaussia* luciferase assay to measure FluPol-NEP interactions. One of the influenza A virus polymerase subunits (PB2, PB1, or PA) was C-terminally tagged in frame with Gluc2 and NEP was C-terminally tagged in frame with Gluc1. If FluPol and NEP interact, luciferase is reconstituted, and its activity is measured using a luciferase assay. (B) 293T cells were transfected with the indicated luciferase-tagged polymerase subunit and NEP together with the remaining two polymerase subunits. As negative controls, two of the three polymerase subunits were omitted in each setting. Luminescence was measured from cell lysate at 24 hpt. Normalized luciferase ratio (NLR) was calculated as described in the Materials and Methods chapter. Data represent at least three independent experiments performed in technical duplicates (mean ± SEM of n=3 biological replicates) $^{**}P < 0.01$, $^{***}P < 0.001$ (two-tailed, unpaired Student's *t*-test).

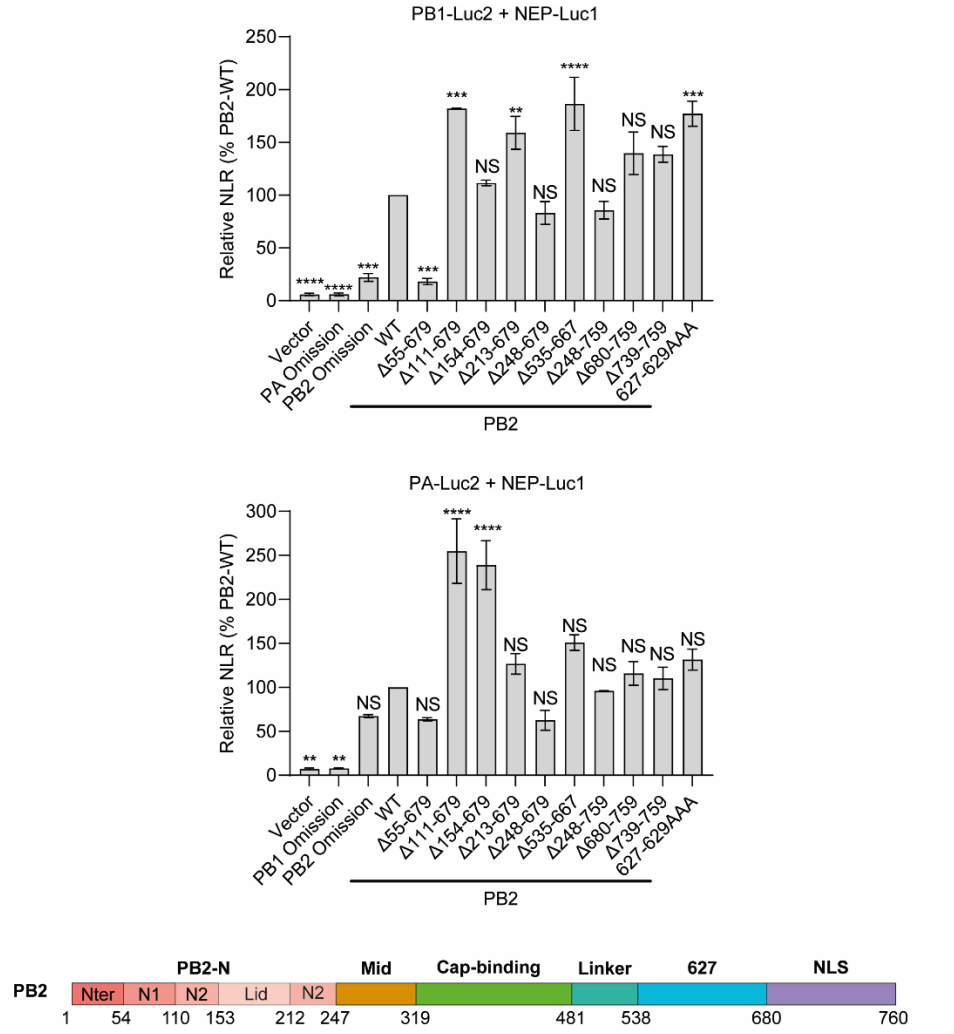

Fig. 6.3 FluPol-NEP interactions are mainly contributed by PB1 and PA.

293T cells were transfected with the indicated PB2 truncated mutants with the split-luciferase constructs to measure FluPol-NP interactions. PB1-Luc2 and NEP-luc1 combination was used in the upper panel; PA-Luc2 and NEP-Luc1 combination was used in the bottom panel. The assay with the omission of two polymerase subunits (Vector) was set as negative control. Luminescence from cell lysates was measured at 24 hpt. The luciferase activities are presented as percentage of NLR changes relative to the NLR for assay with wildtype PB2 (set as 100%). Data represent at least four independent experiments performed in technical duplicates (mean ± SEM of n=4 biological replicates). $^{**}P < 0.01$, $^{***}P < 0.001$, $^{****}P < 0.0001$ (One-way ANOVA; Dunnett's multiple comparisons test). NS, not significant.

6.2.4 NP stimulates FluPol-NEP interactions

A previous study has found that the ablation of NEP inhibits the cytoplasmic accumulation of NP (76); however, there has been no investigation into the effect of NP on FluPol-NEP interactions. To address this question, I co-expressed an increasing amount of NP in the split-luciferase assay measuring FluPol-NEP interactions. Surprisingly, NP promoted FluPol-NEP interactions in a dose-dependent manner. A low amount of NP barely enhanced FluPol-NEP interactions, while a high-dose of NP strongly facilitated FluPol-NEP interactions **(Fig. 6.4A)**. I also assessed the effect of mutant NP-G1 (4), known for its deficiency in RNA-binding (164), on FluPol-NEP interactions. Similarly, co-expression of a high-dose of NP-G1 stimulated FluPol-NEP interactions to a level that is even higher than that achieved by wildtype NP **(Fig. 6.4B)**, indicating the RNA binding ability of NP is dispensable for its stimulation of FluPol-NEP interactions. Treatment with endonuclease Benzonase did not affect the stimulatory effect of NP on FluPol-NEP interactions **(Fig. 6.4C)**. Taken together, these results suggest that NP strengthens FluPol-NEP interactions in a dose-dependent manner and the RNA binding ability of NP is not involved in this stimulation process. However, it should be noted that these data need to be interpreted with caution as the protein expression levels have not been confirmed to be the same at each condition, especially considering a previous study reporting that viral polymerase could be stabilized by viral RNA (239).

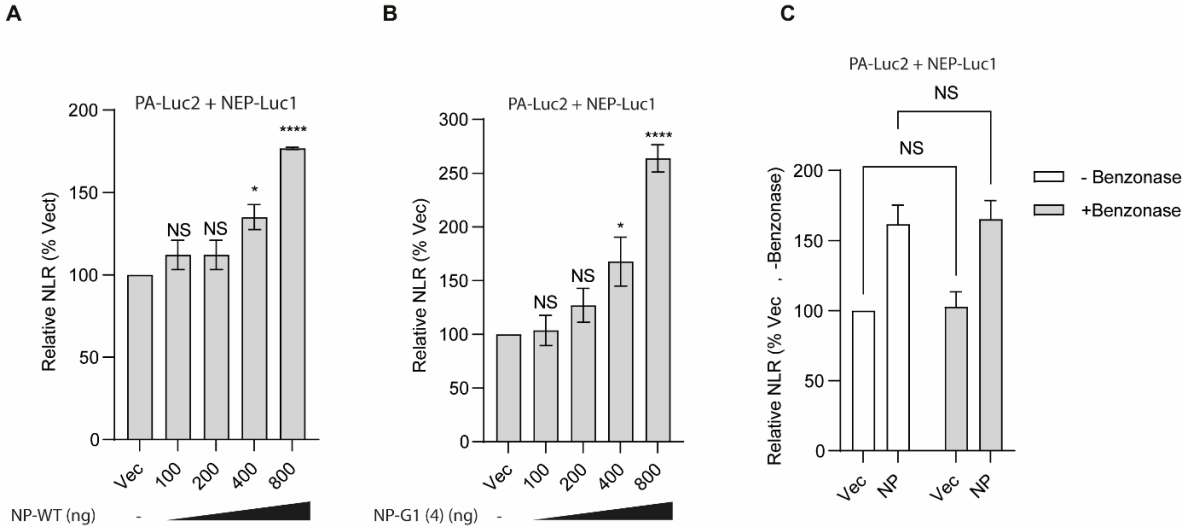

Fig. 6.4 NP stimulates FluPol-NEP interactions in a dose-dependent manner.

293T cells were transfected with plasmids expressing PA-Luc2, NEP-Luc2, PB2, PB1, and the indicated amount of plasmid expressing NP-WT (A) or RNA-binding defective NP-G1 (4) (including amino acid changes R74A, R75A, R174A, R175A, and R221A). (B) The luciferase activities are presented as percentage of NLR changes relative to the NLR in the absence of NP (Vec, set as 100%). Luminescence from cell lysates was measured at 24 hpt. Data represent at least three independent experiments performed in technical duplicates (mean ± SEM of n=3 biological replicates in A-B). *$P < 0.05$, ****$P < 0.0001$ (One-way ANOVA; Dunnett's multiple comparisons test). (C) 293T cells were transfected with plasmids expressing PA-Luc2, NEP-Luc2, PB2, PB1, and 800 ng of plasmid expressing NP-WT. 24 hpt, cell lysates were treated with or without Benzonase for an hour prior to the measurement of luminescence. The luciferase activities are presented as percentage of NLR changes relative to the NLR in the absence of NP and Benzonase treatment (Vec, -Benzonase, set as 100%). Data represent at least three independent experiments performed in technical duplicates (mean ± SEM of n=2 biological replicates in A-B). NS (Two-way ANOVA; Bonferroni's multiple comparisons test).

6.2.5 Both vRNA and cRNA stimulate FluPol-NEP interactions

Given the reported function of NEP in switching from transcription to replication during viral RNA synthesis (171, 173, 176), I sought to explore the effect of replication products on FluPol-NEP interactions. To simulate this scenario, I overexpressed vRNA or cRNA of the NA segment from the WSN virus using RNA polymerase I-driven plasmids in the split-luciferase assay. Surprisingly, both vRNA and cRNA stimulated FluPol-NEP interactions in a dose-dependent manner **(Fig. 6.5A)**. To determine whether the addition of NP, together with vRNA or cRNA, could further promote FluPol-NEP interactions, I simultaneously expressed a high-dose of NP and RNA in the split luciferase assay. The PB1 was replaced with catalytically inactive PB1a to prevent ongoing replication in the presence of NP, which ensures that RNA was only derived from the transfected RNA polymerase I-driven plasmids. As expected, addition of NP further increased this stimulatory effect on FluPol-NEP interactions by both vRNA and cRNA, probably due to the synergistic effect of NP and RNA **(Fig. 6.5B)**. Overall, I demonstrated that both vRNA and cRNA can stimulate FluPol-NEP interactions in a dose-dependent manner. However, it should be noted that these data need to be interpreted with caution as the protein expression levels have not been confirmed to be the same at each condition, especially considering a previous study reporting that viral polymerase could be stabilized by viral RNA (239).

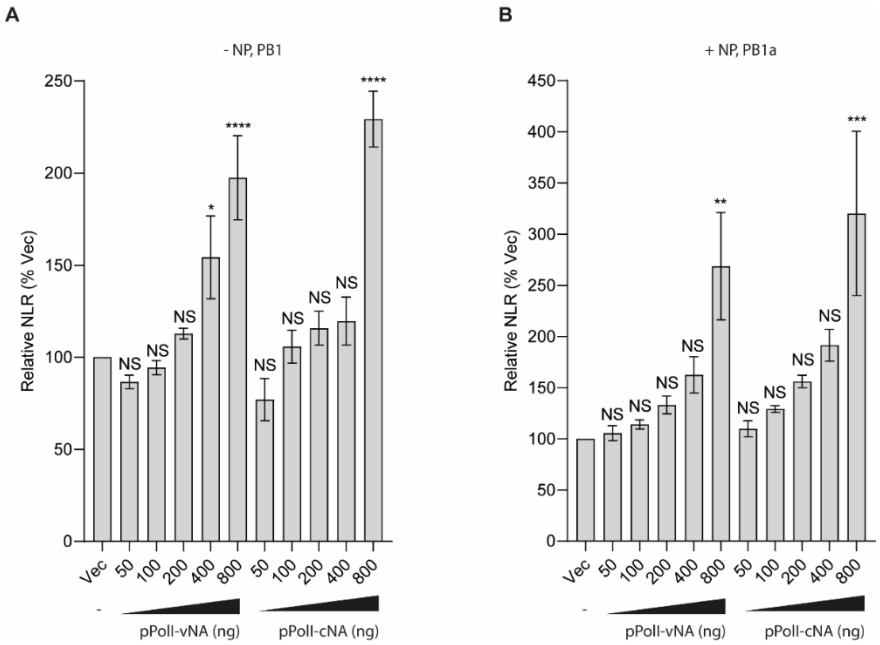

Fig. 6.5 vRNA or cRNA stimulates FluPol-NEP interactions in a dose-dependent manner.

(A) 293T cells were transfected with plasmids expressing PA-Luc2, NEP-Luc1, PB2, PB1, and the indicated amounts of plasmids expressing vRNA or cRNA of NA segment from the WSN virus. (B) 293T cells were transfected with plasmids expressing PA-Luc2, NEP-Luc1, PB2, catalytically inactive PB1a, 800 ng of plasmid expressing NP along with the indicated amounts of plasmids expressing vRNA or cRNA of the NA segment from the WSN virus. Luminescence from cell lysates was measured at 24 hpt. Data represent at least three independent experiments performed in technical duplicates (mean ± SEM of n=3 biological replicates in A-B). *$P < 0.05$, **$P < 0.01$, ***$P < 0.001$, ****$P < 0.0001$ (One-way ANOVA; Dunnett's multiple comparisons test). NS, not significant.

6.2.6 Pol II CTD increases FluPol-NEP interactions

I next determined the effect of the Pol II C-terminal domain (CTD) on FluPol-NEP interactions. CTD interacts with viral polymerase and promotes transcription (178), while NEP is recognised to switch the transcription to replication (171, 173, 176). In turn, I hypothesized that CTD might be able to diminish the interactions between the viral polymerase and NEP. Unexpectedly, I noticed that overexpression of a high-dose of mouse Pol II CTD increased FluPol-NEP interactions by an unknown mechanism **(Fig. 6.6)**. This upregulation of FluPol-NEP interactions by a high-dose of CTD warrants further investigation, especially a validation on protein expression levels. Due to the time constraints and lack of an antibody, I have not evaluated protein expression levels in this assay.

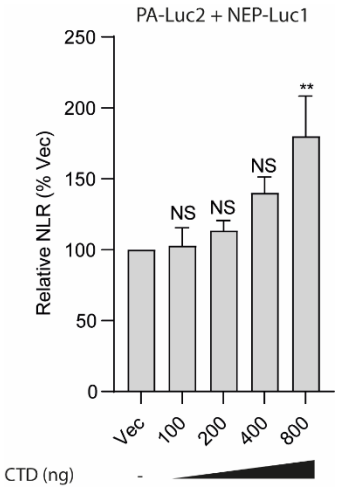

Fig. 6.6 Pol II CTD stimulates FluPol-NEP interactions in a dose-dependent manner. 293T cells were transfected with plasmids expressing PA-Luc2, NEP-Luc1, PB2, PB1, and the indicated amount of plasmid expressing mouse Pol II CTD. Luminescence from cell lysates was measured at 24 hpt. Data represent at least three independent experiments performed in technical duplicates (mean ± SEM of n=3 biological replicates). **P < 0.01 (One-way ANOVA; Dunnett's multiple comparisons test). NS, not significant.

6.2.7 CRM1 dampens FluPol-NEP interactions

One of the key functions of NEP during influenza virus replication is facilitating the nuclear export of vRNP through the cellular CRM1 export pathway (72, 76, 169). To assess the effect of CRM1 on FluPol-NEP interactions, I expressed an increasing amount of CRM1 in the split-luciferase assay, and found that CRM1, especially overexpressed at a high-dose, profoundly damped FluPol-NEP interactions **(Fig. 6.7)**, probably due to the competition of direct binding between NEP and CRM1, which has been reported previously. Due to the time constraints and lack of an antibody, I have not evaluated protein expression levels in this assay.

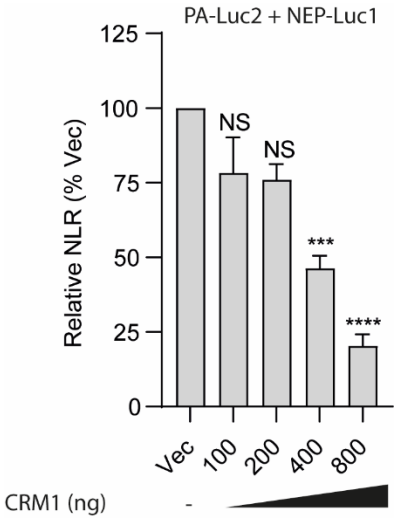

Fig. 6.7 CRM1 dampens FluPol-NEP interactions in a dose-dependent manner.

293T cells were transfected with plasmids expressing PA-Luc2, NEP-Luc1, PB2, PB1, and the indicated amount plasmid expressing CRM1. Luminescence from cell lysates was measured at 24 hpt. Data represent at least three independent experiments performed in technical duplicates (mean ± SEM of n=3 biological replicates). ***$P < 0.001$, ****$P < 0.0001$ (One-way ANOVA; Dunnett's multiple comparisons test). NS, not significant.

6.2.8 M1 enhances FluPol-NEP interactions

M1 has been suggested to mediate the interaction of NEP with vRNPs (79, 240). To ascertain the effect of M1 on FluPol-NEP interactions, an increasing amount of M1 was expressed in the split-luciferase assay. M1 also enhances FluPol-NEP interaction is a dose-dependent manner **(Fig. 6.8)**, strengthening the previous findings that M1 facilitates associating of NEP with vRNPs (21, 79). Due to the time constraints and lack of an antibody, I have not evaluated protein expression levels in this assay.

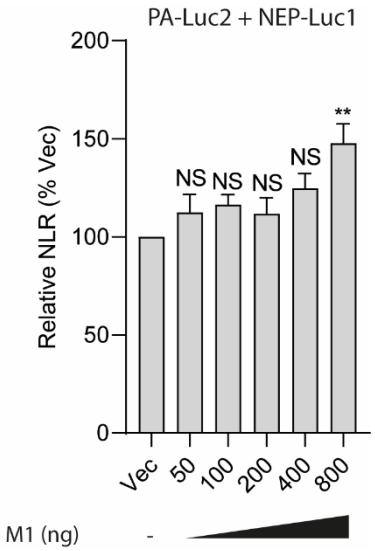

Fig. 6.8 M1 enhances FluPol-NEP interactions in a dose-dependent manner.

293T cells were transfected with plasmids expressing PA-Luc2, NEP-Luc1, PB2, PB1, and the indicated amount plasmid expressing M1. Luminescence from cell lysates was measured at 24 hpt. Data represent at least three independent experiments performed in technical duplicates (mean ± SEM of n=3 biological replicates). **$P < 0.01$ (One-way ANOVA; Dunnett's multiple comparisons test). NS, not significant.

6.2.9 The signature of 627 residue does not affect interactions between NEP and viral polymerase of WSN virus

Adaptive mutations in NEP have been reported to compensate for defective replication and to overcome host restriction of avian influenza viral polymerase in mammalian cells (174). I therefore evaluated the effect of PB2 K627E mutation (avian-signature) on NEP-FluPol interaction. PB2 627E did not affect FluPol-NEP interactions when PB1-Luc2 and NEP-Luc1 were used as probes **(Fig. 6.9A)**. unexpectedly, PB2 627E mutation decreased FluPol-NEP interactions by approximately 15% when using PA-Luc2 and NEP-luc1 as probes **(Fig. 6.9B)**. This reduction is too moderate to being considered as biologically meaningful, albeit it is statistically significant. It should be noted that the NEP used in this assay was from the WSN virus and it carries the previously identified adaptive mutation (174). Further validation by performing the same experiment using an authentic avian NEP is required.

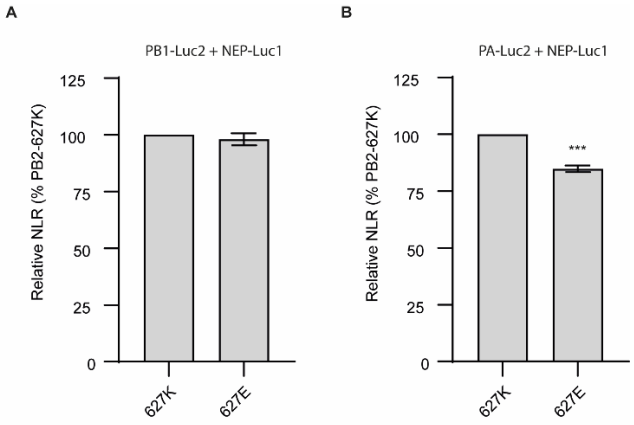

Fig. 6.9 The PB2 K627E mutation does not affect FluPol-NEP interactions.

(A) 293T cells were transfected with plasmids expressing PB1-Luc2, NEP-Luc1, PB2 (627K or 627E), PA; (B) 293T cells were transfected with plasmids expressing PA-Luc2, NEP-Luc1, PB2 (627K or 627E), PB1. Luminescence from cell lysates was measured at 24 hpt. Data represent at least three independent experiments performed in technical duplicates (mean ± SEM of n=3 biological replicates). ***$P < 0.001$ (two-tailed, unpaired Student's *t*-test).

6.2.10 The structure of FluPol-NEP complex

To define the molecular details of how NEP regulates viral RNA synthesis, we then used cryo-electron microscopy (cryo-EM) to solve the structure of NEP in complex with the viral polymerase of the 1918 pandemic H1N1 influenza A virus **(Fig. 6.10)**. In this structure, NEP binds at the C-terminal domain of the PA polymerase subunit (PA-C) and the N-terminus of PB1, involving amino acids from both the N- and C-terminal helices of NEP. Critical residues in the interface include NEP R15, R42, Q96, and Q101. The corresponding interacting residues in viral polymerase include PB1 D2, PA S405A / S413 / S552. To address the functional relevance of this interface between NEP and viral polymerase, I introduced alanine mutations at these interacting residues in either NEP or viral polymerase based on the resolved structure.

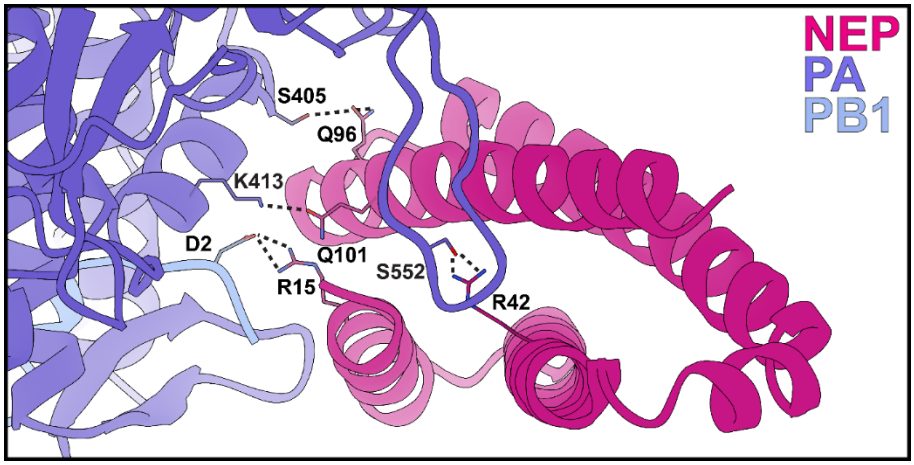

Fig. 6.10 The structure of FluPol-NEP complex

Cryo-EM structure of dimers of 1918 FluPol heterotrimers (purple) bound to WSN NEP (red). Close-up views of the 1918 FluPol-NEP interaction interface. Critical interacting residues in NEP includes: R15, R42, Q96, Q101; the corresponding interacting residues in viral polymerase includes: PB1 D2, PA S552, PA S405, PA K413. Dashed lines indicate hydrogen bonds. (Courtesy of Alison Rep and Loic Carrique).

6.2.11 NEP R15A, R42A, Q96A diminish FluPol-NEP interactions

I examined the effect of individual mutations in NEP at the polymerase interaction interface using the split-luciferase assay, and found that R15A, R42A, and Q96A profoundly dampened interactions between FluPol and NEP to different extents, while Q101A did not affect FluPol-NEP interactions despite the absence or presence of NP **(Fig. 6.11)**. Strikingly, the mutant NEP carrying all these mutations (4A) had almost abolished FluPol-NEP interactions irrespective of whether NP was present or not **(Fig. 6.12)**. Overall, these results suggest that the interacting residues identified in our resolved structure greatly contribute to the interface between viral polymerase and NEP. Due to time constraints and lack of an antibody, I have not evaluated protein expression levels in this assay. The data need to be interpreted with caution because of this issue.

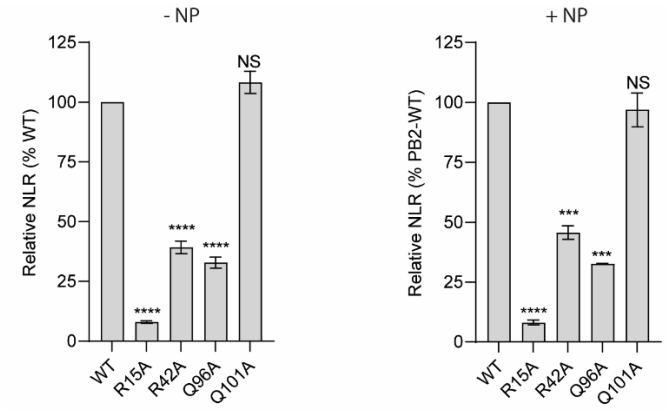

Fig. 6.11 NEP mutations R15A, R42A, and Q96A diminish FluPol-NEP interactions. (A) 293T cells were transfected with plasmids expressing PB2, PB1, PA-Luc2, NEP-Luc1 (wildtype, WT) or mutant NEP-Luc1 with the indicated single mutation. (B) 293T cells were transfected with plasmids expressing PB2, PB1, NP (800 ng), PA-Luc2, NEP-Luc1 (wildtype, WT) or mutant NEP-Luc1 with the indicated single mutation. Luminescence from cell lysates was measured at 24 hpt. Data represent three independent experiments performed in technical duplicates (mean ± SEM of n=3 biological replicates). ***P < 0.001, ****P < 0.0001 (One-way ANOVA; Dunnett's multiple comparisons test). NS, not significant.

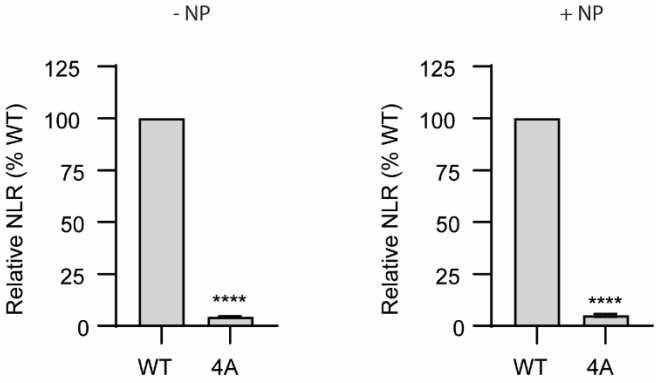

Fig. 6.12 The mutant NEP with quadruple mutation at the interacting residues has abolished FluPol-NEP interactions.

(A) 293T cells were transfected with plasmids expressing PB2, PB1, PA-Luc2, NEP-Luc1 (wildtype, WT), or mutant NEP-Luc1 (4A, R15A, R42A, Q96A, Q101A) in the absence of presence of NP. Luminescence from cell lysates was measured at 24 hpt. Data represent three independent experiments performed in technical duplicates (mean ± SEM of n=3 biological replicates). ****$P < 0.0001$ (One-way ANOVA; Dunnett's multiple comparisons test).

6.2.12 The interface mutations on NEP irreversibly disrupt the FluPol-NEP interactions

To ascertain whether the presence of host or viral factor could render similar levels of interactions between FluPol with NEP (WT) or interface mutant NEP (4A), I subjected NEP (WT)-Luc1 and NEP (4A)-Luc1 to the split-luciferase assay in the presence of the previously mentioned factors and huANP32B at a high-dose. Overexpression of a high-dose of NP, vRNA, cRNA, Pol II CTD, or M1 both enhanced interactions between viral polymerase and NEP (WT) or NEP (4A), whereas overexpression of CRM1 and

huANP32B severely diminished FluPol-NEP (WT) or FluPol-NEP (4A) interactions **(Fig. 6.13)**. Although these factors exhibit similar effects on FluPol-NEP (WT) or FluPol-NEP (4A) interactions, the interactions between FluPol and NEP (4A) are markedly lower compared to the interactions mediated by NEP (WT), suggesting the interface mutations on NEP irreversibly impair the FluPol-NEP interactions. Due to time constraints and lack of an antibody, I have not evaluated protein expression levels in this assay. The data need to be interpreted with caution because of this issue.

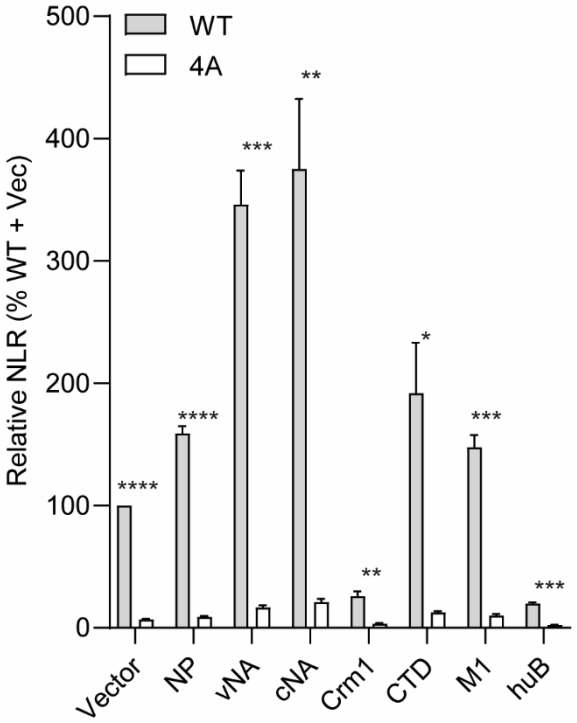

Fig. 6.13 The effect of NP, RNA, CRM1, M1, Pol II CTD, M1, and huANP32B on interactions between viral polymerase and different NEP.

(A) 293T cells were transfected with plasmids expressing PB2, PB1, PA-Luc2, NEP-Luc1(WT) or NEP-Luc1(4A), and 800 ng of plasmids expressing the indicated viral or host factors. Luminescence from cell lysates was measured at 24 hpt. Luminescence from cell lysates was three independent experiments performed in technical duplicates (mean ± SEM of n=3 biological replicates). ****P < 0.001 (two-tailed, unpaired Student's *t*-test).

6.2.13 NEP regulates the switch from transcription to replication.

I next examined whether the FluPol-NEP interactions are associated with the regulatory function of NEP in viral RNA replication and transcription. To this end, I compared the effect of NEP (WT) with NEP (4A) on viral RNA synthesis using vRNP reconstitution assay. Surprisingly, NEP (4A), which is defective in FluPol-NEP interactions, increased vRNA, cRNA, and mRNA levels in a dose-dependent manner. Notably, in cells expressing wildtype NEP, the mRNA level initially reached the plateau (400 ng) and subsequently decreased with the increasing amounts of NEP being expressed in the system, while NEP (4A) constantly enhanced mRNA levels without exhibiting any inhibition on the increased mRNA level **(Fig. 6.14)**. Given our previous finding that NEP (4A) almost abolished FluPol-NEP interactions **(Fig. 6.12)**, these results indicate that the stimulatory effect of NEP on replication is not dependent on FluPol-NEP interactions, while the inhibition of mRNA is dependent on FluPol-NEP interactions.

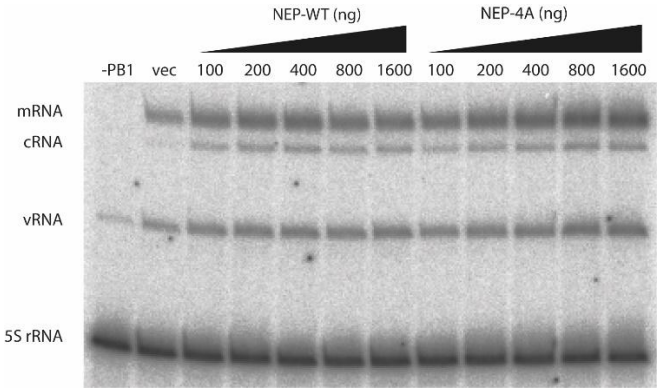

Fig. 6.14 The effect of FluPol-NEP interface mutations on viral RNA synthesis.

(A) 293T cells were transiently transfected with 500 ng of plasmids expressing PB2, PB1, PA, 1000 ng of plasmid expressing NP, 100 ng of pPolI-vNA plasmid expressing the NA segment of the WSN virus along with the indicated increasing amount of NEP (WT) and NEP (4A, R15A, R42A, Q96A, Q101A). PB1 was omitted (-PB1) in the negative control; The setting with empty vector (vec) represents wildtype polymerase activity in the absence of NEP. Total RNA was harvested at 24 hpt and analysed by primer extension assay.

6.3 Discussion

The regulatory function of NEP in viral RNA synthesis has been extensively studied (171-176). In this chapter, effects of several important viral and host factors on FluPol-NEP interactions were evaluated. Our findings reveal that NP, vRNA, cRNA, Pol II CTD all stimulate FluPol-NEP interactions, whereas CRM1 and huANP32B suppress FluPol-NEP interactions **(Fig. 6.13)**. We also resolved the structure of NEP in complex with FluPol and identified critical interacting residues on NEP based on this available structure **(Fig. 6.10)**. Interface mutations on NEP irreversibly disrupt the FluPol-NEP interaction, corroborating the findings from structural analysis **(Fig. 6.2.12)**. By scrutinizing the effect of different doses of NEP and mutant NEP on viral RNA synthesis, I found that the stimulatory effect of NEP on replication is FluPol-NEP interactions-independent, while the inhibitory effect on transcription is FluPol-NEP interaction- dependent **(Fig. 6.14)**.

The resolved FluPol-NEP structure sheds light on the function of NEP in the regulation of RNA synthesis by the influenza virus polymerase. NEP binds to FluPol via PA-C, a binding site shared with Pol II CTD and huANP32B (preliminary data from ongoing work by colleagues in the lab). Pol II CTD and ANP32 proteins are well-known for their supporting functions in viral transcription and replication (66, 238). Therefore, it is tempting to speculate that NEP achieves its regulatory function in viral RNA synthesis by orchestrating fine-tuned interactions between viral polymerase and ANP32 or Pol II CTD. NEP might be able to competitively bind to FluPol with Pol II CTD, and a moderate amount of NEP favours the viral replication by switching the FluPol from transcription conformation to replication confirmation. In contrast, high amounts of NEP might significantly decrease the occupancy of Pol II CTD on the FluPol and thus exhibit the inhibitory effect on viral transcription. The interaction-defective mutant NEP (4A) cannot

associate with the viral polymerase, spatially improving the binding occupancy of ANP32 protein on the FluPol from the very beginning and thereby stimulating viral replication. Even in the presence of high amounts of NEP (4A), Pol II CTD cannot be competed out as NEP (4A) is defective in binding to the FluPol, which could account for the observation that NEP (4A) does not display any inhibitory effect on mRNA accumulation levels.

NEP is recognized to play a role in host adaptation as well as the nuclear export of vRNPs. Data from our ongoing work imply that the nuclear export function is heavily dependent on robust FluPol-NEP interactions. Disrupting FluPol-NEP interactions by mutating critical interacting residues in NEP successfully blocks the nuclear export function (Data not shown in thesis). Nevertheless, these preliminary findings need corroboration by different approaches in the future. (72, 76, 174). Several studies have suggested ANP32 harbouring a nuclear export signal is involved in the nuclear export of viral mRNA (198, 241). It would be interesting to investigate whether ANP32 protein contributes to the nuclear export of vRNP-M1-NEP complex.

In summary, results from this chapter provide insights into the molecular mechanism by which NEP regulates RNA synthesis by the viral polymerase during influenza virus replication. Additionally, the structure of FluPol-NEP allows us to better understand the detailed mechanistic picture of FluPol-NEP interactions during influenza virus life cycle.

SUMMARY AND DISCUSSION

The influenza virus RNA synthesis machinery orchestrates viral transcription and replication via conformational changes induced by fine-tuned interactions with multifunctional viral and host factors. In this study, I investigated three major factors (ANP32, NP, and NEP) that are used by influenza virus to regulate its transcription and genome replication. These viral proteins have multiple functions during viral RNA synthesis, highlighting the high efficiency of the viral RNA synthesis machinery, especially given that the genetic content of influenza virus is very limited.

Through this project, I uncovered that ANP32 LCAR facilitates NP recruitment during influenza virus genome replication, which is a previously unknown role of ANP32 protein (Chapter 3). Moreover, I also demonstrated that the C-terminal tail of NP, a region thought to regulate RNA binding based on structural analysis, is required for robust cRNA stabilization and FluPol-NP interactions (Chapter 4). Finally, I explored the effect of different factors on FluPol-NEP interactions and functionally characterized the FluPol-NEP interaction interface identified in the structure of NEP in complex with FluPol (Chapter 6). My preliminary results strongly suggest that NEP serves as a switch for viral transcription and replication in an allosteric manner. I have also established an *in vitro* cRNP reconstitution assay that can recapitulate vRNA synthesis in a test tube, allowing us to uncouple the two steps of virus replication and to measure vRNA synthesis alone (Chapter 5).

The multifunctional roles of these viral and host factors regulating the viral RNA synthesis machinery warrant further investigation in the future. Revealing these previously unknown

functions could lead to better understanding of the fundamental replication mechanism of influenza A virus and thereby contribute to the development of novel antivirals.

REFERENCES

1. Eccles R. 2005. Understanding the symptoms of the common cold and influenza. Lancet Infect Dis 5:718-25.
2. Berger M. 2015. Influenza, not Ebola, More Likely the Cause of 430 BCE Athenian Outbreak. Clin Infect Dis 61:1492-3.
3. Wilson Smith PL, Christopher Andrews. 1933. A virus obtained from influenza patients. The Lancet ii:66-68.
4. Francis T, Jr. 1940. A New Type of Virus from Epidemic Influenza. Science 92:405-8.
5. WHO. 2023. Influenza (Seasonal), *on* https://www.who.int/news-room/fact-sheets/detail/influenza-(seasonal). Accessed
6. Johnson NP, Mueller J. 2002. Updating the accounts: global mortality of the 1918-1920 "Spanish" influenza pandemic. Bull Hist Med 76:105-15.
7. WHO. 2023. Ongoing avian influenza outbreaks in animals pose risk to humans, *on* https://www.who.int/news/item/12-07-2023-ongoing-avian-influenza-outbreaks-in-animals-pose-risk-to-humans. Accessed
8. Aguero M, Monne I, Sanchez A, Zecchin B, Fusaro A, Ruano MJ, Del Valle Arrojo M, Fernandez-Antonio R, Souto AM, Tordable P, Canas J, Bonfante F, Giussani E, Terregino C, Orejas JJ. 2023. Highly pathogenic avian influenza A(H5N1) virus infection in farmed minks, Spain, October 2022. Euro Surveill 28.
9. WHO. 2022. Assessment of risk associated with recent influenza A(H5N1) clade 2.3.4.4b viruses.
10. Long JS, Mistry B, Haslam SM, Barclay WS. 2019. Host and viral determinants of influenza A virus species specificity. Nat Rev Microbiol 17:67-81.
11. Koutsakos M, Nguyen TH, Barclay WS, Kedzierska K. 2016. Knowns and unknowns of influenza B viruses. Future Microbiol 11:119-35.
12. Hause BM, Collin EA, Liu R, Huang B, Sheng Z, Lu W, Wang D, Nelson EA, Li F. 2014. Characterization of a novel influenza virus in cattle and Swine: proposal for a new genus in the Orthomyxoviridae family. mBio 5:e00031-14.
13. Hause BM, Ducatez M, Collin EA, Ran Z, Liu R, Sheng Z, Armien A, Kaplan B, Chakravarty S, Hoppe AD, Webby RJ, Simonson RR, Li F. 2013. Isolation of a novel swine influenza virus from Oklahoma in 2011 which is distantly related to human influenza C viruses. PLoS Pathog 9:e1003176.
14. Dadonaite B, Vijayakrishnan S, Fodor E, Bhella D, Hutchinson EC. 2016. Filamentous influenza viruses. J Gen Virol 97:1755-1764.
15. Harris A, Cardone G, Winkler DC, Heymann JB, Brecher M, White JM, Steven AC. 2006. Influenza virus pleiomorphy characterized by cryoelectron tomography. Proc Natl Acad Sci U S A 103:19123-7.
16. Zebedee SL, Lamb RA. 1988. Influenza A virus M2 protein: monoclonal antibody restriction of virus growth and detection of M2 in virions. J Virol 62:2762-72.

17. Selzer L, Su Z, Pintilie GD, Chiu W, Kirkegaard K. 2020. Full-length three-dimensional structure of the influenza A virus M1 protein and its organization into a matrix layer. PLoS Biol 18:e3000827.

18. Hutchinson EC, Charles PD, Hester SS, Thomas B, Trudgian D, Martinez-Alonso M, Fodor E. 2014. Conserved and host-specific features of influenza virion architecture. Nat Commun 5:4816.

19. Hutchinson EC, Denham EM, Thomas B, Trudgian DC, Hester SS, Ridlova G, York A, Turrell L, Fodor E. 2012. Mapping the phosphoproteome of influenza A and B viruses by mass spectrometry. PLoS Pathog 8:e1002993.

20. Richardson JC, Akkina RK. 1991. NS2 protein of influenza virus is found in purified virus and phosphorylated in infected cells. Arch Virol 116:69-80.

21. Yasuda J, Nakada S, Kato A, Toyoda T, Ishihama A. 1993. Molecular assembly of influenza virus: association of the NS2 protein with virion matrix. Virology 196:249-55.

22. Shaw ML, Stone KL, Colangelo CM, Gulcicek EE, Palese P. 2008. Cellular proteins in influenza virus particles. PLoS Pathog 4:e1000085.

23. Te Velthuis AJ, Fodor E. 2016. Influenza virus RNA polymerase: insights into the mechanisms of viral RNA synthesis. Nat Rev Microbiol 14:479-93.

24. Pritlove DC, Fodor E, Seong BL, Brownlee GG. 1995. In vitro transcription and polymerase binding studies of the termini of influenza A virus cRNA: evidence for a cRNA panhandle. J Gen Virol 76 (Pt 9):2205-13.

25. Fodor E, Pritlove DC, Brownlee GG. 1994. The influenza virus panhandle is involved in the initiation of transcription. J Virol 68:4092-6.

26. Hsu MT, Parvin JD, Gupta S, Krystal M, Palese P. 1987. Genomic RNAs of influenza viruses are held in a circular conformation in virions and in infected cells by a terminal panhandle. Proc Natl Acad Sci U S A 84:8140-4.

27. Lamb RA, Choppin PW. 1981. Identification of a second protein (M2) encoded by RNA segment 7 of influenza virus. Virology 112:729-37.

28. Lamb RA, Choppin PW. 1979. Segment 8 of the influenza virus genome is unique in coding for two polypeptides. Proc Natl Acad Sci U S A 76:4908-12.

29. Wise HM, Foeglein A, Sun J, Dalton RM, Patel S, Howard W, Anderson EC, Barclay WS, Digard P. 2009. A complicated message: Identification of a novel PB1-related protein translated from influenza A virus segment 2 mRNA. J Virol 83:8021-31.

30. Jagger BW, Wise HM, Kash JC, Walters KA, Wills NM, Xiao YL, Dunfee RL, Schwartzman LM, Ozinsky A, Bell GL, Dalton RM, Lo A, Efstathiou S, Atkins JF, Firth AE, Taubenberger JK, Digard P. 2012. An overlapping protein-coding region in influenza A virus segment 3 modulates the host response. Science 337:199-204.

31. Horimoto T, Kawaoka Y. 2005. Influenza: lessons from past pandemics, warnings from current incidents. Nat Rev Microbiol 3:591-600.

32. Liang Y. 2023. Pathogenicity and virulence of influenza. Virulence 14:2223057.

33. Sempere Borau M, Stertz S. 2021. Entry of influenza A virus into host cells - recent progress and remaining challenges. Curr Opin Virol 48:23-29.

34. Rogers GN, Paulson JC, Daniels RS, Skehel JJ, Wilson IA, Wiley DC. 1983. Single amino acid substitutions in influenza haemagglutinin change receptor binding specificity. Nature 304:76-8.

35. Rogers GN, Paulson JC. 1983. Receptor determinants of human and animal influenza virus isolates: differences in receptor specificity of the H3 hemagglutinin based on species of origin. Virology 127:361-73.

36. Stevens J, Blixt O, Glaser L, Taubenberger JK, Palese P, Paulson JC, Wilson IA. 2006. Glycan microarray analysis of the hemagglutinins from modern and pandemic influenza viruses reveals different receptor specificities. J Mol Biol 355:1143-55.

37. Connor RJ, Kawaoka Y, Webster RG, Paulson JC. 1994. Receptor specificity in human, avian, and equine H2 and H3 influenza virus isolates. Virology 205:17-23.

38. Kuchipudi SV, Nelli R, White GA, Bain M, Chang KC, Dunham S. 2009. Differences in influenza virus receptors in chickens and ducks: Implications for interspecies transmission. J Mol Genet Med 3:143-51.

39. Shinya K, Ebina M, Yamada S, Ono M, Kasai N, Kawaoka Y. 2006. Avian flu: influenza virus receptors in the human airway. Nature 440:435-6.

40. Walther T, Karamanska R, Chan RW, Chan MC, Jia N, Air G, Hopton C, Wong MP, Dell A, Malik Peiris JS, Haslam SM, Nicholls JM. 2013. Glycomic analysis of human respiratory tract tissues and correlation with influenza virus infection. PLoS Pathog 9:e1003223.

41. Karakus U, Thamamongood T, Ciminski K, Ran W, Gunther SC, Pohl MO, Eletto D, Jeney C, Hoffmann D, Reiche S, Schinkothe J, Ulrich R, Wiener J, Hayes MGB, Chang MW, Hunziker A, Yanguez E, Aydillo T, Krammer F, Oderbolz J, Meier M, Oxenius A, Halenius A, Zimmer G, Benner C, Hale BG, Garcia-Sastre A, Beer M, Schwemmle M, Stertz S. 2019. MHC class II proteins mediate cross-species entry of bat influenza viruses. Nature 567:109-112.

42. Matlin KS, Reggio H, Helenius A, Simons K. 1982. Pathway of vesicular stomatitis virus entry leading to infection. J Mol Biol 156:609-31.

43. Marsh M, Helenius A. 1980. Adsorptive endocytosis of Semliki Forest virus. J Mol Biol 142:439-54.

44. Matlin KS, Reggio H, Helenius A, Simons K. 1981. Infectious entry pathway of influenza virus in a canine kidney cell line. J Cell Biol 91:601-13.

45. Sieczkarski SB, Whittaker GR. 2002. Influenza virus can enter and infect cells in the absence of clathrin-mediated endocytosis. J Virol 76:10455-64.

46. de Vries E, Tscherne DM, Wienholts MJ, Cobos-Jimenez V, Scholte F, Garcia-Sastre A, Rottier PJ, de Haan CA. 2011. Dissection of the influenza A virus endocytic routes reveals macropinocytosis as an alternative entry pathway. PLoS Pathog 7:e1001329.

47. Rossman JS, Leser GP, Lamb RA. 2012. Filamentous influenza virus enters cells via macropinocytosis. J Virol 86:10950-60.

48. Boonstra S, Blijleven JS, Roos WH, Onck PR, van der Giessen E, van Oijen AM. 2018. Hemagglutinin-Mediated Membrane Fusion: A Biophysical Perspective. Annu Rev Biophys 47:153-173.

49. Worch R. 2014. Structural biology of the influenza virus fusion peptide. Acta Biochim Pol 61:421-6.

50. Pinto LH, Holsinger LJ, Lamb RA. 1992. Influenza virus M2 protein has ion channel activity. Cell 69:517-28.

51. Manzoor R, Igarashi M, Takada A. 2017. Influenza A Virus M2 Protein: Roles from Ingress to Egress. Int J Mol Sci 18.

52. Mukaigawa J, Nayak DP. 1991. Two signals mediate nuclear localization of influenza virus (A/WSN/33) polymerase basic protein 2. J Virol 65:245-53.

53. Jones IM, Reay PA, Philpott KL. 1986. Nuclear location of all three influenza polymerase proteins and a nuclear signal in polymerase PB2. EMBO J 5:2371-6.

54. Nath ST, Nayak DP. 1990. Function of two discrete regions is required for nuclear localization of polymerase basic protein 1 of A/WSN/33 influenza virus (H1 N1). Mol Cell Biol 10:4139-45.

55. Smith GL, Levin JZ, Palese P, Moss B. 1987. Synthesis and cellular location of the ten influenza polypeptides individually expressed by recombinant vaccinia viruses. Virology 160:336-45.

56. Wang P, Palese P, O'Neill RE. 1997. The NPI-1/NPI-3 (karyopherin alpha) binding site on the influenza a virus nucleoprotein NP is a nonconventional nuclear localization signal. J Virol 71:1850-6.

57. Ozawa M, Fujii K, Muramoto Y, Yamada S, Yamayoshi S, Takada A, Goto H, Horimoto T, Kawaoka Y. 2007. Contributions of two nuclear localization signals of influenza A virus nucleoprotein to viral replication. J Virol 81:30-41.

58. O'Neill RE, Jaskunas R, Blobel G, Palese P, Moroianu J. 1995. Nuclear import of influenza virus RNA can be mediated by viral nucleoprotein and transport factors required for protein import. J Biol Chem 270:22701-4.

59. Nakada R, Hirano H, Matsuura Y. 2015. Structure of importin-alpha bound to a non-classical nuclear localization signal of the influenza A virus nucleoprotein. Sci Rep 5:15055.

60. Cros JF, Garcia-Sastre A, Palese P. 2005. An unconventional NLS is critical for the nuclear import of the influenza A virus nucleoprotein and ribonucleoprotein. Traffic 6:205-13.

61. Bullido R, Gomez-Puertas P, Albo C, Portela A. 2000. Several protein regions contribute to determine the nuclear and cytoplasmic localization of the influenza A virus nucleoprotein. J Gen Virol 81:135-42.

62. Hutchinson EC, Fodor E. 2012. Nuclear import of the influenza A virus transcriptional machinery. Vaccine 30:7353-8.

63. Gabriel G, Herwig A, Klenk HD. 2008. Interaction of polymerase subunit PB2 and NP with importin alpha1 is a determinant of host range of influenza A virus. PLoS Pathog 4:e11.

64. Sediri H, Schwalm F, Gabriel G, Klenk HD. 2015. Adaptive mutation PB2 D701N promotes nuclear import of influenza vRNPs in mammalian cells. Eur J Cell Biol 94:368-74.

65. Gabriel G, Klingel K, Otte A, Thiele S, Hudjetz B, Arman-Kalcek G, Sauter M, Shmidt T, Rother F, Baumgarte S, Keiner B, Hartmann E, Bader M, Brownlee GG, Fodor E, Klenk HD. 2011. Differential use of importin-alpha isoforms governs cell tropism and host adaptation of influenza virus. Nat Commun 2:156.

66. Walker AP, Fodor E. 2019. Interplay between Influenza Virus and the Host RNA Polymerase II Transcriptional Machinery. Trends Microbiol 27:398-407.

67. Te Velthuis AJW, Grimes JM, Fodor E. 2021. Structural insights into RNA polymerases of negative-sense RNA viruses. Nat Rev Microbiol 19:303-318.

68. Stade K, Ford CS, Guthrie C, Weis K. 1997. Exportin 1 (Crm1p) is an essential nuclear export factor. Cell 90:1041-50.

69. Gorlich D, Mattaj IW. 1996. Nucleocytoplasmic transport. Science 271:1513-8.

70. Izaurralde E, Kutay U, von Kobbe C, Mattaj IW, Gorlich D. 1997. The asymmetric distribution of the constituents of the Ran system is essential for transport into and out of the nucleus. EMBO J 16:6535-47.

71. Paterson D, Fodor E. 2012. Emerging roles for the influenza A virus nuclear export protein (NEP). PLoS Pathog 8:e1003019.

72. Brunotte L, Flies J, Bolte H, Reuther P, Vreede F, Schwemmle M. 2014. The nuclear export protein of H5N1 influenza A viruses recruits Matrix 1 (M1) protein to the viral ribonucleoprotein to mediate nuclear export. J Biol Chem 289:20067-77.

73. Elton D, Simpson-Holley M, Archer K, Medcalf L, Hallam R, McCauley J, Digard P. 2001. Interaction of the influenza virus nucleoprotein with the cellular CRM1-mediated nuclear export pathway. J Virol 75:408-19.

74. Lakdawala SS, Wu Y, Wawrzusin P, Kabat J, Broadbent AJ, Lamirande EW, Fodor E, Altan-Bonnet N, Shroff H, Subbarao K. 2014. Influenza a virus assembly intermediates fuse in the cytoplasm. PLoS Pathog 10:e1003971.

75. Watanabe K, Takizawa N, Katoh M, Hoshida K, Kobayashi N, Nagata K. 2001. Inhibition of nuclear export of ribonucleoprotein complexes of influenza virus by leptomycin B. Virus Res 77:31-42.

76. O'Neill RE, Talon J, Palese P. 1998. The influenza virus NEP (NS2 protein) mediates the nuclear export of viral ribonucleoproteins. EMBO J 17:288-96.

77. Martin K, Helenius A. 1991. Nuclear transport of influenza virus ribonucleoproteins: the viral matrix protein (M1) promotes export and inhibits import. Cell 67:117-30.

78. Whittaker G, Kemler I, Helenius A. 1995. Hyperphosphorylation of mutant influenza virus matrix protein, M1, causes its retention in the nucleus. J Virol 69:439-45.

79. Akarsu H, Burmeister WP, Petosa C, Petit I, Muller CW, Ruigrok RW, Baudin F. 2003. Crystal structure of the M1 protein-binding domain of the influenza A virus nuclear export protein (NEP/NS2). EMBO J 22:4646-55.

80. Eisfeld AJ, Kawakami E, Watanabe T, Neumann G, Kawaoka Y. 2011. RAB11A is essential for transport of the influenza virus genome to the plasma membrane. J Virol 85:6117-26.

81. Amorim MJ, Bruce EA, Read EK, Foeglein A, Mahen R, Stuart AD, Digard P. 2011. A Rab11- and microtubule-dependent mechanism for cytoplasmic transport of influenza A virus viral RNA. J Virol 85:4143-56.

82. Momose F, Kikuchi Y, Komase K, Morikawa Y. 2007. Visualization of microtubule-mediated transport of influenza viral progeny ribonucleoprotein. Microbes Infect 9:1422-33.

83. Reuther P, Giese S, Gotz V, Kilb N, Manz B, Brunotte L, Schwemmle M. 2014. Adaptive mutations in the nuclear export protein of human-derived H5N1 strains facilitate a polymerase activity-enhancing conformation. J Virol 88:263-71.

84. Gavazzi C, Isel C, Fournier E, Moules V, Cavalier A, Thomas D, Lina B, Marquet R. 2013. An in vitro network of intermolecular interactions between viral RNA segments of an avian H5N2 influenza A virus: comparison with a human H3N2 virus. Nucleic Acids Res 41:1241-54.

85. Noda T, Sugita Y, Aoyama K, Hirase A, Kawakami E, Miyazawa A, Sagara H, Kawaoka Y. 2012. Three-dimensional analysis of ribonucleoprotein complexes in influenza A virus. Nat Commun 3:639.

86. Noda T, Sagara H, Yen A, Takada A, Kida H, Cheng RH, Kawaoka Y. 2006. Architecture of ribonucleoprotein complexes in influenza A virus particles. Nature 439:490-2.

87. Gog JR, Afonso Edos S, Dalton RM, Leclercq I, Tiley L, Elton D, von Kirchbach JC, Naffakh N, Escriou N, Digard P. 2007. Codon conservation in the influenza A virus genome defines RNA packaging signals. Nucleic Acids Res 35:1897-907.

88. Muramoto Y, Takada A, Fujii K, Noda T, Iwatsuki-Horimoto K, Watanabe S, Horimoto T, Kida H, Kawaoka Y. 2006. Hierarchy among viral RNA (vRNA) segments in their role in vRNA incorporation into influenza A virions. J Virol 80:2318-25.

89. Fujii K, Fujii Y, Noda T, Muramoto Y, Watanabe T, Takada A, Goto H, Horimoto T, Kawaoka Y. 2005. Importance of both the coding and the segment-specific noncoding regions of the influenza A virus NS segment for its efficient incorporation into virions. J Virol 79:3766-74.

90. Fujii Y, Goto H, Watanabe T, Yoshida T, Kawaoka Y. 2003. Selective incorporation of influenza virus RNA segments into virions. Proc Natl Acad Sci U S A 100:2002-7.

91. Dadonaite B, Gilbertson B, Knight ML, Trifkovic S, Rockman S, Laederach A, Brown LE, Fodor E, Bauer DLV. 2019. The structure of the influenza A virus genome. Nat Microbiol 4:1781-1789.

92. Moreira EA, Weber A, Bolte H, Kolesnikova L, Giese S, Lakdawala S, Beer M, Zimmer G, Garcia-Sastre A, Schwemmle M, Juozapaitis M. 2016. A conserved influenza A virus nucleoprotein code controls specific viral genome packaging. Nat Commun 7:12861.

93. Bolte H, Rosu ME, Hagelauer E, Garcia-Sastre A, Schwemmle M. 2019. Packaging of the Influenza Virus Genome Is Governed by a Plastic Network of RNA- and Nucleoprotein-Mediated Interactions. J Virol 93.

94. Gilbertson B, Zheng T, Gerber M, Printz-Schweigert A, Ong C, Marquet R, Isel C, Rockman S, Brown L. 2016. Influenza NA and PB1 Gene Segments Interact during the Formation of Viral Progeny: Localization of the Binding Region within the PB1 Gene. Viruses 8.

95. Cobbin JC, Ong C, Verity E, Gilbertson BP, Rockman SP, Brown LE. 2014. Influenza virus PB1 and neuraminidase gene segments can cosegregate during vaccine reassortment driven by interactions in the PB1 coding region. J Virol 88:8971-80.

96. Barman S, Nayak DP. 2000. Analysis of the transmembrane domain of influenza virus neuraminidase, a type II transmembrane glycoprotein, for apical sorting and raft association. J Virol 74:6538-45.

97. Kundu A, Avalos RT, Sanderson CM, Nayak DP. 1996. Transmembrane domain of influenza virus neuraminidase, a type II protein, possesses an apical sorting signal in polarized MDCK cells. J Virol 70:6508-15.

98. Wohlgemuth N, Lane AP, Pekosz A. 2018. Influenza A Virus M2 Protein Apical Targeting Is Required for Efficient Virus Replication. J Virol 92.

99. Barman S, Ali A, Hui EK, Adhikary L, Nayak DP. 2001. Transport of viral proteins to the apical membranes and interaction of matrix protein with glycoproteins in the assembly of influenza viruses. Virus Res 77:61-9.

100. Zhang J, Pekosz A, Lamb RA. 2000. Influenza virus assembly and lipid raft microdomains: a role for the cytoplasmic tails of the spike glycoproteins. J Virol 74:4634-44.

101. Schroeder C, Heider H, Moncke-Buchner E, Lin TI. 2005. The influenza virus ion channel and maturation cofactor M2 is a cholesterol-binding protein. Eur Biophys J 34:52-66.

102. Enami M, Enami K. 1996. Influenza virus hemagglutinin and neuraminidase glycoproteins stimulate the membrane association of the matrix protein. J Virol 70:6653-7.

103. Rossman JS, Lamb RA. 2011. Influenza virus assembly and budding. Virology 411:229-36.

104. Rossman JS, Jing X, Leser GP, Balannik V, Pinto LH, Lamb RA. 2010. Influenza virus m2 ion channel protein is necessary for filamentous virion formation. J Virol 84:5078-88.

105. Rossman JS, Jing X, Leser GP, Lamb RA. 2010. Influenza virus M2 protein mediates ESCRT-independent membrane scission. Cell 142:902-13.

106. Palese P, Tobita K, Ueda M, Compans RW. 1974. Characterization of temperature sensitive influenza virus mutants defective in neuraminidase. Virology 61:397-410.

107. Palese P, Compans RW. 1976. Inhibition of influenza virus replication in tissue culture by 2-deoxy-2,3-dehydro-N-trifluoroacetylneuraminic acid (FANA): mechanism of action. J Gen Virol 33:159-63.

108. Taubenberger JK, Morens DM. 2006. 1918 Influenza: the mother of all pandemics. Emerg Infect Dis 12:15-22.

109. Taubenberger JK, Kash JC, Morens DM. 2019. The 1918 influenza pandemic: 100 years of questions answered and unanswered. Sci Transl Med 11.

110. Harrington WN, Kackos CM, Webby RJ. 2021. The evolution and future of influenza pandemic preparedness. Exp Mol Med 53:737-749.

111. Neumann G, Noda T, Kawaoka Y. 2009. Emergence and pandemic potential of swine-origin H1N1 influenza virus. Nature 459:931-9.

112. Tumpey TM, Maines TR, Van Hoeven N, Glaser L, Solorzano A, Pappas C, Cox NJ, Swayne DE, Palese P, Katz JM, Garcia-Sastre A. 2007. A two-amino acid change in the hemagglutinin of the 1918 influenza virus abolishes transmission. Science 315:655-9.

113. Tumpey TM, Basler CF, Aguilar PV, Zeng H, Solorzano A, Swayne DE, Cox NJ, Katz JM, Taubenberger JK, Palese P, Garcia-Sastre A. 2005. Characterization of the reconstructed 1918 Spanish influenza pandemic virus. Science 310:77-80.

114. Reid AH, Fanning TG, Hultin JV, Taubenberger JK. 1999. Origin and evolution of the 1918 "Spanish" influenza virus hemagglutinin gene. Proc Natl Acad Sci U S A 96:1651-6.

115. Taubenberger JK, Reid AH, Krafft AE, Bijwaard KE, Fanning TG. 1997. Initial genetic characterization of the 1918 "Spanish" influenza virus. Science 275:1793-6.

116. Kawaoka Y, Krauss S, Webster RG. 1989. Avian-to-human transmission of the PB1 gene of influenza A viruses in the 1957 and 1968 pandemics. J Virol 63:4603-8.

117. Viboud C, Simonsen L, Fuentes R, Flores J, Miller MA, Chowell G. 2016. Global Mortality Impact of the 1957-1959 Influenza Pandemic. J Infect Dis 213:738-45.

118. Mehle A, Doudna JA. 2009. Adaptive strategies of the influenza virus polymerase for replication in humans. Proc Natl Acad Sci U S A 106:21312-6.

119. Eisfeld AJ, Neumann G, Kawaoka Y. 2015. At the centre: influenza A virus ribonucleoproteins. Nat Rev Microbiol 13:28-41.

120. Portela A, Digard P. 2002. The influenza virus nucleoprotein: a multifunctional RNA-binding protein pivotal to virus replication. J Gen Virol 83:723-734.

121. Baudin F, Bach C, Cusack S, Ruigrok RW. 1994. Structure of influenza virus RNP. I. Influenza virus nucleoprotein melts secondary structure in panhandle RNA and exposes the bases to the solvent. EMBO J 13:3158-65.

122. Elton D, Medcalf L, Bishop K, Harrison D, Digard P. 1999. Identification of amino acid residues of influenza virus nucleoprotein essential for RNA binding. J Virol 73:7357-67.

123. Tang YS, Xu S, Chen YW, Wang JH, Shaw PC. 2021. Crystal structures of influenza nucleoprotein complexed with nucleic acid provide insights into the mechanism of RNA interaction. Nucleic Acids Res 49:4144-4154.

124. Ng AK, Zhang H, Tan K, Li Z, Liu JH, Chan PK, Li SM, Chan WY, Au SW, Joachimiak A, Walz T, Wang JH, Shaw PC. 2008. Structure of the influenza virus A H5N1 nucleoprotein: implications for RNA binding, oligomerization, and vaccine design. FASEB J 22:3638-47.

125. Moeller A, Kirchdoerfer RN, Potter CS, Carragher B, Wilson IA. 2012. Organization of the influenza virus replication machinery. Science 338:1631-4.

126. Arranz R, Coloma R, Chichon FJ, Conesa JJ, Carrascosa JL, Valpuesta JM, Ortin J, Martin-Benito J. 2012. The structure of native influenza virion ribonucleoproteins. Science 338:1634-7.

127. Nakano M, Sugita Y, Kodera N, Miyamoto S, Muramoto Y, Wolf M, Noda T. 2021. Ultrastructure of influenza virus ribonucleoprotein complexes during viral RNA synthesis. Commun Biol 4:858.

128. Area E, Martin-Benito J, Gastaminza P, Torreira E, Valpuesta JM, Carrascosa JL, Ortin J. 2004. 3D structure of the influenza virus polymerase complex: localization of subunit domains. Proc Natl Acad Sci U S A 101:308-13.

129. Coloma R, Valpuesta JM, Arranz R, Carrascosa JL, Ortin J, Martin-Benito J. 2009. The structure of a biologically active influenza virus ribonucleoprotein complex. PLoS Pathog 5:e1000491.

130. Martin-Benito J, Area E, Ortega J, Llorca O, Valpuesta JM, Carrascosa JL, Ortin J. 2001. Three-dimensional reconstruction of a recombinant influenza virus ribonucleoprotein particle. EMBO Rep 2:313-7.

131. Li Z, Watanabe T, Hatta M, Watanabe S, Nanbo A, Ozawa M, Kakugawa S, Shimojima M, Yamada S, Neumann G, Kawaoka Y. 2009. Mutational analysis of conserved amino acids in the influenza A virus nucleoprotein. J Virol 83:4153-62.

132. Biswas SK, Boutz PL, Nayak DP. 1998. Influenza virus nucleoprotein interacts with influenza virus polymerase proteins. J Virol 72:5493-501.

133. Poole E, Elton D, Medcalf L, Digard P. 2004. Functional domains of the influenza A virus PB2 protein: identification of NP- and PB1-binding sites. Virology 321:120-33.

134. Wandzik JM, Kouba T, Karuppasamy M, Pflug A, Drncova P, Provaznik J, Azevedo N, Cusack S. 2020. A Structure-Based Model for the Complete Transcription Cycle of Influenza Polymerase. Cell 181:877-893 e21.

135. Fan H, Walker AP, Carrique L, Keown JR, Serna Martin I, Karia D, Sharps J, Hengrung N, Pardon E, Steyaert J, Grimes JM, Fodor E. 2019. Structures of influenza A virus RNA polymerase offer insight into viral genome replication. Nature 573:287-290.

136. Chang S, Sun D, Liang H, Wang J, Li J, Guo L, Wang X, Guan C, Boruah BM, Yuan L, Feng F, Yang M, Wang L, Wang Y, Wojdyla J, Li L, Wang J, Wang M, Cheng G, Wang HW, Liu Y. 2015. Cryo-EM structure of influenza virus RNA polymerase complex at 4.3 A resolution. Mol Cell 57:925-935.

137. Pflug A, Guilligay D, Reich S, Cusack S. 2014. Structure of influenza A polymerase bound to the viral RNA promoter. Nature 516:355-60.

138. Reich S, Guilligay D, Pflug A, Malet H, Berger I, Crepin T, Hart D, Lunardi T, Nanao M, Ruigrok RW, Cusack S. 2014. Structural insight into cap-snatching and RNA synthesis by influenza polymerase. Nature 516:361-6.

139. Biswas SK, Nayak DP. 1994. Mutational analysis of the conserved motifs of influenza A virus polymerase basic protein 1. J Virol 68:1819-26.

140. Guilligay D, Tarendeau F, Resa-Infante P, Coloma R, Crepin T, Sehr P, Lewis J, Ruigrok RW, Ortin J, Hart DJ, Cusack S. 2008. The structural basis for cap binding by influenza virus polymerase subunit PB2. Nat Struct Mol Biol 15:500-6.

141. Yuan P, Bartlam M, Lou Z, Chen S, Zhou J, He X, Lv Z, Ge R, Li X, Deng T, Fodor E, Rao Z, Liu Y. 2009. Crystal structure of an avian influenza polymerase PA(N) reveals an endonuclease active site. Nature 458:909-13.

142. Dias A, Bouvier D, Crepin T, McCarthy AA, Hart DJ, Baudin F, Cusack S, Ruigrok RW. 2009. The cap-snatching endonuclease of influenza virus polymerase resides in the PA subunit. Nature 458:914-8.

143. Lakdawala SS, Fodor E, Subbarao K. 2016. Moving On Out: Transport and Packaging of Influenza Viral RNA into Virions. Annu Rev Virol 3:411-427.

144. Te Velthuis AJ, Robb NC, Kapanidis AN, Fodor E. 2016. The role of the priming loop in influenza A virus RNA synthesis. Nat Microbiol 1:16029.

145. Walker AP, Sharps J, Fodor E. 2020. Mutation of an Influenza Virus Polymerase 3' RNA Promoter Binding Site Inhibits Transcription Elongation. J Virol 94.

146. Robertson JS. 1979. 5' and 3' terminal nucleotide sequences of the RNA genome segments of influenza virus. Nucleic Acids Res 6:3745-57.

147. Desselberger U, Racaniello VR, Zazra JJ, Palese P. 1980. The 3' and 5'-terminal sequences of influenza A, B and C virus RNA segments are highly conserved and show partial inverted complementarity. Gene 8:315-28.

148. Flick R, Neumann G, Hoffmann E, Neumeier E, Hobom G. 1996. Promoter elements in the influenza vRNA terminal structure. RNA 2:1046-57.

149. Neumann G, Hobom G. 1995. Mutational analysis of influenza virus promoter elements in vivo. J Gen Virol 76 (Pt 7):1709-17.

150. Kim HJ, Fodor E, Brownlee GG, Seong BL. 1997. Mutational analysis of the RNA-fork model of the influenza A virus vRNA promoter in vivo. J Gen Virol 78 (Pt 2):353-7.

151. Fodor E, Pritlove DC, Brownlee GG. 1995. Characterization of the RNA-fork model of virion RNA in the initiation of transcription in influenza A virus. J Virol 69:4012-9.

152. Crow M, Deng T, Addley M, Brownlee GG. 2004. Mutational analysis of the influenza virus cRNA promoter and identification of nucleotides critical for replication. J Virol 78:6263-70.

153. Thierry E, Guilligay D, Kosinski J, Bock T, Gaudon S, Round A, Pflug A, Hengrung N, El Omari K, Baudin F, Hart DJ, Beck M, Cusack S. 2016. Influenza Polymerase Can Adopt an Alternative Configuration Involving a Radical Repacking of PB2 Domains. Mol Cell 61:125-37.

154. Pflug A, Lukarska M, Resa-Infante P, Reich S, Cusack S. 2017. Structural insights into RNA synthesis by the influenza virus transcription-replication machine. Virus Res 234:103-117.

155. Hu Y, Sneyd H, Dekant R, Wang J. 2017. Influenza A Virus Nucleoprotein: A Highly Conserved Multi-Functional Viral Protein as a Hot Antiviral Drug Target. Curr Top Med Chem 17:2271-2285.

156. Ye Q, Krug RM, Tao YJ. 2006. The mechanism by which influenza A virus nucleoprotein forms oligomers and binds RNA. Nature 444:1078-82.

157. Chenavas S, Estrozi LF, Slama-Schwok A, Delmas B, Di Primo C, Baudin F, Li X, Crepin T, Ruigrok RW. 2013. Monomeric nucleoprotein of influenza A virus. PLoS Pathog 9:e1003275.

158. Knight ML, Fan H, Bauer DLV, Grimes JM, Fodor E, Keown JR. 2021. Structure of an H3N2 influenza virus nucleoprotein. Acta Crystallogr F Struct Biol Commun 77:208-214.

159. Turrell L, Lyall JW, Tiley LS, Fodor E, Vreede FT. 2013. The role and assembly mechanism of nucleoprotein in influenza A virus ribonucleoprotein complexes. Nat Commun 4:1591.

160. Momose F, Basler CF, O'Neill RE, Iwamatsu A, Palese P, Nagata K. 2001. Cellular splicing factor RAF-2p48/NPI-5/BAT1/UAP56 interacts with the influenza virus nucleoprotein and enhances viral RNA synthesis. J Virol 75:1899-908.

161. Wang F, Sheppard CM, Mistry B, Staller E, Barclay WS, Grimes JM, Fodor E, Fan H. 2022. The C-terminal LCAR of host ANP32 proteins interacts with the influenza A virus nucleoprotein to promote the replication of the viral RNA genome. Nucleic Acids Res 50:5713-5725.

162. Kawaguchi A, Momose F, Nagata K. 2011. Replication-coupled and host factor-mediated encapsidation of the influenza virus genome by viral nucleoprotein. J Virol 85:6197-204.

163. Vreede FT, Jung TE, Brownlee GG. 2004. Model suggesting that replication of influenza virus is regulated by stabilization of replicative intermediates. J Virol 78:9568-72.

164. Vreede FT, Ng AK, Shaw PC, Fodor E. 2011. Stabilization of influenza virus replication intermediates is dependent on the RNA-binding but not the homo-oligomerization activity of the viral nucleoprotein. J Virol 85:12073-8.

165. Zhu Z, Fan H, Fodor E. 2023. Defining the minimal components of the influenza A virus replication machinery via an in vitro reconstitution system. PLoS Biol 21:e3002370.

166. Lamb RA, Lai CJ. 1980. Sequence of interrupted and uninterrupted mRNAs and cloned DNA coding for the two overlapping nonstructural proteins of influenza virus. Cell 21:475-85.

167. Inglis SC, Barrett T, Brown CM, Almond JW. 1979. The smallest genome RNA segment of influenza virus contains two genes that may overlap. Proc Natl Acad Sci U S A 76:3790-4.

168. Iwatsuki-Horimoto K, Horimoto T, Fujii Y, Kawaoka Y. 2004. Generation of influenza A virus NS2 (NEP) mutants with an altered nuclear export signal sequence. J Virol 78:10149-55.

169. Huang S, Chen J, Chen Q, Wang H, Yao Y, Chen J, Chen Z. 2013. A second CRM1-dependent nuclear export signal in the influenza A virus NS2 protein contributes to the nuclear export of viral ribonucleoproteins. J Virol 87:767-78.

170. Bullido R, Gomez-Puertas P, Saiz MJ, Portela A. 2001. Influenza A virus NEP (NS2 protein) downregulates RNA synthesis of model template RNAs. J Virol 75:4912-7.

171. Robb NC, Smith M, Vreede FT, Fodor E. 2009. NS2/NEP protein regulates transcription and replication of the influenza virus RNA genome. J Gen Virol 90:1398-1407.

172. Zhang L, Shao Y, Wang Y, Yang Q, Guo J, Gao GF, Deng T. 2023. Twenty natural amino acid substitution screening at the last residue 121 of influenza A virus NS2 protein reveals the critical role of NS2 in promoting virus genome replication by coordinating with viral polymerase. J Virol doi:10.1128/jvi.01166-23:e0116623.

173. Zhang L, Wang Y, Shao Y, Guo J, Gao GF, Deng T. 2023. Fine Regulation of Influenza Virus RNA Transcription and Replication by Stoichiometric Changes in Viral NS1 and NS2 Proteins. J Virol 97:e0033723.

174. Manz B, Brunotte L, Reuther P, Schwemmle M. 2012. Adaptive mutations in NEP compensate for defective H5N1 RNA replication in cultured human cells. Nat Commun 3:802.

175. Perez JT, Zlatev I, Aggarwal S, Subramanian S, Sachidanandam R, Kim B, Manoharan M, tenOever BR. 2012. A small-RNA enhancer of viral polymerase activity. J Virol 86:13475-85.

176. Perez JT, Varble A, Sachidanandam R, Zlatev I, Manoharan M, Garcia-Sastre A, tenOever BR. 2010. Influenza A virus-generated small RNAs regulate the switch from transcription to replication. Proc Natl Acad Sci U S A 107:11525-30.

177. Chua MA, Schmid S, Perez JT, Langlois RA, Tenoever BR. 2013. Influenza A virus utilizes suboptimal splicing to coordinate the timing of infection. Cell Rep 3:23-9.

178. Lukarska M, Fournier G, Pflug A, Resa-Infante P, Reich S, Naffakh N, Cusack S. 2017. Structural basis of an essential interaction between influenza polymerase and Pol II CTD. Nature 541:117-121.

179. Serna Martin I, Hengrung N, Renner M, Sharps J, Martinez-Alonso M, Masiulis S, Grimes JM, Fodor E. 2018. A Mechanism for the Activation of the Influenza Virus Transcriptase. Mol Cell 70:1101-1110 e4.

180. Plotch SJ, Bouloy M, Ulmanen I, Krug RM. 1981. A unique cap(m7GpppXm)-dependent influenza virion endonuclease cleaves capped RNAs to generate the primers that initiate viral RNA transcription. Cell 23:847-58.

181. Gu W, Gallagher GR, Dai W, Liu P, Li R, Trombly MI, Gammon DB, Mello CC, Wang JP, Finberg RW. 2015. Influenza A virus preferentially snatches noncoding RNA caps. RNA 21:2067-75.

182. Koppstein D, Ashour J, Bartel DP. 2015. Sequencing the cap-snatching repertoire of H1N1 influenza provides insight into the mechanism of viral transcription initiation. Nucleic Acids Res 43:5052-64.

183. Kouba T, Drncova P, Cusack S. 2019. Structural snapshots of actively transcribing influenza polymerase. Nat Struct Mol Biol 26:460-470.

184. Pflug A, Gaudon S, Resa-Infante P, Lethier M, Reich S, Schulze WM, Cusack S. 2018. Capped RNA primer binding to influenza polymerase and implications for the mechanism of cap-binding inhibitors. Nucleic Acids Res 46:956-971.

185. Bier K, York A, Fodor E. 2011. Cellular cap-binding proteins associate with influenza virus mRNAs. J Gen Virol 92:1627-1634.

186. Poon LL, Pritlove DC, Fodor E, Brownlee GG. 1999. Direct evidence that the poly(A) tail of influenza A virus mRNA is synthesized by reiterative copying of a U track in the virion RNA template. J Virol 73:3473-6.

187. Deng T, Vreede FT, Brownlee GG. 2006. Different de novo initiation strategies are used by influenza virus RNA polymerase on its cRNA and viral RNA promoters during viral RNA replication. J Virol 80:2337-48.

188. Carrique L, Fan H, Walker AP, Keown JR, Sharps J, Staller E, Barclay WS, Fodor E, Grimes JM. 2020. Host ANP32A mediates the assembly of the influenza virus replicase. Nature 587:638-643.

189. Oymans J, Te Velthuis AJW. 2018. A Mechanism for Priming and Realignment during Influenza A Virus Replication. J Virol 92.

190. Jorba N, Coloma R, Ortin J. 2009. Genetic trans-complementation establishes a new model for influenza virus RNA transcription and replication. PLoS Pathog 5:e1000462.

191. York A, Hengrung N, Vreede FT, Huiskonen JT, Fodor E. 2013. Isolation and characterization of the positive-sense replicative intermediate of a negative-strand RNA virus. Proc Natl Acad Sci U S A 110:E4238-45.

192. Nilsson-Payant BE, tenOever BR, Te Velthuis AJW. 2022. The Host Factor ANP32A Is Required for Influenza A Virus vRNA and cRNA Synthesis. J Virol 96:e0209221.

193. Malek SN, Katumuluwa AI, Pasternack GR. 1990. Identification and preliminary characterization of two related proliferation-associated nuclear phosphoproteins. J Biol Chem 265:13400-9.

194. Matsuoka K, Taoka M, Satozawa N, Nakayama H, Ichimura T, Takahashi N, Yamakuni T, Song SY, Isobe T. 1994. A nuclear factor containing the leucine-rich repeats expressed in murine cerebellar neurons. Proc Natl Acad Sci U S A 91:9670-4.

195. Vaesen M, Barnikol-Watanabe S, Gotz H, Awni LA, Cole T, Zimmermann B, Kratzin HD, Hilschmann N. 1994. Purification and characterization of two putative HLA class II associated proteins: PHAPI and PHAPII. Biol Chem Hoppe Seyler 375:113-26.

196. Reilly PT, Yu Y, Hamiche A, Wang L. 2014. Cracking the ANP32 whips: important functions, unequal requirement, and hints at disease implications. Bioessays 36:1062-71.

197. Matilla A, Radrizzani M. 2005. The Anp32 family of proteins containing leucine-rich repeats. Cerebellum 4:7-18.

198. Wang Y, Zhang H, Na L, Du C, Zhang Z, Zheng YH, Wang X. 2019. ANP32A and ANP32B are key factors in the Rev-dependent CRM1 pathway for nuclear export of HIV-1 unspliced mRNA. J Biol Chem 294:15346-15357.

199. Gunther M, Bauer A, Muller M, Zaeck L, Finke S. 2020. Interaction of host cellular factor ANP32B with matrix proteins of different paramyxoviruses. J Gen Virol 101:44-58.

200. Bauer A, Neumann S, Karger A, Henning AK, Maisner A, Lamp B, Dietzel E, Kwasnitschka L, Balkema-Buschmann A, Keil GM, Finke S. 2014. ANP32B is a nuclear target of henipavirus M proteins. PLoS One 9:e97233.

201. Naffakh N, Tomoiu A, Rameix-Welti MA, van der Werf S. 2008. Host restriction of avian influenza viruses at the level of the ribonucleoproteins. Annu Rev Microbiol 62:403-24.

202. Manz B, Schwemmle M, Brunotte L. 2013. Adaptation of avian influenza A virus polymerase in mammals to overcome the host species barrier. J Virol 87:7200-9.

203. Almond JW. 1977. A single gene determines the host range of influenza virus. Nature 270:617-8.

204. Subbarao EK, London W, Murphy BR. 1993. A single amino acid in the PB2 gene of influenza A virus is a determinant of host range. J Virol 67:1761-4.

205. Mehle A, Doudna JA. 2008. An inhibitory activity in human cells restricts the function of an avian-like influenza virus polymerase. Cell Host Microbe 4:111-22.

206. Paterson D, te Velthuis AJ, Vreede FT, Fodor E. 2014. Host restriction of influenza virus polymerase activity by PB2 627E is diminished on short viral templates in a nucleoprotein-independent manner. J Virol 88:339-44.

207. Weber M, Sediri H, Felgenhauer U, Binzen I, Banfer S, Jacob R, Brunotte L, Garcia-Sastre A, Schmid-Burgk JL, Schmidt T, Hornung V, Kochs G, Schwemmle M, Klenk HD, Weber F. 2015. Influenza virus adaptation PB2-627K modulates nucleocapsid inhibition by the pathogen sensor RIG-I. Cell Host Microbe 17:309-319.

208. Pinto RM, Bakshi S, Lytras S, Zakaria MK, Swingler S, Worrell JC, Herder V, Hargrave KE, Varjak M, Cameron-Ruiz N, Collados Rodriguez M, Varela M, Wickenhagen A, Loney C, Pei Y, Hughes J, Valette E, Turnbull ML, Furnon W, Gu Q, Orr L, Taggart A, Diebold O, Davis C, Boutell C, Grey F, Hutchinson E, Digard P, Monne I, Wootton SK, MacLeod MKL, Wilson SJ, Palmarini M. 2023. BTN3A3 evasion promotes the zoonotic potential of influenza A viruses. Nature 619:338-347.

209. Swann OC, Rasmussen AB, Peacock TP, Sheppard CM, Barclay WS. 2023. Avian Influenza A Virus Polymerase Can Utilize Human ANP32 Proteins To Support cRNA but Not vRNA Synthesis. mBio 14:e0339922.

210. Moncorge O, Mura M, Barclay WS. 2010. Evidence for avian and human host cell factors that affect the activity of influenza virus polymerase. J Virol 84:9978-86.

211. Staller E, Sheppard CM, Neasham PJ, Mistry B, Peacock TP, Goldhill DH, Long JS, Barclay WS. 2019. ANP32 Proteins Are Essential for Influenza Virus Replication in Human Cells. J Virol 93.

212. Zhang H, Zhang Z, Wang Y, Wang M, Wang X, Zhang X, Ji S, Du C, Chen H, Wang X. 2019. Fundamental Contribution and Host Range Determination of ANP32A and ANP32B in Influenza A Virus Polymerase Activity. J Virol 93.

213. Long JS, Giotis ES, Moncorge O, Frise R, Mistry B, James J, Morisson M, Iqbal M, Vignal A, Skinner MA, Barclay WS. 2016. Species difference in ANP32A underlies influenza A virus polymerase host restriction. Nature 529:101-4.

214. Domingues P, Hale BG. 2017. Functional Insights into ANP32A-Dependent Influenza A Virus Polymerase Host Restriction. Cell Rep 20:2538-2546.

215. Baker SF, Ledwith MP, Mehle A. 2018. Differential Splicing of ANP32A in Birds Alters Its Ability to Stimulate RNA Synthesis by Restricted Influenza Polymerase. Cell Rep 24:2581-2588 e4.

216. Peacock TP, Sheppard CM, Lister MG, Staller E, Frise R, Swann OC, Goldhill DH, Long JS, Barclay WS. 2023. Mammalian ANP32A and ANP32B Proteins Drive Differential Polymerase Adaptations in Avian Influenza Virus. J Virol 97:e0021323.

217. Sheppard CM, Goldhill DH, Swann OC, Staller E, Penn R, Platt OK, Sukhova K, Baillon L, Frise R, Peacock TP, Fodor E, Barclay WS. 2023. An Influenza A virus can evolve to use human ANP32E through altering polymerase dimerization. Nat Commun 14:6135.

218. Long JS, Idoko-Akoh A, Mistry B, Goldhill D, Staller E, Schreyer J, Ross C, Goodbourn S, Shelton H, Skinner MA, Sang H, McGrew MJ, Barclay W. 2019. Species specific differences in use of ANP32 proteins by influenza A virus. Elife 8.

219. Zhang Z, Zhang H, Xu L, Guo X, Wang W, Ji Y, Lin C, Wang Y, Wang X. 2020. Selective usage of ANP32 proteins by influenza B virus polymerase: Implications in determination of host range. PLoS Pathog 16:e1008989.

220. Mistry B, Long JS, Schreyer J, Staller E, Sanchez-David RY, Barclay WS. 2020. Elucidating the Interactions between Influenza Virus Polymerase and Host Factor ANP32A. J Virol 94.

221. Camacho-Zarco AR, Kalayil S, Maurin D, Salvi N, Delaforge E, Milles S, Jensen MR, Hart DJ, Cusack S, Blackledge M. 2020. Molecular basis of host-adaptation interactions between influenza virus polymerase PB2 subunit and ANP32A. Nat Commun 11:3656.

222. Kawakami E, Watanabe T, Fujii K, Goto H, Watanabe S, Noda T, Kawaoka Y. 2011. Strand-specific real-time RT-PCR for distinguishing influenza vRNA, cRNA, and mRNA. J Virol Methods 173:1-6.

223. Cassonnet P, Rolloy C, Neveu G, Vidalain PO, Chantier T, Pellet J, Jones L, Muller M, Demeret C, Gaud G, Vuillier F, Lotteau V, Tangy F, Favre M, Jacob Y. 2011. Benchmarking a luciferase complementation assay for detecting protein complexes. Nat Methods 8:990-2.

224. Wandzik JM, Kouba T, Cusack S. 2021. Structure and Function of Influenza Polymerase. Cold Spring Harb Perspect Med 11.

225. Ogino T, Green TJ. 2019. RNA Synthesis and Capping by Non-segmented Negative Strand RNA Viral Polymerases: Lessons From a Prototypic Virus. Front Microbiol 10:1490.

226. Ruigrok RW, Crepin T, Kolakofsky D. 2011. Nucleoproteins and nucleocapsids of negative-strand RNA viruses. Curr Opin Microbiol 14:504-10.

227. Elton D, Medcalf E, Bishop K, Digard P. 1999. Oligomerization of the influenza virus nucleoprotein: identification of positive and negative sequence elements. Virology 260:190-200.

228. Sugiyama K, Kawaguchi A, Okuwaki M, Nagata K. 2015. pp32 and APRIL are host cell-derived regulators of influenza virus RNA synthesis from cRNA. Elife 4.

229. Ye Q, Guu TS, Mata DA, Kuo RL, Smith B, Krug RM, Tao YJ. 2012. Biochemical and structural evidence in support of a coherent model for the formation of the double-helical influenza A virus ribonucleoprotein. mBio 4:e00467-12.

230. Ng AK, Chan WH, Choi ST, Lam MK, Lau KF, Chan PK, Au SW, Fodor E, Shaw PC. 2012. Influenza polymerase activity correlates with the strength of interaction between nucleoprotein and PB2 through the host-specific residue K/E627. PLoS One 7:e36415.

231. Nilsson BE, Te Velthuis AJW, Fodor E. 2017. Role of the PB2 627 Domain in Influenza A Virus Polymerase Function. J Virol 91.

232. Rameix-Welti MA, Tomoiu A, Dos Santos Afonso E, van der Werf S, Naffakh N. 2009. Avian Influenza A virus polymerase association with nucleoprotein, but not polymerase assembly, is impaired in human cells during the course of infection. J Virol 83:1320-31.

233. Nilsson-Payant BE, Blanco-Melo D, Uhl S, Escudero-Perez B, Olschewski S, Thibault P, Panis M, Rosenthal M, Munoz-Fontela C, Lee B, tenOever BR. 2021. Reduced Nucleoprotein Availability Impairs Negative-Sense RNA Virus Replication and Promotes Host Recognition. J Virol 95.

234. Shimizu K, Handa H, Nakada S, Nagata K. 1994. Regulation of influenza virus RNA polymerase activity by cellular and viral factors. Nucleic Acids Res 22:5047-53.

235. Vreede FT, Brownlee GG. 2007. Influenza virion-derived viral ribonucleoproteins synthesize both mRNA and cRNA in vitro. J Virol 81:2196-204.

236. Shapiro GI, Krug RM. 1988. Influenza virus RNA replication in vitro: synthesis of viral template RNAs and virion RNAs in the absence of an added primer. J Virol 62:2285-90.

237. Hogg JR, Collins K. 2007. RNA-based affinity purification reveals 7SK RNPs with distinct composition and regulation. RNA 13:868-80.

238. Zhu Z, Fodor E, Keown JR. 2023. A structural understanding of influenza virus genome replication. Trends Microbiol 31:308-319.

239. Brownlee GG, Sharps JL. 2002. The RNA polymerase of influenza a virus is stabilized by interaction with its viral RNA promoter. J Virol 76:7103-13.

240. Bui M, Wills EG, Helenius A, Whittaker GR. 2000. Role of the influenza virus M1 protein in nuclear export of viral ribonucleoproteins. J Virol 74:1781-6.

241. Fries B, Heukeshoven J, Hauber I, Gruttner C, Stocking C, Kehlenbach RH, Hauber J, Chemnitz J. 2007. Analysis of nucleocytoplasmic trafficking of the HuR ligand APRIL and its influence on CD83 expression. J Biol Chem 282:4504-4515.